FEASIBILITY STUDY OF TOWER DESIGN AND VIBRATION SUPPRESSION FOR AN ANTARCTIC INFRARED TELESCOPE

by

Anderson Michael Furlanetto

A thesis submitted to Johns Hopkins University in conformity with the requirements for the degree of Master of Science in Engineering

Baltimore, Maryland

December 2022

Abstract

There is increasing interest to develop a dedicated near-infrared (NIR) observatory in Antarctica due to the advantages of a colder, darker sky in the NIR band and because the turbulent ground layer, responsible for seeing, is limited to the first 30 m above the ice shelf. A telescope mounted atop a 25 to 30 m tower will have enhanced performance by operating at the top of the boundary layer and unprecedented sensitivity due to the Antarctic climate.

Cryoscope is one such telescope and will be mounted atop a 30 m tower at Dome C, Antarctica. This presents a challenge for image stability since vibration-induced image motion must be less than 0.1 arcsec while the tower is subjected to 10 m/s wind buffeting. Seven tower designs were assessed using structural analysis programs to determine each tower's stability and natural frequency from wind loads determined using ASCE Standards 7-16 and wind data from Dome C. Power law analysis was conducted to evaluate the relationships between stability and mass if a tower was linearly scaled. Furthermore, in case the tower designs provide insufficient stability, vibration isolation mounts are explored to provide additional compensation, mainly damping mounts and friction mounts. In addition, we hold in reserve the possibility of active cancellation of forces on the telescope by applying torques with direct drive motors in response to forces measured by rotary flexures and encoders incorporated into the bearing mounts. The primary purpose of this work is to assess the feasibility and degree of difficulty of designing a 30 m tower for Antarctica with sufficient stability through passive and active mitigation methods while considering construction and transportation constraints.

Reviewers

Primary Reader and Advisor:

David Kraemer, Ph.D.

Associate Teaching Professor, Department of Mechanical Engineering

Johns Hopkins University

Secondary Reader:

Cristopher Moen, Ph.D., P.E.

Associate Research Professor and Director, M.S.E. in Civil Engineering

Johns Hopkins University

Tertiary Reader:

Roger M. Smith

Principal Electronics Engineer, Caltech Optical Observatories

California Institute of Technology

Dedication

To my mother, Rosineia Furlanetto, and my sister, Margarete Furlanetto.

Acknowledgements

I would like to thank the academy… When I came to Johns Hopkins University as an undergraduate, I never thought I would be designing the next generation of telescopes or solving problems related to astronaut health. I am very grateful to have worked with the brilliant folks at the JHU Instrument Development Group. Especially Dr. Stephen Smee and Stephen Hope who gave me the opportunity to discover my passion for engineering and astronomy instrumentation. Your unwavering support and guidance provided an environment that nurtured my engineering development. Your brilliance and passion for engineering has been incredibly inspiring to me during my undergraduate and Master's journey. Without you, I would not be where I am today.

I would also like to thank Roger Smith for making this project possible by introducing me to Cryoscope and letting me be part of its development team. Your mentorship and insight pushed me to grow into a better engineer. Thank you for being a soundboard for my ideas and for I hope this work will help lead us to one day visiting Cryoscope in the Antarctic.

Additionally, thank you to Dr. Kraemer and Dr. Moen for agreeing to advise and review this essay without necessarily knowing what you were getting into. Your patience and dedication helped make this work something I am truly proud of.

Finally, I would like to express my sincere love and thanks to friends and family believed in me through and through. You kept my head afloat through difficult times and made the good times all the more memorable. From U-Haul trips to foodie escapades and crazy workouts, you made Baltimore all the better.

Contents

List of Tables

List of Figures

1. Aims

This work supports the development of Cryoscope and the larger effort of deploying an optical or infrared observatory to Antarctica. The primary aim of this work is to:

- Assess the feasibility of a 0.1 arcsec RMS tilt requirement atop a ~30 m tower at Dome C, Antarctica for Cryoscope.

with secondary aims:

1. Determine whether 25 to 30 m tower designs can maintain 0.1 arcsec stability or better during nominal wind conditions at Dome C.
2. Ensure these designs conform to construction, transportation, and other logistic constraints at Dome C.
3. Assess vibration suppression methods that could decouple the telescope from the tower and improve the stability of the telescope.

2. Introduction

Time-domain astronomy studies how astronomical objects vary in intensity or position by observing the larger areas of sky after some time interval and comparing to reference images compiled by averaging previous images of the same areas. Such observations provide insight into phenomena on many scales, ranging from asteroids in our solar system, to stars of various brightness, eclipsing binary stars, exploding stars (supernovae), and the destruction of stars when consumed by black holes (tidal disruption events). Current ground-based, time-domain surveys like the Zwicky Transient Facility (ZTF) operate in the visual light spectrum and are blind to infrared emissions, so their capacity to observe time-domain phenomena is limited those which emit in the optical. Some events of considerable interest only produce infrared emission. For example, theories for the formation of the heavy elements invoke Neutron Star-Black Hole mergers which produce material that is opaque in the optical but transparent in the near infrared. The timing of these events is provided by the Laser Interferometer Gravitational-Wave Observatory (LIGO), but localization by LIGO is poor. Spectroscopy of these transient events is required to understand them, but this requires a fast wide field NIR (near-infrared) camera to provide accurate positions. For this reason, there is increasing interest to develop telescopes that operate in the NIR. These telescopes can see infrared radiation which penetrate the cosmic dust that obscures 90% of the Milky Way in the optical band. By deploying these telescopes in the Antarctica, sensitivity is no longer limited by background atmospheric emission. Antarctica is an attractive location to perform NIR imaging and time-domain astronomy since the sky is “25 to 40 times darker” [compared to temperate latitudes] [1]. The sensitivity of an infrared camera is significantly reduced by the strong infrared emissions from the sky itself. Narrow band emission lines of OH radicals dominate to 2.35 μm; while at temperate latitudes the blackbody emission dominates from 2.35 μm to 2.55 μm, where the sky becomes opaque due to water absorption.

Antarctica is very attractive for K-band imaging since the lower sky temperature moves the rising edge of the Plank curve beyond 2.55 μm leaving a dark sky between 2.35 μm and 2.55 μm. The cold, dry atmosphere allows for observations in the K_{dark} band from 2.35 μm to 2.5 μm. Furthermore, the turbulent boundary layer, responsible for image degradation known as seeing, is mostly constrained to an altitude of 25 m (above the ice) for relatively small wind speeds with a median seeing of 0.25 [1]. Therefore, a telescope will have unprecedented sensitivity and enhanced performance by placing it atop a tower above the turbulent boundary layer in Antarctica.

One such telescope is Cryoscope. Its optical design will deliver diffraction-limited imaging over the whole field of view at the 2.4 μm wavelength. Given a planned 1.2 m diameter, the diffraction limit is 0.5 arcsec. This diffraction-limited imaging can be achieved at nearly all times if the telescope is mounted on a 25- to 30-meter-high tower. This reduces the median image quality degradation due to the atmosphere to 0.25 arcsec since the telescope is at the top of the atmospheric "ground layer", which is only 30m thick at Dome C, Antarctica. We allocate the same full width at half maximum (FWHM) to image motion as to seeing, so that the total delivered image quality is 0.54 arcsec, slightly greater than the 0.4 arcsec set by optics alone.

To preserve Cryoscope's performance, vibration-induced image motion must be less than 0.1 arcsec. Vibration-induced image motion is created by wind forces acting on the tower, causing it to tilt and oscillate. If bearings in the telescope mount were completely frictionless, then rotations of the tower would not affect where the telescope is pointing. Unfortunately, friction cannot be reduced to be negligible, so the tower must be optimized for stability against wind buffeting. The coupling of these rotations to the telescope may be reduced by vibration-isolation mounts, selection and understanding of bearings for the telescope mount, and active compensation of residual torques transmitted by the bearing using the direct drive torque motors

planned to point the telescope. The primary goal of this study is to demonstrate whether Cryoscope's 0.1 arcsec pointing requirement can be achieved by exploring the mitigation measures listed above and understanding their relative degree of difficulty.

Additionally, tower design is constrained by the construction capabilities at Dome C, such as the limited availability of heavy machinery and manpower and increased cost of material transportation to assemble such a tall structure. This essay addresses these issues, as well as other feasibility constraints, by proposing a modular, workable design for a 30-meter Antarctic tower, modelling the displacement transmissibility through the telescope's bearings, and design of a vibration isolation system that meets the performance requirements for Cryoscope.

3. Antarctica

Wind buffeting and temperature gradients can cause undesirable motion of a telescope – whose pointing precision is often a fraction of an arcsecond. Therefore, understanding the weather is essential for performing astronomical observations. Several locations around Antarctica have been assessed as possible candidates for telescope deployments, particularly Dome A, Dome C, Dome F, and the Filchner Ice Shelf, each with similar climates and seeing characteristics.

3.1 Why Dome C

Dome C is an attractive location to deploy a telescope on a tower in Antarctica since the minimum tower height to achieve good seeing is only 30 m, and there is available infrastructure at the Concordia Research Station (Dome C) for construction, servicing, and operations. Swain and Gallée (2006) studied the boundary layer seeing during the Antarctic winter, seeing at several locations that could serve as possible telescope sites, and found the elevation to limit the average seeing to 0.1" or better 50% of the time, what they call the "minimal boundary layer contribution (MBLC)". Figure 1 below is a plot taken from their paper showing their results. The seeing during the winter is of particular interest since this is when the atmosphere is at its coldest and the black body emissions of the atmosphere are at their lowest. Domes A, C, and F, West Antarctica Crest (WA) and Filchner Ice Shelf (Fi) have a MBLC elevation of less than 30 m. Their respective MBLC elevation can be seen in Table 1 below. Domes A and F have the lowest MBLC and would be ideal locations based on MBLC elevation alone, however neither have year-round bases (they only have summer bases), which increases the amount of infrastructure that must be built up to establish a year-round base at either location. Dome C, Filchner Ice Shelf, and the West Antarctic Crest have the same MBLC elevation, however both the Filchner Ice Shelf and the West Antarctic Crest are both prone to calving and neither have year-round

bases. That leaves Dome C, which already has a year-round base, called the Concordia Research Station, and has an airfield for personnel and light material transport as well as ground routes for winterized caterpillar tractors to transport heavy material and equipment to the base. Therefore, Dome C is the most suitable location to deploy a telescope atop a tower since the MBLC is less than 30 m and there already exists significant infrastructure to build, operate, and maintain an observatory.

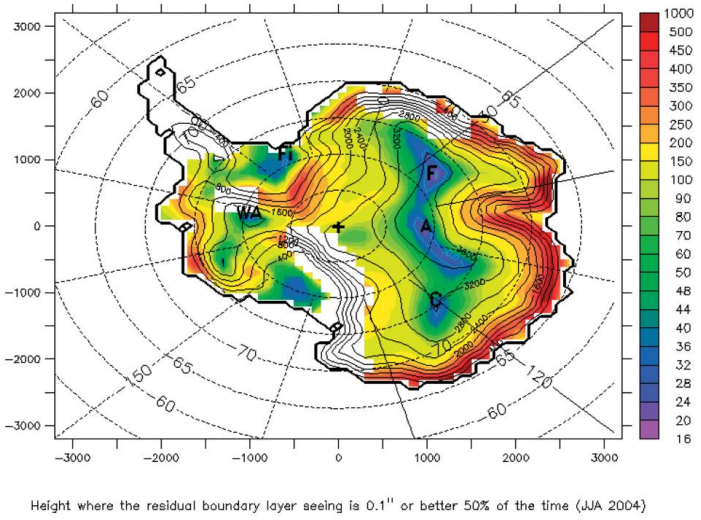

Figure 1. *"Elevation (meters) required to limit the atmospheric seeing contribution from the boundary layer to ≤ 0.1" at least 50% of the time during the 2004 winter (June, July, August) season" [13].*

Table 1. Locations in Antarctica where the MBLC elevation is less than 30 meters [13].

Location	MBLC Elevation (m)
Dome A	21.7
Dome C	27.5
Dome F	18.5
Filchner Ice Shelf	27.5
West Antarctic Crest	27.5

3.2 Weather at Dome C

Dome C lies on the Antarctic Plateau, which has been an attractive location for long-wavelength astronomy due to its extremely cold and dry climate [2][3]. The high altitude (the Plateau has an average altitude of 3.2 km) and very stable atmosphere (compared against more temperate latitudes) reduces the seeing to a few fractions of an arcsecond (often better than at Mauna Kea), provides high atmospheric transmission, and low sky brightness. Dome C is of particular interest, compared to being directly at the South Pole, since the ground layer is only about 30 m high compared to being 100 m to 300 m at the South Pole. The sensitivity (sky emission and atmospheric transparency) are about two times better in the near- to mid-infrared range and, though not relevant to Cryoscope, is about ten times better in the mid- to far-infrared [4].

Data collection and analysis of the weather behavior at Dome C at various altitudes is abundant [5][6]. Genthon et al. 2021 conducted climatology studies over a 10-year period (from 2010 to 2019) on a 42-meter tower. Sensors were placed at the 3 m, 9 m, 18 m, 25 m, 33 m, and 42 m heights of the tower. The most relevant figures from the paper are displayed below:

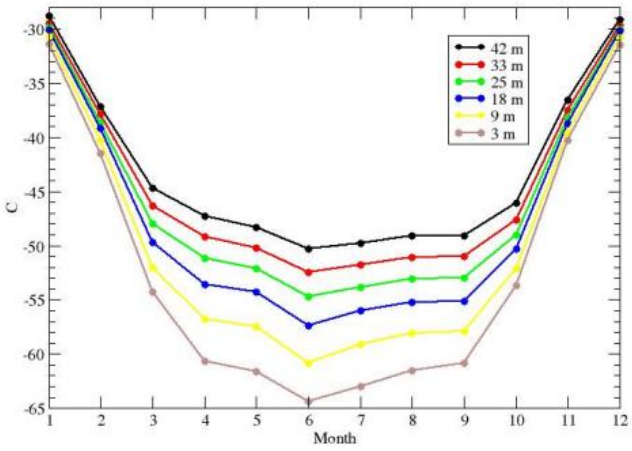

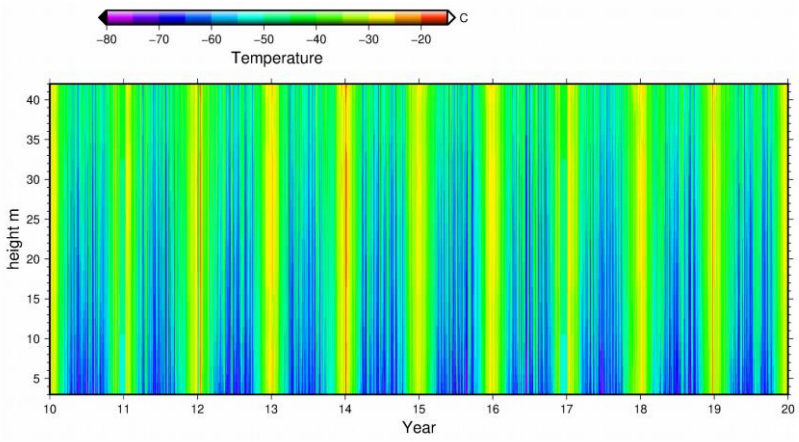

Figure 2. *Mean 10-year seasonal cycle of temperature at six Dome C tower levels [5].*

Note the temperature extremes of the data in Figure 2, -10℃ and -80℃. Mechanisms and electronics must either be designed for low temperatures or heated so they are at their operating temperature. Special attention to bearing selection and design for the telescope mount are made so that they retain their near frictionless properties and do not seize during operation.

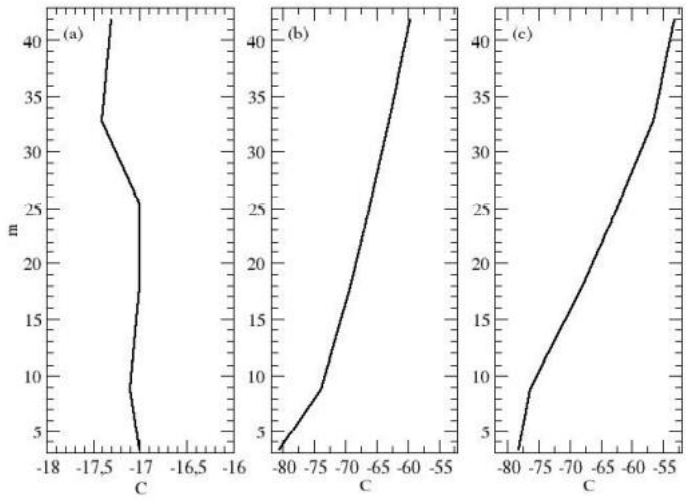

Figure 3. *Vertical profile of daily-mean temperature on 2 January 2014 (a), 22 June 2017 (b), 24 June 2017 (c), the days with the warmest and coldest temperatures and the steepest temperature inversion, respectively [5].*

Figure 3 shows that temperature is not constant with height; temperature gradients are apparent. Therefore, any tower design and control system must account for material contraction

and expansion due to temperature as well as the oscillatory temperature change from the day-night cycle. These changes will be small and slow so they are not of significant as a source of excitation but must be noted, nevertheless.

Data of wind speed was also collected:

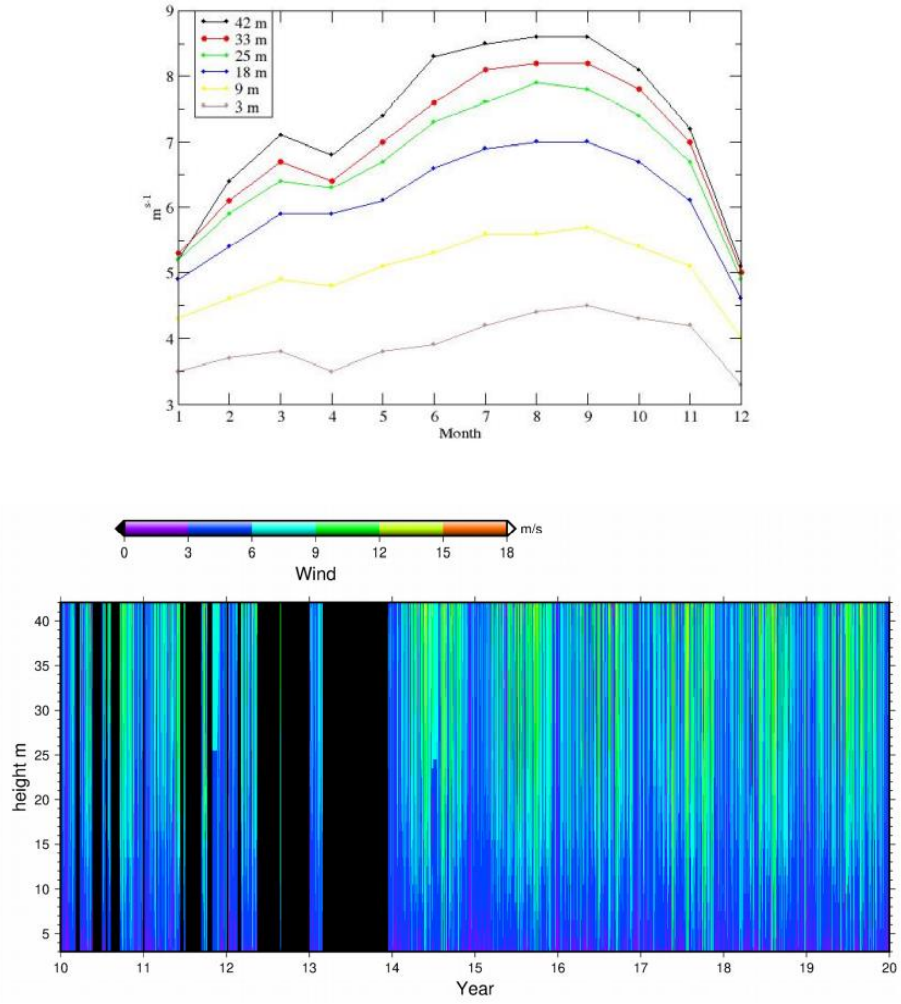

Figure 4. *Mean 6-year seasonal cycle of wind speed at the six levels along the tower. Years 2010 to 2013 are not included in the averaging process due to large gaps in the data in these years [5].*

Wind speeds vary from 0 m/s to as high as 18 m/s but peak at around 10 m/s for an altitude of 30 m. The average wind speeds are at their greatest during late winter and early spring. This data is corroborated by a study by Aristidi et al. 2005 who used balloon-borne

weather sondes to measure wind behavior high in the atmosphere. Their relevant results are shown in Figure 5 below:

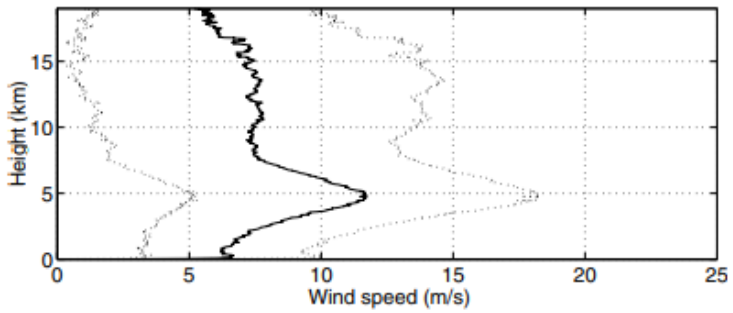

Figure 5. *Mean wind speed profile at Dome C. The two outer lines delimit the standard deviation [6].*

Their results and information from Wendler et al. 1992, the wind speeds and direction (see Figure 6) are consistent [7]. This could be factored into tower design, so it is stiffer in the direction the wind blows (between 150° and 260°) or includes add-ons to the tower beams such that the wind remains laminar as it passes through the tower and reduces the force applied directly to the beams due to flow stagnation (i.e., creating an airfoil-like cross section).

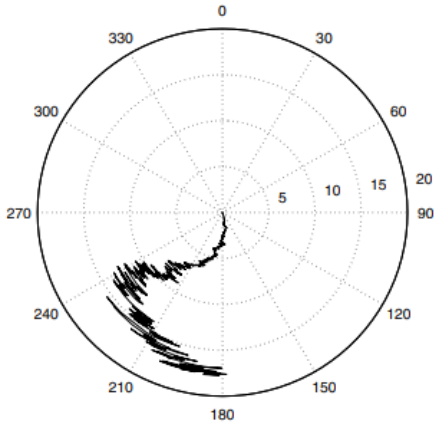

Figure 6. *Average wind direction profile as a function of altitude [6].*

Lastly, it is important to note the spectral distribution of wind behavior since its frequency range drives the design and selection of compensation techniques:

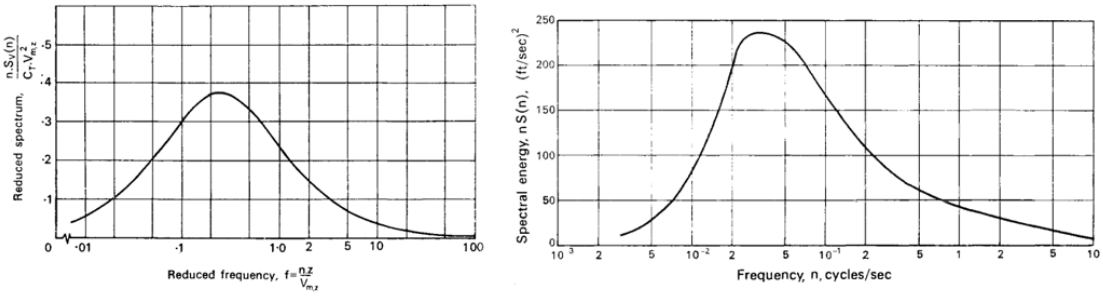

Figure 7. *Spectra of gustiness in strong winds: vertical gustiness (left) and horizontal gustiness (right) [8].*

Figure 7 shows that vertical gustiness of wind peaks between 0.1 Hz and 1 Hz before quickly dropping off and horizontal gustiness peaks between 0.02 Hz and 0.05 Hz, but the spectral intensity of horizontal gusts are significantly more disruptive than vertical gusts (~400 times greater). Although the frequencies that lie at around the peak spectral energy for horizontal gustiness are low, there is still significant energy within the 1-10 Hz range, but quickly drops off. Therefore, the tower and vibration isolation system design should filter out these frequencies as much as possible and maximize their natural frequency to be beyond 1 Hz.

4. Tower Design

Placing a telescope atop a tower in Antarctica will improve the local seeing by being above the turbulent ground layer of air. At the same time, image motion must be kept below 0.25 arcsec FWHM or 0.106 arcsec RMS if normally distributed. The principal load acting on the tower is air pressure from sustained winds and gusts, so the tower must be designed to resist these loads while minimizing angular deflections. Wind loads are quantified from the data provided in Section 3.2 using the American Society of Civil Engineers (ASCE) Standards 7-16 in Section 4.1. This is followed by an assessment of contemporary telescope tower geometries and a discussion of space-truss designs in Sections 4.2 and 4.3.1. Design solutions are proposed in Section 4.3.3 and assessed using the methods discussed in Section 4.3.2 with results presented in Section 4.3.4. The results show that the designs proposed herein offer better performance than most contemporary towers for less mass and easier assembly. These designs offer a modular, compensating structure that promises sufficient mechanical stability through purely passive means – avoiding the expense of active systems, which can be relegated to a contingency measure.

4.1 Quantifying Wind Loading

This section provides the method to determine wind loads from available data from Dome C. Loading from sustained winds and 3-s gusts are determined according to ASCE 7-16, "Minimum Design Loads and Associated Criteria for Buildings and Other Structures." Table 1 provides the results for sustained winds and gusts. Section 4.1.1 contains screen captures from Chapters 26 through 28 showing the pertaining instructions, tables, and formula from the procedure.

Sustained winds between 0 m/s to 10 m/s are the service conditions expected for the tower with 72 m/s 3-second gusts being the ultimate condition that the tower must survive.

Table 27.2-1 Steps to Determine MWFRS Wind Loads for Enclosed, Partially Enclosed, and Open Buildings of All Heights

Step 1: Determine Risk Category of building; see Table 1.5-1.

Step 2: Determine the basic wind speed, V, for the applicable Risk Category; see Figs. 26.5-1 and 26.5-2.

Step 3: Determine wind load parameters:

- Wind directionality factor, K_d; see Section 26.6 and Table 26.6-1.
- Exposure category; see Section 26.7.
- Topographic factor, K_{zt}; see Section 26.8 and table in Fig. 26.8-1.
- Ground elevation factor, K_e; see Section 26.9
- Gust-effect factor, G or G_f; see Section 26.11.
- Enclosure classification; see Section 26.12.
- Internal pressure coefficient, (GC_{pi}); see Section 26.13 and Table 26.13-1.

Step 4: Determine velocity pressure exposure coefficient, K_z or K_h; see Table 26.10-1.

Step 5: Determine velocity pressure q_z or q_h, Eq. (26.10-1).

Step 6: Determine external pressure coefficient, C_p or C_N:

- Fig. 27.3-1 for walls and flat, gable, hip, monoslope, or mansard roofs.
- Fig. 27.3-2 for domed roofs.
- Fig. 27.3-3 for arched roofs.
- Fig. 27.3-4 for monoslope roof, open building.
- Fig. 27.3-5 for pitched roof, open building.
- Fig. 27.3-6 for troughed roof, open building.
- Fig. 27.3-7 for along-ridge/valley wind load case for monoslope, pitched, or troughed roof, open building.

Step 7: Calculate wind pressure, p, on each building surface:

- Eq. (27.3-1) for rigid and flexible buildings.
- Eq. (27.3-2) for open buildings.

Figure 8. *General procedure to determine wind load.*

Table 2. Wind load parameters determined using ASCE Standard 7-16.

Wind Load Parameters	Value	Reasoning
Wind Directionality Factor, K_d	0.85	Trussed Tower, Figure 11
Exposure Category	Exposure D	Surface Roughness D, Figure 12
Topographic Factor K_{zt}	1	No topographic obstructions/features, Figure 13
Ground Elevation Factor, K_e	0.68	Dome C as altitude of ~3.2km so use Note 2 from Figure 14
Gust-effect Factor, G	0.85	Rigid structure, Figure 15
Enclose Classification	Open	Each wall is at least 80% open, Figure 16
Internal Pressure Coefficient, GC_{pi}	0	Figure 16
Velocity Pressure Exposure Coefficients, K_h or K_z	1.42	For Exposure D, interpolating for 30m, Figure 17
Velocity Pressure, q_z	2630 N/m^2	Equation from Figure 18
External Pressure Coefficient, CN	1.2	Flat roof, angle is zero, Figure 19
Wind Pressure @ 72 m/s	**2700 N/m^2**	**Equation for open buildings, Figure 20**
Wind Pressure @ 10 m/s	**50 N/m^2**	

4.1.1 ASCE Standards 7-16

Step 1: Determine Risk Category of Building; Table 1.5-1.

Table 1.5-1 Risk Category of Buildings and Other Structures for Flood, Wind, Snow, Earthquake, and Ice Loads

Use or Occupancy of Buildings and Structures	Risk Category
Buildings and other structures that represent low risk to human life in the event of failure	I
All buildings and other structures except those listed in Risk Categories I, III, and IV	II
Buildings and other structures, the failure of which could pose a substantial risk to human life	III
Buildings and other structures, not included in Risk Category IV, with potential to cause a substantial economic impact and/or mass disruption of day-to-day civilian life in the event of failure	
Buildings and other structures not included in Risk Category IV (including, but not limited to, facilities that manufacture, process, handle, store, use, or dispose of such substances as hazardous fuels, hazardous chemicals, hazardous waste, or explosives) containing toxic or explosive substances where the quantity of the material exceeds a threshold quantity established by the Authority Having Jurisdiction and is sufficient to pose a threat to the public if released[a]	
Buildings and other structures designated as essential facilities	IV
Buildings and other structures, the failure of which could pose a substantial hazard to the community Buildings and other structures (including, but not limited to, facilities that manufacture, process, handle, store, use, or dispose of such substances as hazardous fuels, hazardous chemicals, or hazardous waste) containing sufficient quantities of highly toxic substances where the quantity of the material exceeds a threshold quantity established by the Authority Having Jurisdiction and is sufficient to pose a threat to the public if released[a]	
Buildings and other structures required to maintain the functionality of other Risk Category IV structures	

[a]Buildings and other structures containing toxic, highly toxic, or explosive substances shall be eligible for classification to a lower Risk Category if it can be demonstrated to the satisfaction of the Authority Having Jurisdiction by a hazard assessment as described in Section 1.5.3 that a release of the substances is commensurate with the risk associated with that Risk Category.

Figure 9. *Risk factor criteria.*

Risk factor IV is used due to the tower requiring arcsecond stability.

Step 2: Determine the basic wind speed, *V*, for applicable Risk Category

There does appear to be any published data on the 3-second wind gusts of Antarctica or any of the candidate locations so the 3-s wind gust speed for northern coastal Alaska will be used as a preliminary estimate until said data is published. Basic wind speed, *V*, is selected as 72 m/s from the northernmost point of Alaska from Figure 10.

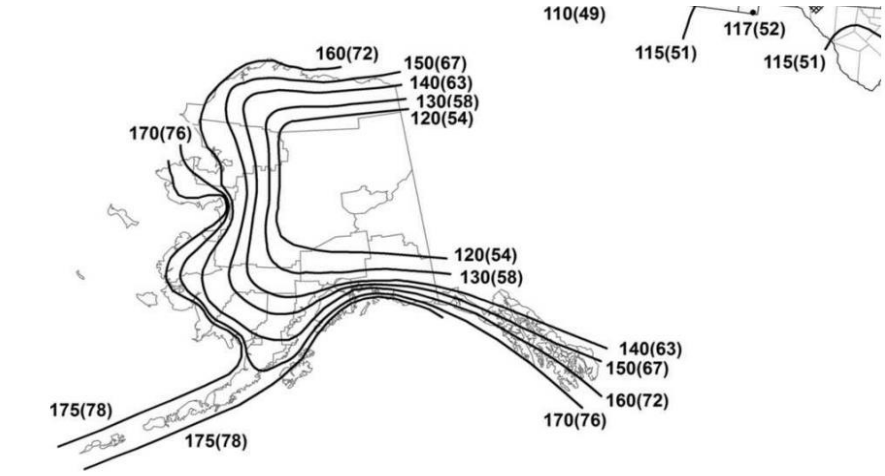

Notes

1. Values are nominal design 3-s gust wind speeds in mi/h (m/s) at 33 ft (10 m) above ground for Exposure Category C.
2. Linear interpolation is permitted between contours. Point values are provided to aid with interpolation.
3. Islands, coastal areas, and land boundaries outside the last contour shall use the last wind speed contour.
4. Mountainous terrain, gorges, ocean promontories, and special wind regions shall be examined for unusual wind conditions.
5. Wind speeds correspond to approximately a 1.6% probability of exceedance in 50 years (Annual Exceedance Probability = 0.00033, MRI = 3,000 years).
6. Location-specific basic wind speeds shall be permitted to be determined using www.atcouncil.org/windspeed.

FIGURE 26.5-1D Basic Wind Speeds for Risk Category IV Buildings and Other Structures

Figure 10. *Basic wind speeds map of Alaska for Risk Category IV structures.*

Step 3: Determine wind load parameters

Table 26.6-1 Wind Directionality Factor, K_d

Structure Type	Directionality Factor K_d
Buildings	
Main Wind Force Resisting System	0.85
Components and Cladding	0.85
Arched Roofs	0.85
Circular Domes	1.0[a]
Chimneys, Tanks, and Similar Structures	
Square	0.90
Hexagonal	0.95
Octagonal	1.0[a]
Round	1.0[a]
Solid Freestanding Walls, Roof Top Equipment, and Solid Freestanding and Attached Signs	0.85
Open Signs and Single-Plane Open Frames	0.85
Trussed Towers	
Triangular, square, or rectangular	0.85
All other cross sections	0.95

[a]Directionality factor $K_d = 0.95$ shall be permitted for round or octagonal structures with nonaxisymmetric structural systems.

Figure 11. *Table for Wind Directionality Factor, K_d.*

26.7.2 Surface Roughness Categories. A ground surface roughness within each 45° sector shall be determined for a distance upwind of the site, as defined in Section 26.7.3, from the categories defined in the following text, for the purpose of assigning an exposure category as defined in Section 26.7.3.

Surface Roughness B: Urban and suburban areas, wooded areas, or other terrain with numerous, closely spaced obstructions that have the size of single-family dwellings or larger.

Surface Roughness C: Open terrain with scattered obstructions that have heights generally less than 30 ft (9.1 m). This category includes flat, open country and grasslands.

Surface Roughness D: Flat, unobstructed areas and water surfaces. This category includes smooth mud flats, salt flats, and unbroken ice.

26.7.3 Exposure Categories.

Exposure B: For buildings or other structures with a mean roof height less than or equal to 30 ft (9.1 m), Exposure B shall apply where the ground surface roughness, as defined by Surface Roughness B, prevails in the upwind direction for a distance greater than 1,500 ft (457 m). For buildings or other structures with a mean roof height greater than 30 ft (9.1 m), Exposure B shall apply where Surface Roughness B prevails in the upwind direction for a distance greater than 2,600 ft (792 m) or 20 times the height of the building or structure, whichever is greater.

Exposure C: Exposure C shall apply for all cases where Exposure B or D does not apply.

Exposure D: Exposure D shall apply where the ground surface roughness, as defined by Surface Roughness D, prevails in the upwind direction for a distance greater than 5,000 ft (1,524 m) or 20 times the building or structure height, whichever is greater. Exposure D shall also apply where the ground surface roughness immediately upwind of the site is B or C, and the site is within a distance of 600 ft (183 m) or 20 times the building or structure height, whichever is greater, from an Exposure D condition as defined in the previous sentence.

For a site located in the transition zone between exposure categories, the category resulting in the largest wind forces shall be used.

Figure 12. *Excerpts to determine Exposure Category*

Step 3: Determine wind load parameters (continued)

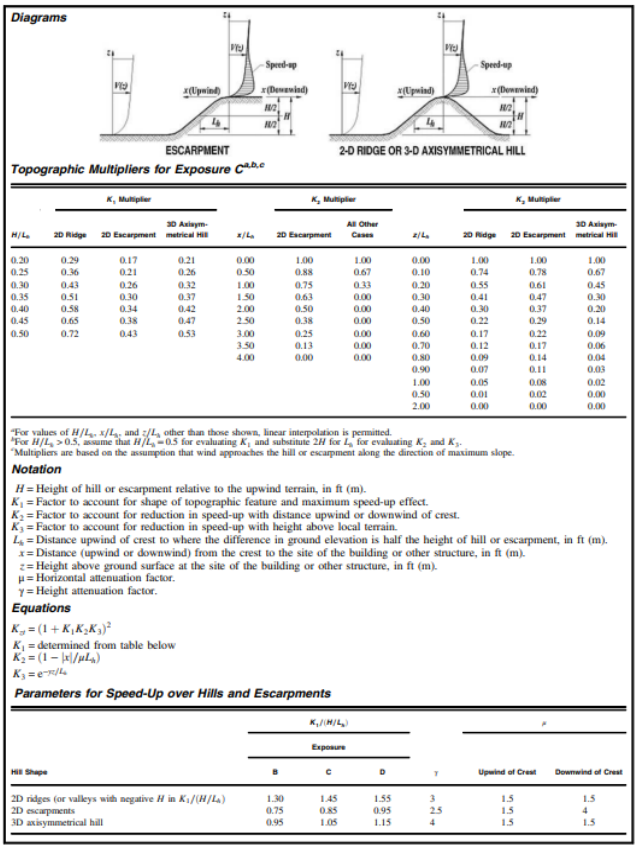

Diagrams

ESCARPMENT

2-D RIDGE OR 3-D AXISYMMETRICAL HILL

Topographic Multipliers for Exposure C[a,b,c]

	K_1 Multiplier				K_2 Multiplier			K_3 Multiplier		
H/L_h	2D Ridge	2D Escarpment	3D Axisymmetrical Hill	x/L_h	2D Escarpment	All Other Cases	z/L_h	2D Ridge	2D Escarpment	3D Axisymmetrical Hill
0.20	0.29	0.17	0.21	0.00	1.00	1.00	0.00	1.00	1.00	1.00
0.25	0.36	0.21	0.26	0.50	0.88	0.67	0.10	0.74	0.78	0.67
0.30	0.43	0.26	0.32	1.00	0.75	0.33	0.20	0.55	0.61	0.45
0.35	0.51	0.30	0.37	1.50	0.63	0.00	0.30	0.41	0.47	0.30
0.40	0.58	0.34	0.42	2.00	0.50	0.00	0.40	0.30	0.37	0.20
0.45	0.65	0.38	0.47	2.50	0.38	0.00	0.50	0.22	0.29	0.14
0.50	0.72	0.43	0.53	3.00	0.25	0.00	0.60	0.17	0.22	0.09
				3.50	0.13	0.00	0.70	0.12	0.17	0.06
				4.00	0.00	0.00	0.80	0.09	0.14	0.04
							0.90	0.07	0.11	0.03
							1.00	0.05	0.08	0.02
							0.50	0.01	0.02	0.00
							2.00	0.00	0.00	0.00

[a]For values of H/L_h, x/L_h, and z/L_h other than those shown, linear interpolation is permitted.
[b]For $H/L_h > 0.5$, assume that $H/L_h = 0.5$ for evaluating K_1 and substitute $2H$ for L_h for evaluating K_2 and K_3.
[c]Multipliers are based on the assumption that wind approaches the hill or escarpment along the direction of maximum slope.

Notation

H = Height of hill or escarpment relative to the upwind terrain, in ft (m).
K_1 = Factor to account for shape of topographic feature and maximum speed-up effect.
K_2 = Factor to account for reduction in speed-up with distance upwind or downwind of crest.
K_3 = Factor to account for reduction in speed-up with height above local terrain.
L_h = Distance upwind of crest to where the difference in ground elevation is half the height of hill or escarpment, in ft (m).
x = Distance (upwind or downwind) from the crest to the site of the building or other structure, in ft (m).
z = Height above ground surface at the site of the building or other structure, in ft (m).
μ = Horizontal attenuation factor.
γ = Height attenuation factor.

Equations

$K_{zt} = (1 + K_1 K_2 K_3)^2$

K_1 = determined from table below
$K_2 = (1 - |x|/\mu L_h)$
$K_3 = e^{-\gamma z/L_h}$

Parameters for Speed-Up over Hills and Escarpments

	$K_1/(H/L_h)$				μ	
	Exposure					
Hill Shape	B	C	D	γ	Upwind of Crest	Downwind of Crest
2D ridges (or valleys with negative H in $K_1/(H/L_h)$	1.30	1.45	1.55	3	1.5	1.5
2D escarpments	0.75	0.85	0.95	2.5	1.5	4
3D axisymmetrical hill	0.95	1.05	1.15	4	1.5	1.5

FIGURE 26.8-1 Topographic Factor, K_{zt}

Figure 13. *Table to determine Topographic Factor, K_{Zt}.*

Table 26.9-1 Ground Elevation Factor, K_e

Ground Elevation above Sea Level		Ground Elevation Factor
ft	m	K_e
<0	<0	See note 2
0	0	1.00
1,000	305	0.96
2,000	610	0.93
3,000	914	0.90
4,000	1,219	0.86
5,000	1,524	0.83
6,000	1,829	0.80
>6,000	>1,829	See note 2

Notes

1. The conservative approximation $K_e = 1.00$ is permitted in all cases.
2. The factor K_e shall be determined from the above table using interpolation or from the following formula for all elevations:
   $K_e = e^{-0.0000362 z_g}$ (z_g = ground elevation above sea level in ft).
   $K_e = e^{-0.000119 z_g}$ (z_g = ground elevation above sea level in m).
3. K_e is permitted to be take as 1.00 in all cases.

Figure 14. *Table to determine Ground Elevatio Factor, K_e.*

Step 3: Determine wind load parameters (continued)

26.11.4 Rigid Buildings or Other Structures. For rigid buildings or other structures as defined in Section 26.2, the gust-effect factor shall be taken as 0.85 or calculated by this formula:

$$G = 0.925\left(\frac{1 + 0.7 g_Q I_{\bar{z}} Q}{1 + 0.7 g_v I_{\bar{z}}}\right) \quad (26.11\text{-}6)$$

$$I_{\bar{z}} = c\left(\frac{33}{\bar{z}}\right)^{1/6} \quad (26.11\text{-}7)$$

$$I_{\bar{z}} = c\left(\frac{10}{\bar{z}}\right)^{1/6} \quad (26.11\text{-}7.si)$$

where $I_{\bar{z}}$ = intensity of turbulence at height $\bar{z}$, where $\bar{z}$ is the equivalent height of the building or structure defined as $0.6h$, but not less than z_{min} for all building or structure heights h. z_{min} and c are listed for each exposure in Table 26.11-1; g_Q and g_v shall be taken as 3.4. The background response Q is given by

$$Q = \sqrt{\frac{1}{1 + 0.63\left(\frac{B+h}{L_{\bar{z}}}\right)^{0.63}}} \quad (26.11\text{-}8)$$

where B and h are defined in Section 26.3; and $L_{\bar{z}}$ = integral length scale of turbulence at the equivalent height given by

$$L_{\bar{z}} = \ell\left(\frac{\bar{z}}{33}\right)^{\bar{\varepsilon}} \quad (26.11\text{-}9)$$

$$L_{\bar{z}} = \ell\left(\frac{\bar{z}}{10}\right)^{\bar{\varepsilon}} \quad (26.11\text{-}9.si)$$

in which ℓ and $\bar{\varepsilon}$ = constants listed in Table 26.11-1.

26.11.5 Flexible or Dynamically Sensitive Buildings or Other Structures. For flexible or dynamically sensitive buildings or other structures as defined in Section 26.2, the gust-effect factor shall be calculated by

$$G_f = 0.925\left(\frac{1 + 1.7 I_{\bar{z}}\sqrt{g_Q^2 Q^2 + g_R^2 R^2}}{1 + 1.7 g_v I_{\bar{z}}}\right) \quad (26.11\text{-}10)$$

g_Q and g_v shall be taken as 3.4, and g_R is given by

$$g_R = \sqrt{2\ln(3{,}600 n_1)} + \frac{0.577}{\sqrt{2\ln(3{,}600 n_1)}} \quad (26.11\text{-}11)$$

R, the resonant response factor, is given by

$$R = \sqrt{\frac{1}{\beta} R_n R_h R_B (0.53 + 0.47 R_L)} \quad (26.11\text{-}12)$$

$$R_n = \frac{7.47 N_1}{(1 + 10.3 N_1)^{5/3}} \quad (26.11\text{-}13)$$

$$N_1 = \frac{n_1 L_{\bar{z}}}{\bar{V}_{\bar{z}}} \quad (26.11\text{-}14)$$

$$R_\ell = \frac{1}{\eta} - \frac{1}{2\eta^2}(1 - e^{-2\eta}) \quad \text{for } \eta > 0 \quad (26.11\text{-}15a)$$

$$R_l = 1 \quad \text{for } \eta = 0 \quad (26.11\text{-}15b)$$

where the subscript ℓ in Eqs. (26.11-15a) and (26.11-15b) shall be taken as h, B, and L, respectively, where h, B, and L are defined in Section 26.3, and

n_1 = fundamental natural frequency.
$R_\ell = R_h$ setting $\eta = 4.6 n_1 h/\bar{V}_{\bar{z}}$.
$R_\ell = R_B$ setting $\eta = 4.6 n_1 B/\bar{V}_{\bar{z}}$.
$R_\ell = R_L$ setting $\eta = 15.4 n_1 L/\bar{V}_{\bar{z}}$;
β = damping ratio, percent of critical (i.e., for 2% use 0.02 in the equation).
$\bar{V}_{\bar{z}}$ = mean hourly wind speed (ft/s) (m/s) at height $\bar{z}$ determined from Eq. (26.11-16):

$$\bar{V}_{\bar{z}} = \bar{b}\left(\frac{\bar{z}}{33}\right)^{\bar{\alpha}}\left(\frac{88}{60}\right)V \quad (26.11\text{-}16)$$

$$\bar{V}_{\bar{z}} = \bar{b}\left(\frac{\bar{z}}{10}\right)^{\bar{\alpha}} V \quad (26.11\text{-}16.si)$$

where $\bar{b}$ and $\bar{\alpha}$ are constants listed in Table 26.9-1; and V is the basic wind speed in mi/h (m/s).

Figure 15. *Details for determining Gust-effect Factor, G.*

Step 3: Determine wind load parameters (continued)

Table 26.13-1 Main Wind Force Resisting System and Components and Cladding (All Heights): Internal Pressure Coefficient, (GC_{pi}), for Enclosed, Partially Enclosed, Partially Open, and Open Buildings (Walls and Roof)

Enclosure Classification	Criteria for Enclosure Classification	Internal Pressure	Internal Pressure Coefficient, (GC_{pi})
Enclosed buildings	A_o is less than the smaller of $0.01A_g$ or 4 sq ft (0.37 m) and $A_{oi}/A_{gi} \leq 0.2$	Moderate	+0.18 −0.18
Partially enclosed buildings	$A_o > 1.1A_{oi}$ and $A_o >$ the lesser of $0.01A_g$ or 4 sq ft (0.37 m) and $A_{oi}/A_{gi} \leq 0.2$	High	+0.55 −0.55
Partially open buildings	A building that does not comply with Enclosed, Partially Enclosed, or Open classifications	Moderate	+0.18 −0.18
Open buildings	Each wall is at least 80% open	Negligible	0.00

Notes

1. Plus and minus signs signify pressures acting toward and away from the internal surfaces, respectively.
2. Values of (GC_{pi}) shall be used with q_z or q_h as specified.
3. Two cases shall be considered to determine the critical load requirements for the appropriate condition:
   a. A positive value of (GC_{pi}) applied to all internal surfaces, or
   b. A negative value of (GC_{pi}) applied to all internal surfaces.

Figure 16. *Table to determine enclosure classification and Internal Pressure Coefficient, GC_{pi}.*

Step 4: Determine velocity pressure exposure coefficient, K_z or K_h

Use exposure determined from Figure 12 (Exposure D). Use linear interpolation as is allowed from Note 3 to determined K_z at 30 m.

Table 26.10-1 Velocity Pressure Exposure Coefficients, K_h and K_z

Height above Ground Level, z		Exposure		
ft	m	B	C	D
0–15	0–4.6	0.57 (0.70)[a]	0.85	1.03
20	6.1	0.62 (0.70)[a]	0.90	1.08
25	7.6	0.66 (0.70)[a]	0.94	1.12
30	9.1	0.70	0.98	1.16
40	12.2	0.76	1.04	1.22
50	15.2	0.81	1.09	1.27
60	18.0	0.85	1.13	1.31
70	21.3	0.89	1.17	1.34
80	24.4	0.93	1.21	1.38
90	27.4	0.96	1.24	1.40
100	30.5	0.99	1.26	1.43
120	36.6	1.04	1.31	1.48
140	42.7	1.09	1.36	1.52
160	48.8	1.13	1.39	1.55
180	54.9	1.17	1.43	1.58
200	61.0	1.20	1.46	1.61
250	76.2	1.28	1.53	1.68
300	91.4	1.35	1.59	1.73
350	106.7	1.41	1.64	1.78
400	121.9	1.47	1.69	1.82
450	137.2	1.52	1.73	1.86
500	152.4	1.56	1.77	1.89

[a]Use 0.70 in Chapter 28, Exposure B, when $z < 30$ ft (9.1 m).

Notes

1. The velocity pressure exposure coefficient K_z may be determined from the following formula:
   For 15 ft (4.6 m) $\le z \le z_g$ $K_z = 2.01(z/z_g)^{2/\alpha}$
   For $z < 15$ ft (4.6 m) $K_z = 2.01(15/z_g)^{2/\alpha}$
2. α and z_g are tabulated in Table 26.11-1.
3. Linear interpolation for intermediate values of height z is acceptable.
4. Exposure categories are defined in Section 26.7.

Figure 17. *Table for Velocity Pressure Exposure Coefficients.*

Step 5: Determine velocity pressure, q_z or q_h

26.10.2 Velocity Pressure. Velocity pressure, q_z, evaluated at height z above ground shall be calculated by the following equation:

$$q_z = 0.00256 K_z K_{zt} K_d K_e V^2 \text{ (lb/ft}^2\text{)}; \; V \text{ in mi/h} \qquad (26.10\text{-}1)$$

$$q_z = 0.613 K_z K_{zt} K_d K_e V^2 \text{ (N/m}^2\text{)}; \; V \text{ in m/s} \qquad (26.10\text{-}1.si)$$

where

K_z = velocity pressure exposure coefficient, see Section 26.10.1.
K_{zt} = topographic factor, see Section 26.8.2.
K_d = wind directionality factor, see Section 26.6.
K_e = ground elevation factor, see Section 26.9.
V = basic wind speed, see Section 26.5.
q_z = velocity pressure at height z.

The velocity pressure at mean roof height is computed as $q_h = q_z$ evaluated from Eq. (26.10-1) using K_z at mean roof height h.

The basic wind speed, V, used in determination of design wind loads on rooftop structures, rooftop equipment, and other

Figure 18. *Equation to determine velocity pressure, q_z.*

Step 6: Determine external pressure coefficient, *CN*

Fig. 27.3-1 for walls and flat, gable, hip, monoslope, or mansard roofs.
Fig. 27.3-2 for domed roofs.
Fig. 27.3-3 for arched roofs.
Fig. 27.3-4 for monoslope roof, open building.
Fig. 27.3-5 for pitched roof, open building.
Fig. 27.3-6 for troughed roof, open building.
Fig. 27.3-7 for along-ridge/valley wind load case for monoslope, pitched, or troughed roof, open building.

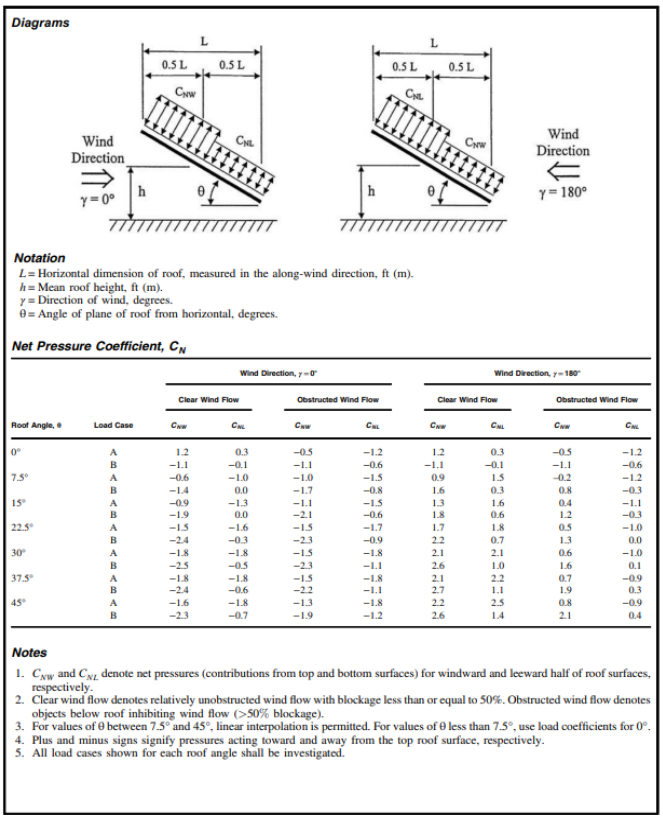

Diagrams

Notation

L = Horizontal dimension of roof, measured in the along-wind direction, ft (m).
h = Mean roof height, ft (m).
γ = Direction of wind, degrees.
θ = Angle of plane of roof from horizontal, degrees.

Net Pressure Coefficient, C_N

		Wind Direction, $\gamma = 0°$				Wind Direction, $\gamma = 180°$			
		Clear Wind Flow		Obstructed Wind Flow		Clear Wind Flow		Obstructed Wind Flow	
Roof Angle, θ	Load Case	C_{NW}	C_{NL}	C_{NW}	C_{NL}	C_{NW}	C_{NL}	C_{NW}	C_{NL}
0°	A	1.2	0.3	−0.5	−1.2	1.2	0.3	−0.5	−1.2
	B	−1.1	−0.1	−1.1	−0.6	−1.1	−0.1	−1.1	−0.6
7.5°	A	−0.6	−1.0	−1.0	−1.5	0.9	1.5	−0.2	−1.2
	B	−1.4	0.0	−1.7	−0.8	1.6	0.3	0.8	−0.3
15°	A	−0.9	−1.3	−1.1	−1.5	1.3	1.6	0.4	−1.1
	B	−1.9	0.0	−2.1	−0.6	1.8	0.6	1.2	−0.3
22.5°	A	−1.5	−1.6	−1.5	−1.7	1.7	1.8	0.5	−1.0
	B	−2.4	−0.3	−2.3	−0.9	2.2	0.7	1.3	0.0
30°	A	−1.8	−1.8	−1.5	−1.8	2.1	2.1	0.6	−1.0
	B	−2.5	−0.5	−2.3	−1.1	2.6	1.0	1.6	0.1
37.5°	A	−1.8	−1.8	−1.5	−1.8	2.1	2.2	0.7	−0.9
	B	−2.4	−0.6	−2.2	−1.1	2.7	1.1	1.9	0.3
45°	A	−1.6	−1.8	−1.3	−1.8	2.2	2.5	0.8	−0.9
	B	−2.3	−0.7	−1.9	−1.2	2.6	1.4	2.1	0.4

Notes

1. C_{NW} and C_{NL} denote net pressures (contributions from top and bottom surfaces) for windward and leeward half of roof surfaces, respectively.
2. Clear wind flow denotes relatively unobstructed wind flow with blockage less than or equal to 50%. Obstructed wind flow denotes objects below roof inhibiting wind flow (>50% blockage).
3. For values of θ between 7.5° and 45°, linear interpolation is permitted. For values of θ less than 7.5°, use load coefficients for 0°.
4. Plus and minus signs signify pressures acting toward and away from the top roof surface, respectively.
5. All load cases shown for each roof angle shall be investigated.

FIGURE 27.3-4 Main Wind Force Resisting System, Part 1 ($0.25 \le h/L \le 1.0$): Net Pressure Coefficient, C_N, for Open Buildings with Monoslope Free Roofs, $\theta \le 45°$, $\gamma = 0°$, 180°)

Figure 19. *Table to determine external pressure coefficient, CN.*

Step 7: Calculate wind pressure, *p*, on building surface

- Eq. (27.3-1) for rigid and flexible buildings.
- Eq. (27.3-2) for open buildings.

27.3.2 Open Buildings with Monoslope, Pitched, or Troughed Free Roofs. The net design pressure for the MWFRS of open buildings with monoslope, pitched, or troughed free roofs in lb/ft^2 (N/m^2), shall be determined by the following equation:

$$p = q_h G C_N \qquad (27.3\text{-}2)$$

where

q_h = velocity pressure evaluated at mean roof height h using the exposure as defined in Section 26.7.3 that results in the highest wind loads for any wind direction at the site.
G = gust-effect factor from Section 26.11.
C_N = net pressure coefficient determined from Figs. 27.3-4 through 27.3-7.

Figure 20. *Equation to determine wind pressure on open building.*

4.2 Previous Telescope Tower Designs

Operating telescopes atop a tower is not new to astronomy. In 1908, a 60-foot (18 m) tower was built to house Dr. George Hale's first solar telescope and was soon followed by his second in 1912, built atop a 150-foot tower (the tower height is actually 176 ft [54 m] tall), both located at Mt. Wilson, California.

Figure 21. *150-Foot Solar Tower at Mt. Wilson, CA.*

Since then, additional towers for telescopes have been built such as a 15-meter tower for the Dutch Open Telescope (DOT) in La Palma, Spain, a 7.5-meter tower at the South Pole for testing the Advanced Technology Solar Telescope (ATST), a 41-meter tower for the Dunn Solar Telescope (DST) in New Mexico, and a 38-meter tower for the Vacuum Tower Telescope (VTT) in the Canary Islands [9]. The design of these towers and their stability characteristics can be used to derive a successful tower design for the Antarctic.

Note from Figure 21, Figure 22, and Figure 23, that the design of each tower differs dramatically. The 150-Foot Solar Tower has a seemingly simple truss design but is really two towers, with one inside the other (this will be discussed shortly). The 7.5-meter tower at the South Pole and the 15-meter tower for the DOT have an open-air design, similar to the 150-foot solar tower, but involve isosceles triangle supports. Lastly, the 41-meter tower for the Dunn

Solar Telescope and 38-meter tower for the Vacuum Tower Telescope are made up of a concrete-slab outer hull – such structures will not be used for an Antarctic telescope due to the high cost and practicality of creating and transporting concrete in Antarctica compared to steel.

The open-air design of the 150-Foot Solar Tower, 7.5-meter South Pole tower, and 15-meter DOT tower are of particular interest since they reduce wind loading by minimizing the surface area that wind pressure can act upon; in contrast, the 41-meter DST tower and 38-meter VTT tower have large surface areas so are subjected to greater wind forces. This load reduction is confirmed by the ASCE Standards 7-16 as indicated in Section 4.1, which shows that open towers are subjected to lower wind loads compared to closed or semi-closed structures. Additionally, open-towers require less material to construct, offering lower cost compared to a non-open-air design. Therefore, the tower designs considered herein will focus on open-air designs for the tower in Antarctica.

Figure 22. *7.5-meter tower at the South Pole (left). 15-meter tower for DOT at La Palma, Spain (right) [9].*

Figure 23. *41-meter tower for the Dunn Solar Telescope (left), 38-meter tower for the Vacuum Tower Telescope (right).*

4.2.1 The 150-Foot Solar Tower

When the 150-Foot Solar Tower was commissioned in 1912, Hale published notes stating, “there has never been an occasion when it was necessary to stop work because of trembling of the image,” even “when the wind was blowing twenty miles an hour” [10]. This would make it appear that the “classical” open-air tower design could be adapted for a tower in the Antarctic. However, modern measuring techniques show that the image shake can be as great as 10 to 20 arcseconds, significantly greater than the stability requirements for a modern, high-resolution telescope. Although the image instability of the 150-Foot Solar Telescope is beyond what is acceptable, the tower design provides insight that can serve as a basis for future iterations.

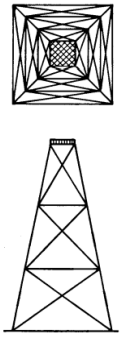

Figure 24. *Classical framework open-air tower [9].*

The classical framework tower, shown in Figure 24, is very stiff against translations of the upper platform but is not sufficiently stiff against rotation [11]. To compensate for this deficiency, the 150-Foot Solar Tower is comprised of an inner and outer tower, so that wind only affects the outer tower. The outer tower is a hollow I-beam structure held together with rivets, and the inner tower is a matching I-beam structure that fits in the cavity created by the outer I-beam (see Figure 25). There is a gap in the floor at the top of the tower to maintain separation of the two towers, with the inner tower and optics inside the circle and the dome and catwalk outside the circle. In principle, when the outer tower rotates, the inner optics remain motionless.

Figure 25. *Highlighting the inner and outer tower of the 150-Foot Solar Tower at Mt. Wilson, CA [12].*

In reality, the inner tower deflects as much as 10 to 20 arcseconds, as per private conversations with Larry Webster, retired site manager of the Mt. Wilson Observatory. This is due to coupling between the outer and inner tower through the underground foundation and the inner tower resonating often due to a very low natural frequency, about 0.5 Hz [11]. Therefore, any tower design for this application should minimize coupling through the foundation of the tower and ensure that the tower's natural frequency is greater than 1 Hz.

4.2.2 The DOT Tower

The DOT tower takes the classical open-air design of the 150-Foot Solar Tower and improves its mechanical stability by two orders of magnitude to 0.2 arcsec. The design principle for the DOT tower involves large angle isosceles triangles to minimize angular deflections and maximize the natural frequency of the tower.

The top platform is in the shape of a rhombus supported by four broad-based isosceles triangles without small angles (top angle is greater than 30°) made up of circular tubes. When 10 m/s winds buffet the platform, translations are 0.1 mm with height differences between the corner points less than 1 μm [9]. This should mean that if the platform is 2 m x 2 m, then the supposed maximum angular displacement is about 0.01 arcseconds but the stability is about 0.2 arcsec. By keeping the tower more than 80% transparent and selecting tubes such that the natural frequency of the tower is greater than 5 Hz, the wind forces acting on the tower are dramatically reduced [9].

The high stability of the 15 m DOT tower suggests that the tower can be simply elongated to meet requirements for a 30 m tower in Antarctica; however, this adversely affects the tower's natural frequency. The equation for determining the natural frequency of transverse vibrations of a round tube is [9]:

$$f_n = \frac{c}{8\pi}\frac{\sqrt{\frac{(D^2 + d^2)E}{\rho}}}{L^2}. \quad (1)$$

Where:

f_n = natural frequency in Hz

c = constant depending on connection of endpoints (both ends pinned, one pinned and one fixed, or both fixed)

E = modulus of elasticity of the material

ρ = material density

D = outside tube diameter

d = inside tube diameter

L = length of the tube

If the length of the tubes is simply increased to 30 m, then the natural frequency of transverse vibrations of the tower supports will be less than 1 Hz and within the peak power spectrum for wind loads. The diameter of the tubes could be increased; however, such a solution may not be practical since the weight and size of these tubes becomes difficult and costly to transport to Antarctica. Instead, the tower can be decomposed into stories that are built separately and integrated together. Doing so would simplify logistics and reduce cost. Dome C has limited construction equipment and heavy machinery to construct a 30 m tower; therefore, a symmetric tower design with consistent beam lengths would consolidate the number of parts, transportation items, and installation equipment required. Hammerschlag et al. 2006 has proposes decomposing the 30-meter tower into 4 stories to reduce individual tube lengths. It looks as follows:

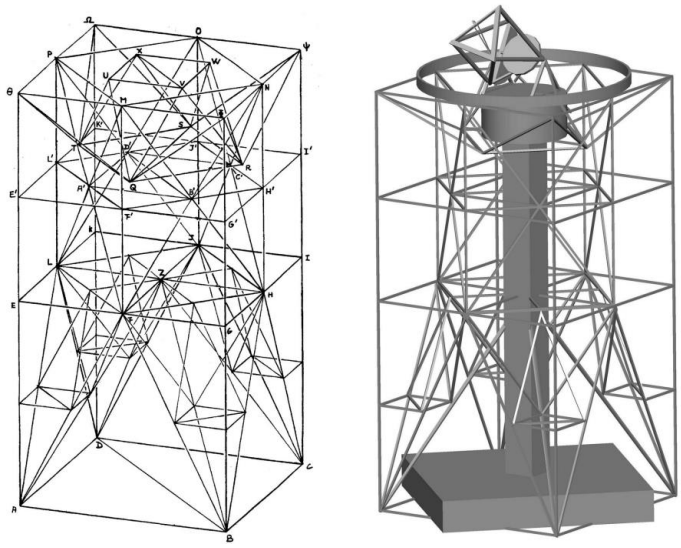

Figure 26. *30-meter tower for Antarctica designed to be separated into 4 stories with a 15 m x 15 m base. Simple framework (left). Rendering with elevator shaft and 2 m telescope primary mirror (right) [11].*

The central gray column is a proposed elevator shaft but has not been yet designed for their 30 m tower but will likely be some sort of lattice design as in the DOT.

The 30 m tower design provided by Hammerschlag (referred as HT going forward) divides the tower into four stories that could be constructed separately before being assembled into the full tower. However, the paper does not provide any assembly procedures accounting for the fact that Dome C has a limited inventory of cranes and a maximum reach of 20 m. One could try hoisting higher stories using a pulley system before resting them on lower stories or jacking up higher modules and then installing the lower module beneath it, but such infrastructure is not included in the design. A tower with modules that can be assembled before arriving to Antarctica and easily interface with their traversing infrastructure should be prioritized to reduce cost and complexity of assembly at Dome C. In addition, simplifications to the tower design could be made to reduce cost by introducing uniformity in beam sizes, thus improving the modularity and assembly of each tower module. The designers of this tower also fail to include how the tower behaves when subjected to an ultimate condition or what that ultimate condition could be, for

example a 72 m/s 3-second wind gust. They have only solved the forced vibration case for 10 m/s sustained winds and have not looked at the free vibration response from an ultimate condition.

Finally, there is no indication of the Hammerschlag tower's natural frequency for different telescope masses. The natural frequency of a fixed-fixed beam decreases for increasing distributed load as show in the equation below:

$$f_n = 3.56\sqrt{\frac{EI}{qL^4}} \qquad (2)$$

where E is the Young's modulus, I is the area-moment of inertia, q is the distributed load, and L is the length of the beam. Simulations in MASTAN2, shown in Section 4.3.4, show that for a 12,000 kg telescope, the tower's natural frequency drops to about 3.3 Hz for the first two modes, less than the 4.3 Hz and 5.9 Hz as discussed in ref. 42.

4.3 Telescope Tower for Antarctica

The open-air tower concept provides advantages in stability, cost, and assembly compared to closed towers that make it a competitive design option for a 30 m Antarctic tower at Dome C. The 150-Foot Solar Tower and DOT Tower are two examples of open-air towers designed specifically for telescopes, but many other open-air tower designs exist in the form of transmission towers, masts, and other structures that fall under the category of "lattice towers." The factors that define their performance vary but those most important to us are the stability, natural frequency, and mass, which are influenced by the geometry of the lattice and the beam cross-section. Many beam options exist, as illustrated in Figure 27. To constrain the design problem, this analysis focuses on the geometry of the lattice using a similar carbon steel round Hollow Structural Section (HSS) as in the 15 m DOT tower and the proposed Hammerschlag 30 m Antarctic tower, referred to HT from now on. The motivation to use round HSS is also

influenced by their good torsional stiffness and natural frequency characteristics that make them well suited for a tower that should minimize angular displacements while maintaining a large natural frequency.

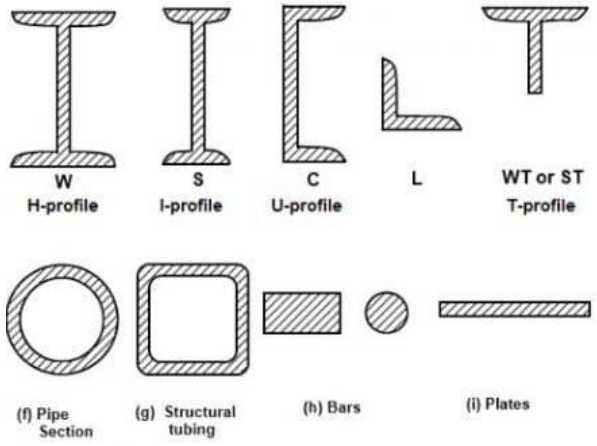

Figure 27. *Various standard steel beam types [14].*

4.3.1 Triangles and Tetrahedra

The DOT tower and proposed HT utilize the structural advantage of triangles over other polygons. In Hammerschlag et al. 2006, they highlight the importance of large angle (greater than 30°) isosceles triangles and design their towers around this principle. The benefit of large angle isosceles triangles is confirmed by analyzing the forces within the members of a simply supported isosceles truss structure as shown in Figure 29. When the top angle is increased, the internal forces within the angled members decrease and are distributed to the horizontal member. This is important since the deflection of a beam is governed by the force acting on it as show in the equation:

$$\delta = \frac{PL}{AE} \tag{3}$$

where P is the force acting on the beam, L is the length of the beam, A is the area of the beam's cross section, and E is the Young's modulus of the material the beam is made of. Since either

vertical member will be in compression and tension, the resulting deflection is angular. Increasing the top angle increases the internal force on the horizontal member which increases the horizontal displacement thereby reducing the angular displacement. Horizontal displacements are tolerable since the telescope is only sensitive to angular displacements. Therefore, the tower structure should incorporate this compensating geometry.

However, increasing the top angle of the triangle reduces its height, increasing the number of triangles and material needed to scale the necessary height, and increases the length of the angled members, which increases their deflection. Therefore, the top angle should be within the range of 30° to 60° to maintain a balance between rigidity and material cost.

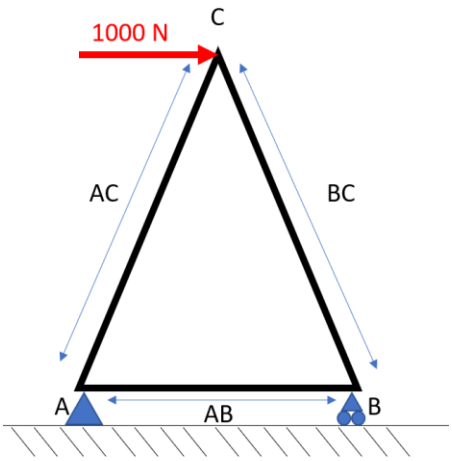

Figure 28. *Simply supported triangle truss structure.*

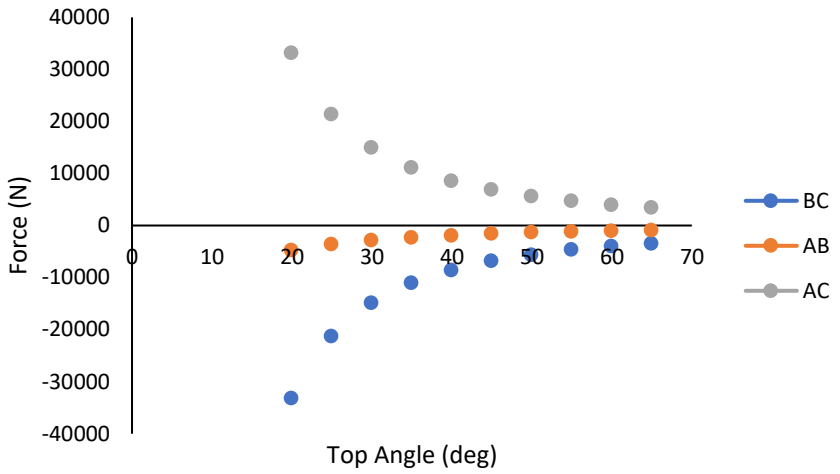

Figure 29. *Results showing effect of top angle on internal forces in the three members. Positive implies tension and negative, compression.*

To bring the benefits of a two-dimensional triangle to three-dimensional space there are many design possibilities. The DOT tower does so by bringing together four such triangles to form a kind of pyramid (square base to a rhombus top). HT builds upon this principle but requires additional bracing and design to maintain the compensating mechanism. Both structures contain multiple tetrahedra, many of which are irregular.

Tetrahedra are common in the design of spaceframes and other lattice structures, and they are ever present in nature. Various tetrahedral geometries can be built into modular cubes that can be combined to create larger tetrahedra and other advantageous polyhedrons, such as octahedrons. For example, a module consisting of a 3-orthoscheme, combined with a trirectangular tetrahedron, can be brought together with four similar modules to form a demihypercube which forms a large tetrahedral structure – providing rigidity to the single module and to the whole four-module unit. Therefore, a 30 m tower for the Antarctic should leverage the stability and modularity benefits of tetrahedra in its design.

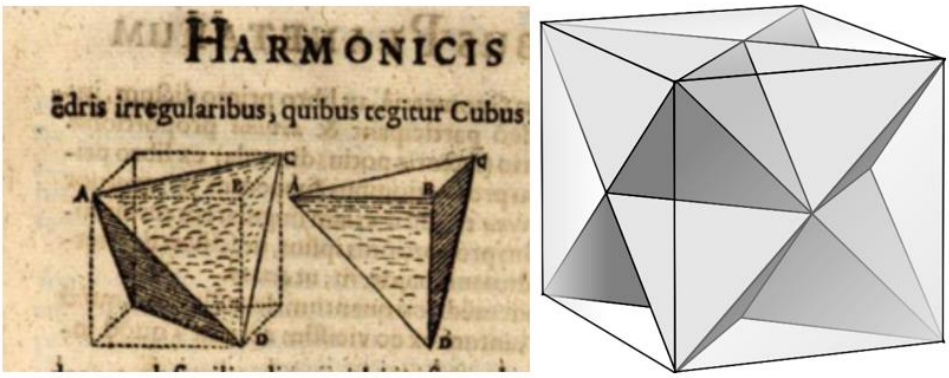

Figure 30. *Trirectangular tetrahedron (left). Demihypercube (right) [15][16].*

4.3.2 Tower Evaluation & Simulation Setup

In order to offer a competitive design to HT, new tower designs should possess similar or better stability when subjected to 10 m/s sustained winds, while offering reduced cost and easier assembly. Stability is evaluated based on minimizing telescope base rotation and tilt caused by differential vertical deflection of the tower's top nodes for 10 m/s wind loads, maximizing natural frequency for the first bending and torsional modes beyond 1 Hz to avoid the peak spectral density of horizontal wind frequencies, and survival of the ultimate condition of a 72 m/s 3-s wind gust. The deflection from the sustained winds and wind gusts are used in Section 5 to build the forced vibration and free vibration models for evaluating coupling through the bearings. Although a general assembly procedure was not proposed for HT, assembly can still be evaluated by considering how tower segments will be transported and constructed by ensuring the constraints for constructing each tower are the same (i.e., availability of machinery and personnel).

Analyses of each tower were conducted in MASTAN2, a MATLAB structural analysis program that provides linear and nonlinear analysis routines based on the text: *Matrix Structural Analysis,* 2nd Edition, by McGuire, Gallagher, and Ziemian. MASTAN2 was selected over FEA software, like Ansys, because it provides rapid, broad-stroke results that are sufficient for comparing performance without becoming mired in granular details. Future work, however, must

include additional analysis into specific aspects of the tower's designs, such as comparing the stress distribution for steel joint and connection designs.

HT was modeled in MASTAN2 first to establish a baseline of which future designs would be compared against. Below is a diagram of the tower from the paper and how it appears in MASTAN2. While they provide details for the tubes in their design, they do not match standardized round HSS dimensions, so nominal section properties for the closest standardized size were taken from *Hollow Structural Sections: Dimensions and Section Properties*, by the Steel Tube Institute of North America. Structural carbon steel is the building material for all the structures discussed here, and their material properties are defined according to *ASTM A36/A36M-08 Standard Specification for Carbon Structural Steel*. The basic characteristics of HT are provided in the table below:

Table 3. Characteristics of HT.

Tower	Structural Details	Weight (tonnes)	Estimated Cost ($)
HT	15 m x 15 m base, 30m tall. Beams are round HSS of 9.625" x 0.375", tetrahedra leg supports extending halfway up the tower height (15 m). Decomposed into four sections that are 15 m x 15 m x 7.5 m	70.8	105,678

The cost listed is only the material and shipping cost and does not include assembly cost, so it is an underestimate of the actual cost of each tower. The number presented is determined from the cost per kilogram of 1020 steel ($0.50/kg) and cost of hauling cargo by ship from Port Hueneme, CA to the South Pole ($0.20/kg) via the United States Antarctic Program since there is no available information online on the cost of shipping to Dome C [17][18].

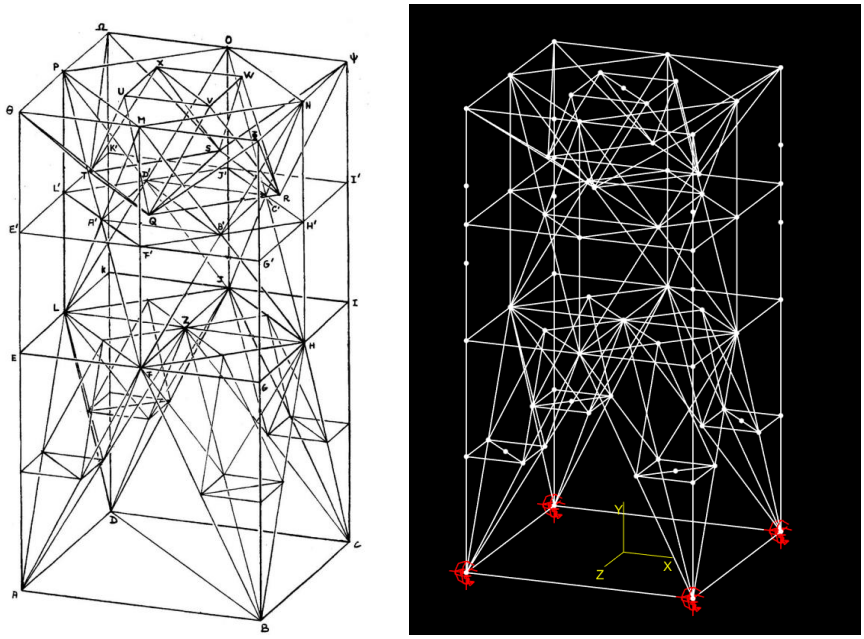

Figure 31. *(left) Two-story tower taken from Hammerschlag et al. 2006, (right) same tower but in MASTAN2.*

A second-order, inelastic analysis is performed to determine the deflection of the nodes at the top of the tower, and these results are fed into an eigenvalue analysis to determine the first thirty natural frequencies for each tower. The natural frequencies are compared between the dead load of the tower elements and the inclusion of a live load simulating different telescope masses atop the tower (between 0 kg and 12,000 kg). For this reason, a second-order, inelastic analysis was performed – to account for the geometric, elastic, and material factors that influence the response of the structure. The deflection of each node at the top of the tower is then compared when no wind loading is applied for a tower with a 12,000 kg telescope against deflection due to wind generated pressure for 10 m/s sustained winds and 72 m/s 3-s wind gusts. These pressures were determined using ASCE Standards 7-16 in Section 4.1 and are multiplied by the diameter of the beam element to convert the pressure (N/m^2) into a distributed load (N/m). This distributed load is applied to members that are in direct confrontation with the wind, not including vortex shedding.

The distributed load should be a function of tower height since the velocity pressure exposure coefficient increases with height, see Figure 17, but MASTAN2 cannot apply triangular distributed loads, so the distributed loads are uniform and are from the 30 m height calculations. This approach overestimates the wind load since velocity pressure exposure coefficient is greater for 30 m than for lower heights, see Figure 17.

At the time of writing this essay, it is not clear whether a dome or enclosure will be mounted atop the tower and the telescope housed within during observations. Should a dome be included, and the telescope would be observing while the dome is deployed, then additional analysis is required to account for the wind loading transmitted to the tower from the added surface area of the dome and the impact of the mass of the dome on the natural frequency of the tower.

4.3.3 Tower Designs & Assembly

4.3.3.1 Tower Designs

Using the large angle isosceles triangle design philosophy with tetrahedra and incorporating a modularity requirement and construction limitations to the design problem, six tower designs were created and are compared against the characteristics of HT. These towers, T1, T2, T3, T4, T5, and T6 are workable solutions with different weighting allocated to performance, cost, and ease of construction.

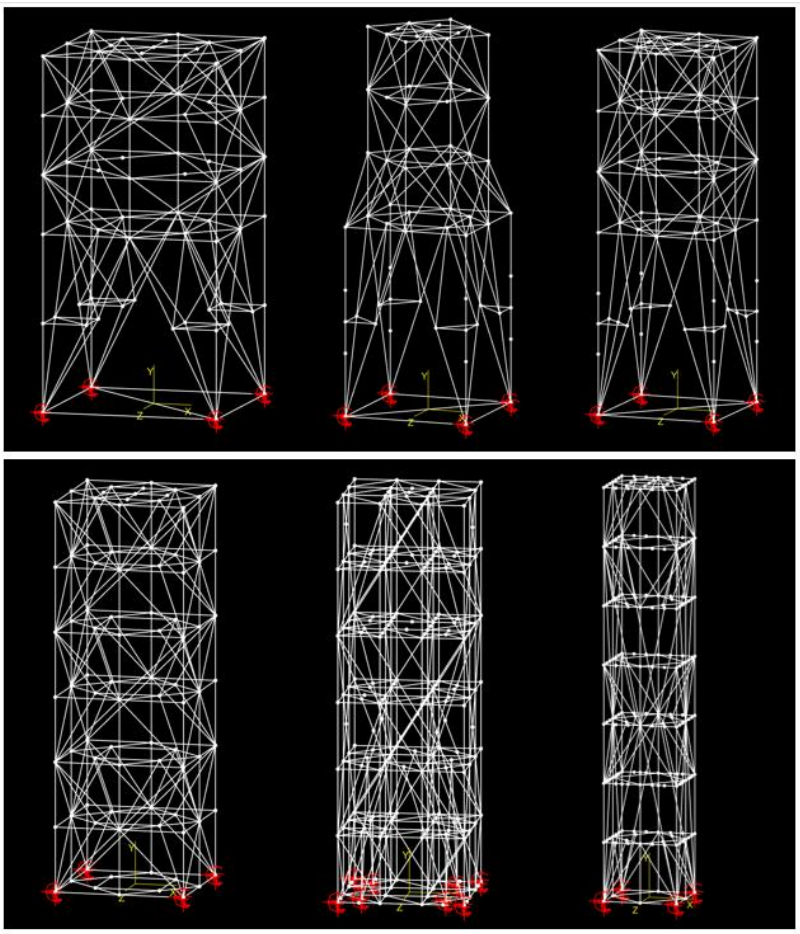

Figure 32. *Top to bottom, left to right: T1, T2, T3, T4, T5, T6.*

Table 4. Characteristics of proposed towers.

Tower	Structural Details	Weight (tonnes)	Estimated Cost ($)
T1	Closely follows HT design. 15 m x 15 m base, 30 m tall. Beams are the same round HSS at HT (9.625" x 0.375"), with tetrahedra leg supports extending halfway up the tower height (15 m). Implements tetrahedra geometry to maximize torsional and lateral stiffness. Top half made up of three levels, each 15 m x 15 m x 5 m and comprised of four modules with dimensions 7.5 m x 7.5 m x 5 m. The bottom half is comprised of two levels, each 15 m x 15 m x 7.5 m and comprised of four modules with dimensions 7.5 m x 7.5 m x 7.5 m. Height-width aspect ratio of 2.	78.0	116,327

T2	A slimmed version of T1. Prioritizes cost. 10 m x 10 m base, 30 m tall. Same round HSS. Top half made up of three levels, each with dimensions of 7 m x 7 m x 5 m and comprised of four modules with dimensions 3.5 m x 3.5 m x 5 m. The bottom half is comprised of two levels, each 10 m x 10 m x 7.5 m and comprised of four modules with dimensions 5 m x 5 m x 7.5 m. Height-width aspect ratio of 3.	46.0	68,584
T3	A balance of T1 and T2 between cost and performance. 10 m x 10 m base, 30 m tall. Same round HSS. Top half made up of three levels, each with dimensions of 10 m x 10 m x 5 m and comprised of four modules with dimensions 5 m x 5 m x 5 m. The bottom half is comprised of two levels, each 10 m x 10 m x 7.5 m and comprised of four modules with dimensions 5 m x 5 m x 7.5 m. Height-width aspect ratio of 3.	59.9	89,379
T4	Maximizes natural frequency and modularity. Forgoes tetrahedra legs for repeating tetrahedra sections. 10 m x 10 m base, 30 m tall. Same round HSS. Comprised of six levels, each 10 m x 10 m x 5 m and made up of four modules with dimensions 5 m x 5 m x 5 m. Height-width aspect ratio of 3.	77.1	115,122
T5	The second most modular design. A near 80% reduction of T3 with a 7.5 m x 7.5 m base, 24 m tall. Round HSS size decreased by 20% to 7.625 in x 0.328 in. Repeating tetrahedra sections. Comprised of six levels, each 7.5 m x 7.5 m x 4 m and made up of eight modules with dimensions 2.5 m x 2.5 m x 4 m. Module dimensions closely resemble shipping container width x height dimensions. Height-width aspect ratio of 3.2.	57.0	85,023
T6	The most modular design. Similar to T5 but with a 5 m x 5 m base, 28 m tall. Same round HSS as T1-T4, Modules are 2.5 m x 2.5 m x 4 m, with four modules per level with a total of seven levels. Height-width aspect ratio of 5.6.	53.9	80,442

A noticeable difference in the tower designs is their width. T2, T3, and T4 are no more than 10 m x 10 m wide, T5 is 7.5 m x 7.5 m wide, and T6 is 5 m x 5 m wide compared to the 15 m x 15 m width of HT and T1. Narrower tower designs than HT were created in order to

simplify the logistics of transportation and assembly, to increase the natural frequency of the individual beams through shorter strut length, and to determine the impact of smaller widths on tower mass and stability. Recall equation 1:

$$v_m = \frac{c}{8\pi}\frac{\sqrt{\frac{(D^2 + d^2)E}{\rho}}}{L^2} \quad (1)$$

The transverse vibration of a 15 m tube with fixed ends is 6.6 Hz but if its weight is considered, from equation 2:

$$f_n = 3.56\sqrt{\frac{EI}{qL^4}} \quad (2)$$

then the natural frequency for the same 15 m tube is 2.1 Hz. Although still greater than 1 Hz, the natural frequency of individual beams is of particular importance because of the possibility of resonance due to vortex shedding. When wind flows over a cylindrical member, vortices form which create oscillatory transverse forces on that member. The equation for determining the frequency of these oscillations is as follows:

$$f_v = \frac{sv}{D} \quad (3)$$

Where *v* is the wind velocity, *D* is the diameter of the cylindrical member, and *s* is the Strouhal number, which is about 0.2 for round tubes. If this frequency coincides with a modal frequency of the member, then troublesome vibrations can occur. Using the above equation, the wind velocity that resonates the 9.625 in x 0.375 in tubes of the HT tower due to vortex shedding can be determined, which is 2.6 m/s from its 2.1 Hz the natural frequency. This result is well within the maximum operating condition of 10 m/s wind speed and is of grave concern since a resonating tower will be inherently unstable and hurt the telescope's performance. For this reason, beam lengths are less than 7.6 m, with most being between 3 m to 5 m. This ensures that the natural frequencies of the beams are large enough that vortex induced vibrations occur at

wind velocities beyond 10 m/s. Should beam lengths need to be longer than 7.6 m, some countermeasures may be required. Peter Gillingham of the PILOT Telescope, per private conversations, suggests that deploying mechanical dampers and helical fences near the midpoint of the members could increase the natural frequency of longer beams so as to avoid resonance from vortex shedding. Additional analysis into this area should be pursued should a large tower design be selected.

The tetrahedra design philosophy is reliant on maintaining stiff members and stiff nodes. Although, this essay does not provide analysis on specific joint designs, Figure 33 is meant to demonstrate feasibility by showing joining methods for structural joints. Methods include weldments and rivets or other fasteners directly to adjoining beams or to intermediate plates and blocks that serve as a hub for connections.

Figure 33. *Examples of structural joints.*

4.3.3.2 Tower Assembly

Dome C has limited heavy equipment, for example the largest crane there has a maximum reach of only 20 m, and cargo transportation, which is mainly via land on winterized

tractors four times out of the year from the Antarctic coast, see Figure 34. With this in mind, all six tower designs were created to be modular, allowing tower construction to be completed in segments and to simplify transportation to Dome C. Figure 36 through Figure 38 breaks down the modules for a few tower designs and

Table **5** and Figure 39 through Figure 42 describes their dimensions and shipping.

Figure 34. *Traversal tractors and trailers to get to Dome C [43].*

The design of T5 and T6 are such that each module keeps within the width and height of a standard shipping container so they could readily integrate with existing traversal gear and transportation infrastructure but at the cost of stability. The modules for T1, bottom half of T2, T3, T4, and T5 are much wider (5 m wide) than the widths of flatbed truck trailers, which are about 2.5 m wide. In the United States, truck loads with widths beyond 2.5 m constitute an oversized load and will require state permits to travel on public highways with the possible requirement of escort vehicles and limited permitted travel times and routes. Any load beyond 5 m wide becomes a "superload" and would be subject to more requirements [44]. Additionally, transportation from the factory to the port may be limited due to height restrictions for hauling cargo under overpasses and bridges. This could be circumvented by transporting struts for modules to the port and constructing the modules at the port before loading onto the ship, but this is rather obtuse. Therefore, transportation of the modules to a port for the aforementioned towers would be more difficult and require more oversight and approval than T5 or T6. Unloading these larger-than-container-sized modules may also pose a challenge since unloading is done by cranes on the transport vessel, rather than port cranes, which support container-sized loads, see Figure 35 below. These wider modules would also require new traversal infrastructure so they can be hauled by the tractors. T5 and T6 avoid these complex logistical challenges of transporting oversized loads by utilizing shipping container-sized modules.

Figure 35. *Photos of MV American Tern, a container ship that carries cargo to McMurdo Station, Antarctica [46].*

Additional motivation to modularize the towers comes from the foreseen difficulty of erecting a tower in subfreezing temperatures and with limited cargo space for transportation. I expect that it would be rather difficult to assemble a large construction crew that will fasten together tubing by hand while wearing mittens, whereby touching metal with a bare hand would leave the person stuck to it! Instead, modules would arrive at Dome C preassembled and would only have to be fastened to their sister modules to complete the level. There are a few ways this could be done. One way would be to use the 20 m crane available at Dome C whereby up to 15 m of tower could be erected, building from the bottom up. A larger crane could be brought to Dome C to complete the construction, or each level could be jacked up by hydraulic jacks one level at a time and additional modules assembled underneath. Although it may appear unconventional, this construction method has already seen applications in constructing high-rise buildings [45]. Another benefit of the jacking method is that the assembly process only occurs at the base of the tower, as opposed to construction crews assembling the tower 10 m, 15 m, 20 m, etc. above the ground in subfreezing temperatures. See Figure 43 for how the first four levels can be constructed using the jacking method. The jacking system would provide the means of erecting the tower without being limited by the 20 m crane and allow for progressive, yearly

assembly of the tower while modules are shipped to Dome C. Only four modules would be required to construct one level of the tower, except for T5 which requires eight modules, so an entire traverse does not have to be dedicated to simply hauling the tower. This means that the tower can be built over a few years, one level at a time.

Since both the crane and jacking method are based in hydraulics, they require hydraulic fluid capable of working in the Antarctic climate. Heaters are probably not required since assembly of the towers will occur in summer when ambient temperatures are above -35°C and common low temperature hydraulic oil is rated to -50°C and specialized oils are rated for -78°C [19][20].

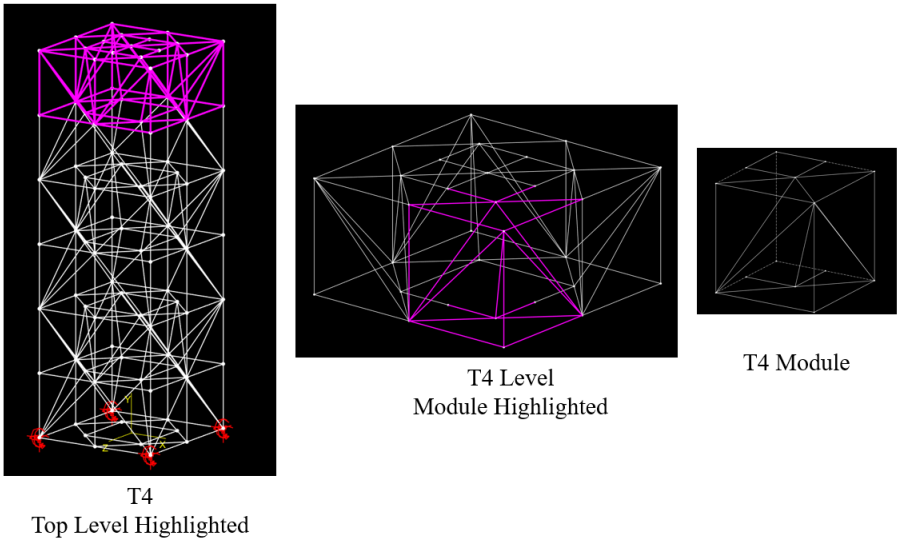

Figure 36. *Breakdown of T4 individual level and module.*

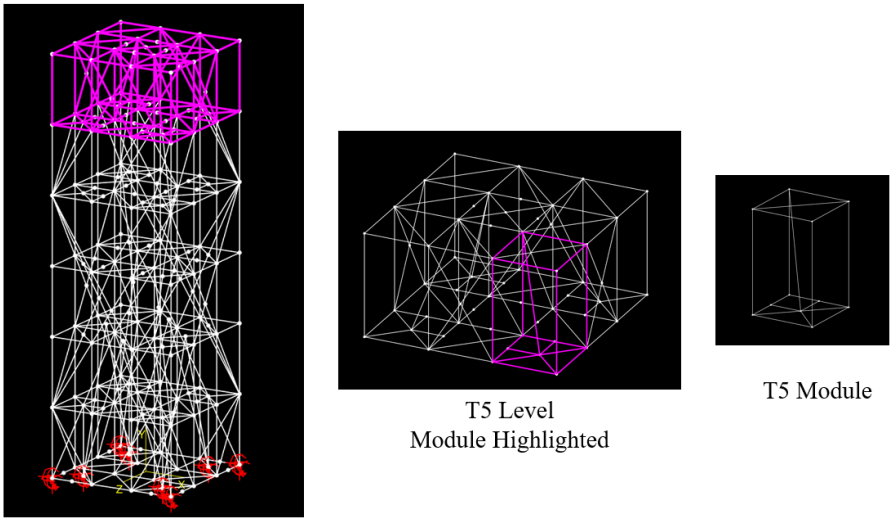

Figure 37. *Breakdown of T5 individual level and module.*

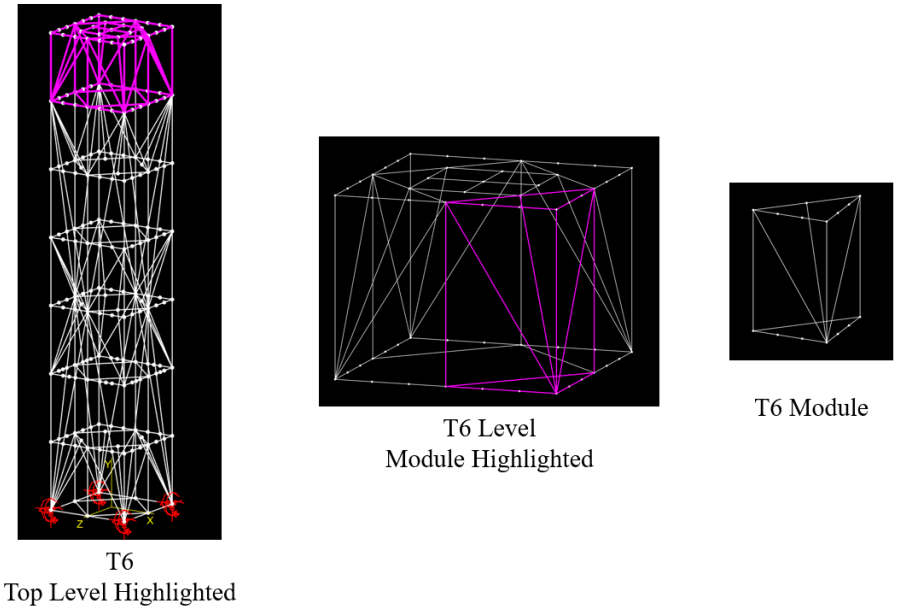

Figure 38. *Breakdown of T6 individual level and module.*

T1-T4 Module Dimensions

Truss design viewed from top. Comprised of four square modules, with square opening in center for elevator.

Height of each module can be up to 20’ if placing to standard 20’ length container volume but thus is becoming a bit unwieldy for jacking system. Two modules each 5m tall fit nicely onto a 40’ long truck trailer bed.

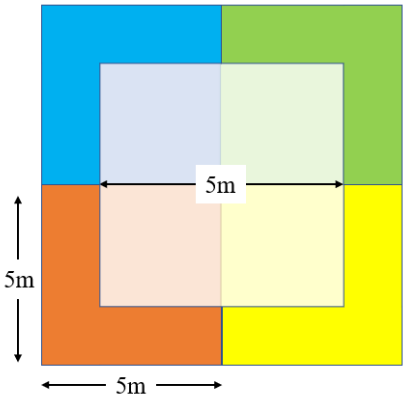

Figure 39. *General description of module sizes of T1-T4 from top view.*

T5 Module Dimensions

Truss design viewed from top. Comprised of eight square modules, with square opening in center for elevator.

Height of each module can be up to 20’ if placing to standard 20’ length container volume but this is becoming a bit unwieldy for jacking system. Three modules each 4m tall fit nicely into a 40’ long container volume.

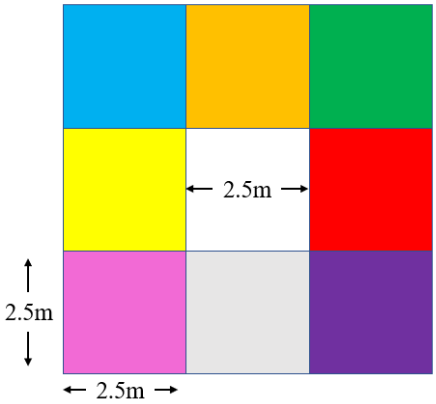

Figure 40. *General description of module sizes of T5 from top view.*

T6 Module Dimensions

Truss design viewed from top is approximately four 45 deg right triangles, with square opening in center for elevator.

Note flats at apexes to allow sections for be bolted together.

Height of each module can be up to 20' if placing to standard 20' length container volume but this is becoming a bit unwieldy for jacking system. Three modules each 4m tall fit nicely into a 40' long container volume.

Tower can be 7*4m tall for aspect ratio height:width = 5.8:1.

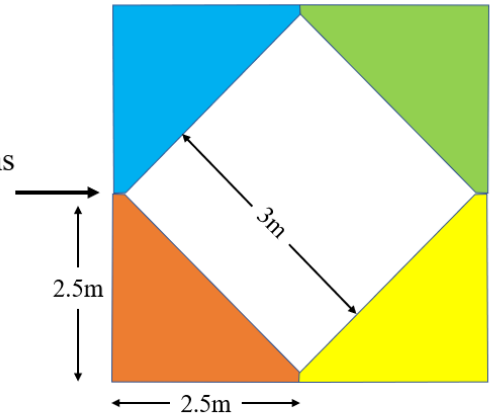

By the time area is allocated to counterweights, rails and cables, the elevator platform will be closer to about 2.5 wide, which is ok.

Figure 41. *General description of module sizes of T6 from top view.*

T5 &T6 Module Shipping

- Shipping containers: 8' wide, 8.5' high (standard) or to 9.5' (tall), length = 10', 20', 40'.
- If total tower width is ~5m, can pack modules into shipping container volume thus:

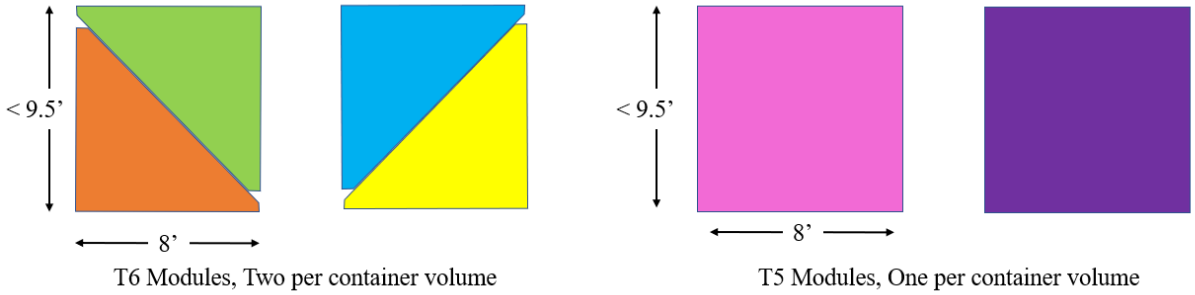

T6 Modules, Two per container volume

T5 Modules, One per container volume

Figure 42. *General dimensions of how T5 and T6 modules fit with shipping container standard width and height.*

Table 5. Breakdown of tower modules for cargo shipment.

Tower	Module Dimensions (meters)	Est. Module Mass (tonnes)	Cargo Container Size (Width x Height)			Total Containers Required (40ft length)	Modules per Level
			Standard	Oversized	Supersized		
HT	7.5 x 7.5 x 7.5	5.6	0	0	20	20	4
T1	7.5 x 7.5 x 5	5.2	0	0	12	20	4
	7.5 x 7.5 x 7.5	5.6	0	0	8		
T2	5 x 5 x 7.5	3.0	0	0	8	20	4
	3.5 x 3.5 x 5	2.8	0	12	0		
T3	5 x 5 x 5	5.1	0	0	10	20	4
	5 x 5 x 7.5	3.0	0	0	10		
T4	5 x 5 x 5	5.1	0	0	24	24	4
T5	2.5 x 2.5 x 4	2.7	48	0	0	24	8
T6	**2.5 x 2.5 x 4**	**2.3**	**28**	**0**	**0**	**7 (4 per)**	**4**

Modules with dimensions larger than 5 m could be decomposed into smaller modules but doing so trades simpler transportation with increased construction costs.

1. Assemble platform

Bolt together platform to provide wide base.

2. Install hydraulic cylinders

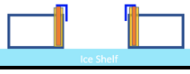

3. 1st Tower level

Assemble tower level from 4 prefabricated modules

Roll on rails into gap in platform.

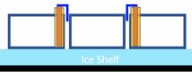

4. Install dome

With crane

Could install telescope and stop here for first observing season

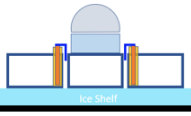

5. Lift

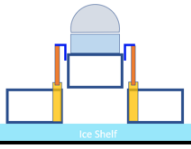

6. Position next level

Assemble next level and roll under tower

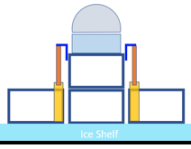

7. Lower and join

Rest tower on new level and join

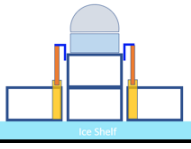

8. Retract

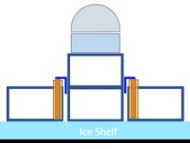

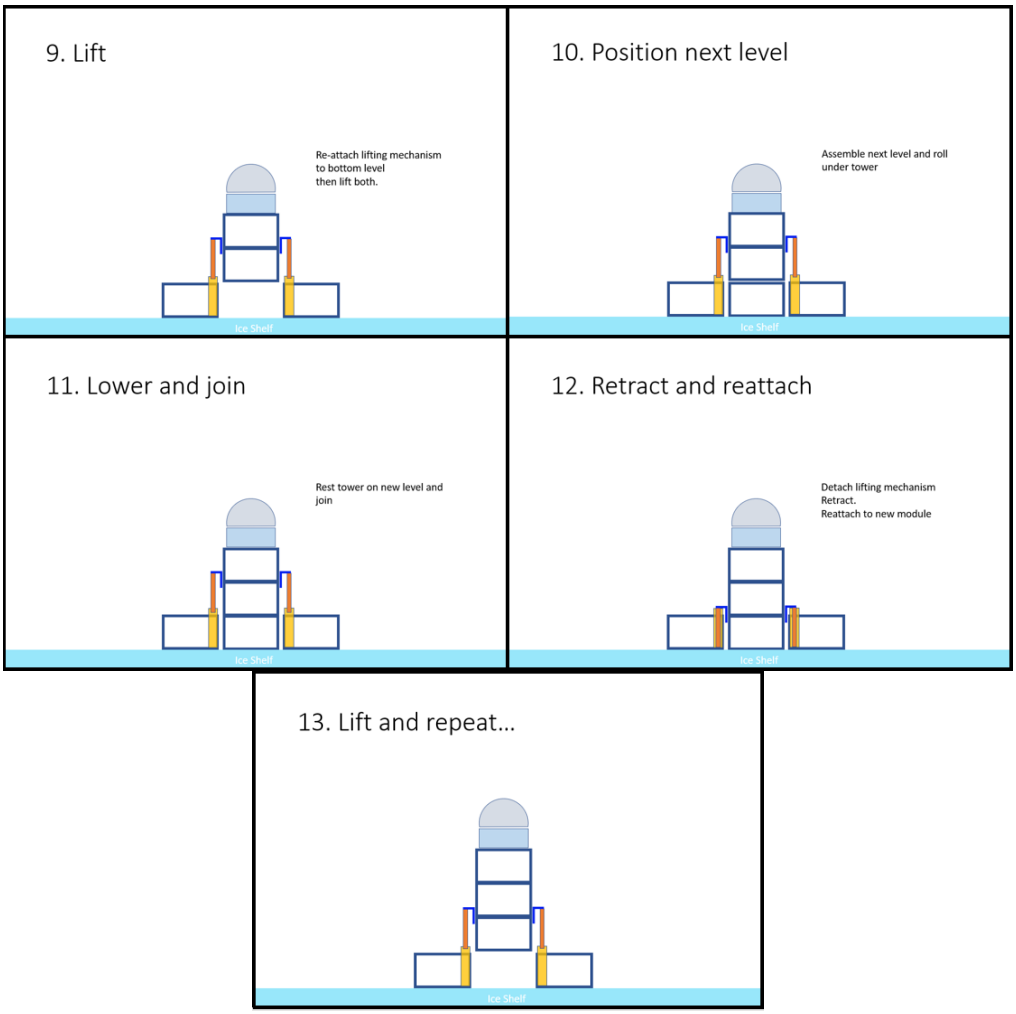

Figure 43. *How tower would be erected using the jacking method described. This procedure can be repeated for the full 30 m. Provided by Roger Smith.*

4.3.4 Simulation Results

Simulation results show that each of the six proposed tower designs and HT optimize for different parameters, such as tilt and base rotation, mass, and natural frequency. Tilt refers to the angular displacement caused by differential vertical deflection of the top nodes, causing the telescope base to "tilt" as in Figure 44. Base rotation refers to the rotation of the top of the tower about its vertical axis, creating a twisting motion as in Figure 44. The operating condition is that the tower should have less than 0.1 arcsec of angular displacement (tilt and base rotation) for a maximum sustained wind speed of 10 m/s and each tower should survive the ultimate condition of a 72 m/s 3-sec wind gust.

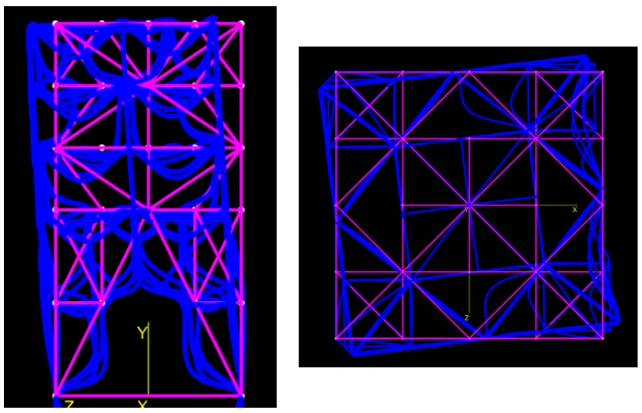

Figure 44. *Exaggerated tower tilt (left) and exaggerated based rotation from top view (right).*

Surprisingly, the HT tower deflects the second most when subjected to 10 m/s winds but maintains the third highest torsional mode behind T5 and T4 as shown in Figure 45. T1 maintains the lowest deflections but has the most mass and has intermediate modes of vibration with 2.53 Hz and 6.21 Hz for the first mode and torsional mode, respectively. T2 is the lowest mass design, being 41% lighter than T1 and 35% lighter than HT, while offering less deflection than HT and a higher first mode than both but at the cost of a lower torsional vibration mode. All vibration modes are greater than 2 Hz, providing a frequency ratio greater than 20 at 1σ for horizontal wind frequencies, but the first mode for each tower varies for different telescope

masses. Figure 51 shows some tower designs are more sensitive than others to changes in telescope mass. For example, T2 has the second lowest natural frequency for a 600 kg telescope, but it has the second greatest natural frequency for a 12,000 kg telescope and with the least variance compared to the other tower designs.

Table 6. Mass & natural frequency of tower designs.

Tower	Mass (tonnes)	First Mode Frequency for 0 kg (Hz)	Torsional Mode Frequency for 0 kg (Hz)	First Mode Frequency with 12000 kg Telescope (Hz)	Torsional Mode Frequency with 12000 kg Telescope (Hz)
HT	70.8	4.93	6.45	2.45	6.45
T1	78.0	4.57	6.21	2.53	6.21
T2	46.0	4.13	5.56	3.61	5.56
T3	59.9	3.89	4.85	3.38	4.85
T4	66.2	4.35	9.43	3.52	9.43
T5	57.0	5.06	7.76	3.90	7.76
T6	53.9	3.49	5.30	2.67	5.30

Table 7. Stability of tower designs.

Tower	Operating Condition		Survival Condition	
	Max Tilt (arcsec)	Max Field Rotation (arcsec)	Max Tilt (arcsec)	Max Field Rotation (arcsec)
HT	0.550	0.056	11.441	3.008
T1	0.078	0.072	6.600	3.424
T2	0.413	0.014	21.518	0.737
T3	0.110	0.016	5.445	0.889
T4	0.413	0.014	27.392	0.979
T5	0.330	0.004	22.937	0.349
T6	0.660	0.016	36.633	0.570

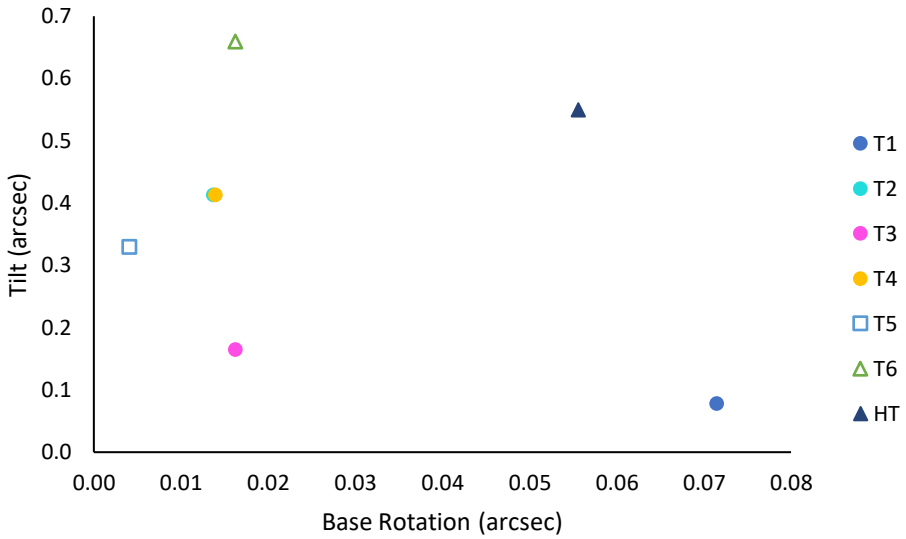

Figure 45. *Plot of maximum tilt and field rotation for each tower at maximum operating condition.*

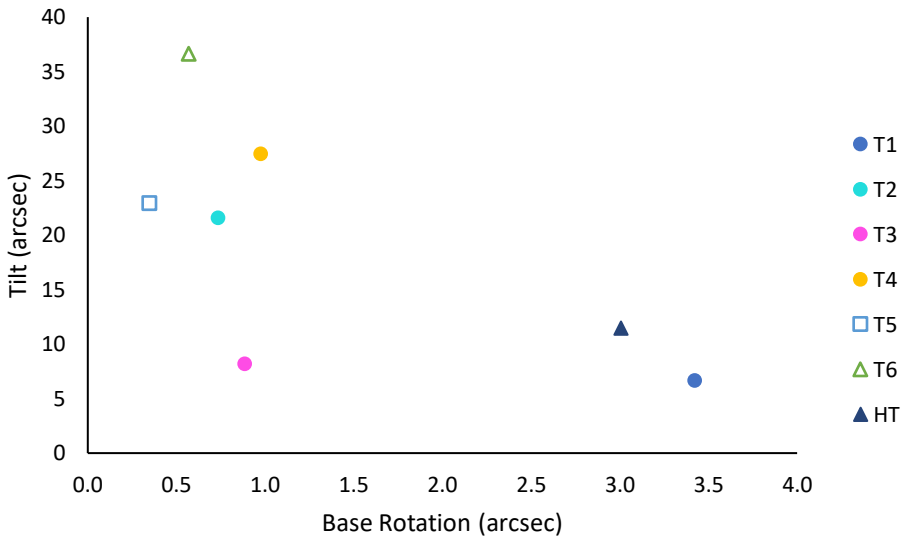

Figure 46. *Plot of maximum tilt and field rotation for each tower during survival condition.*

Since base rotation at the maximum operating condition for all towers is less than 0.1 arcsec, towers should be assessed by other performance factors, like natural frequency and mass. See below:

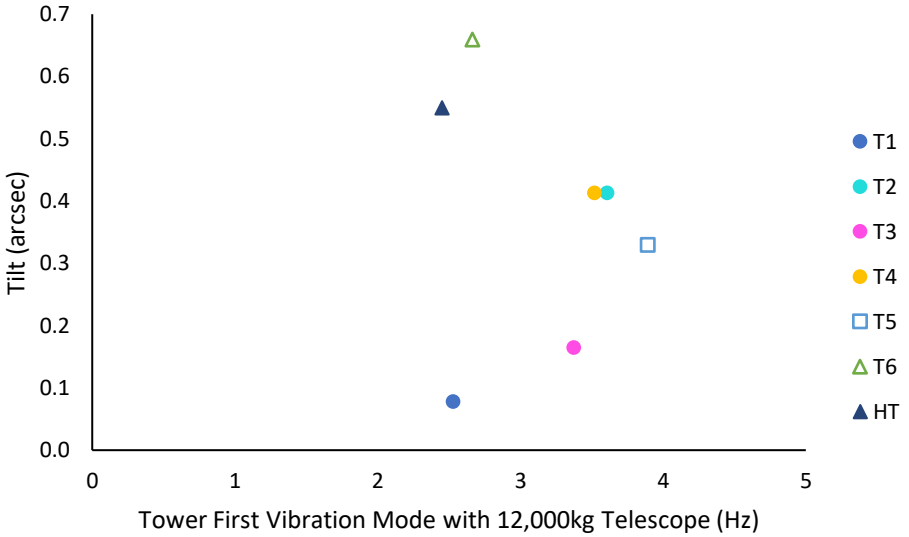

Figure 47. *Plot of each tower's maximum tilt against first vibration mode.*

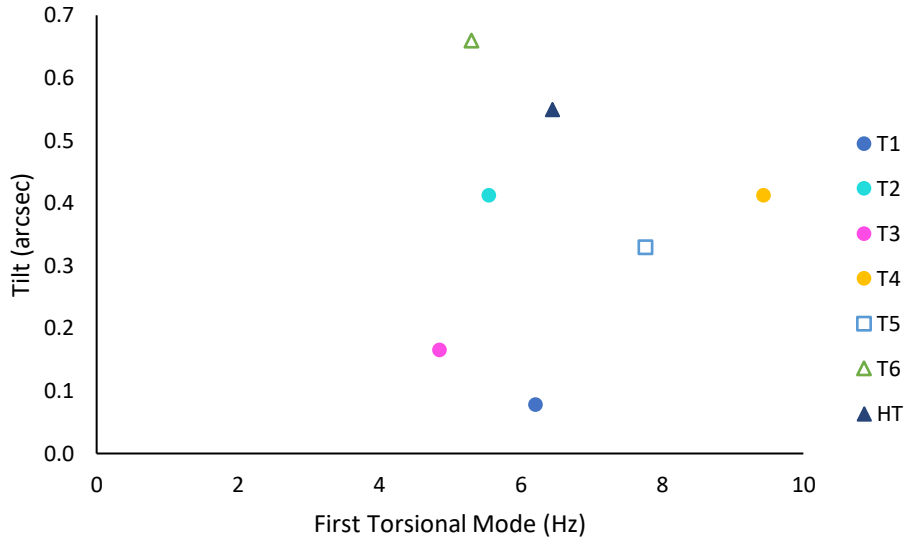

Figure 48. *Plot of each tower's maximum tilt against first torsional vibration mode.*

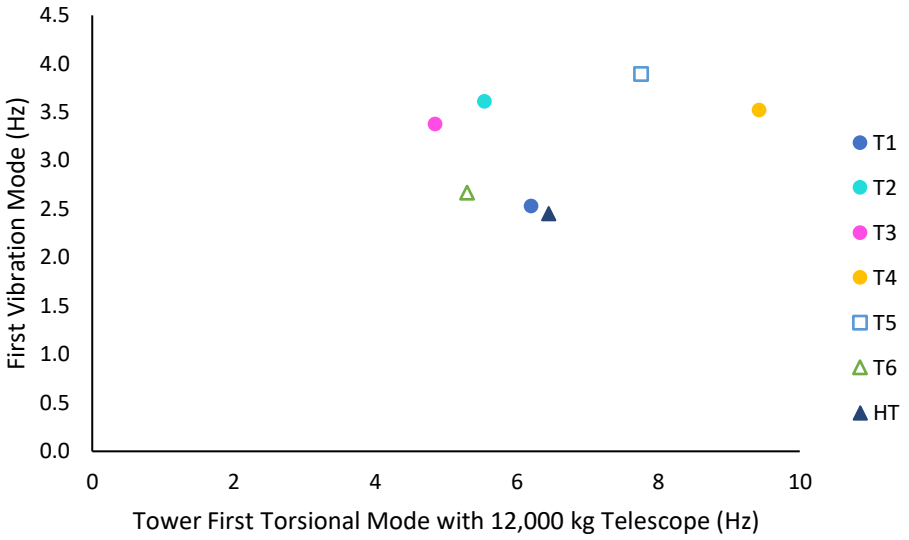

Figure 49. *Plot of each tower's first vibration mode against its first torsional vibration mode.*

The first vibration mode and first torsional mode vary from tower to tower, but all provide a frequency ratio greater than 20 and 40, respectively, at 1σ for horizontal wind frequencies. It becomes easier to differentiate and rank the towers when tower mass is plotted against tilt and natural frequency against increasing telescope masses.

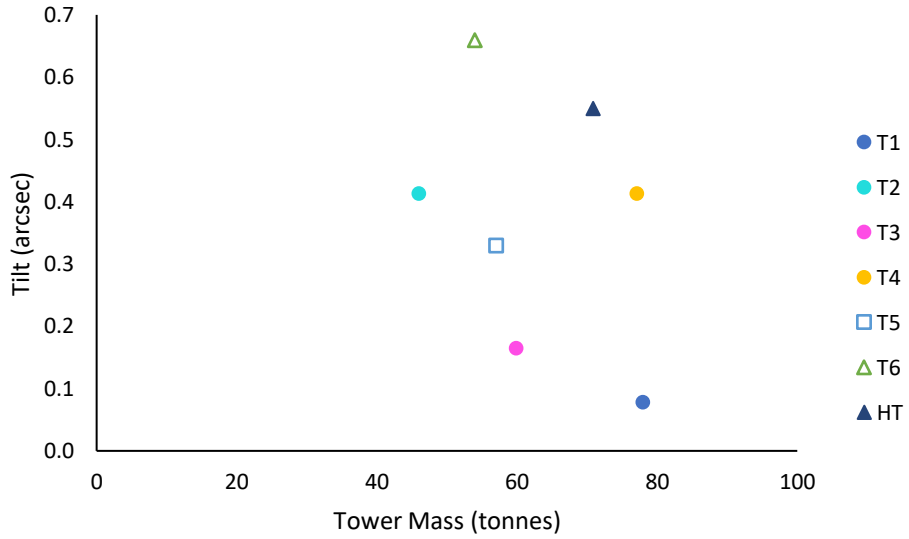

Figure 50. *Plot of each tower's maximum tilt against their mass.*

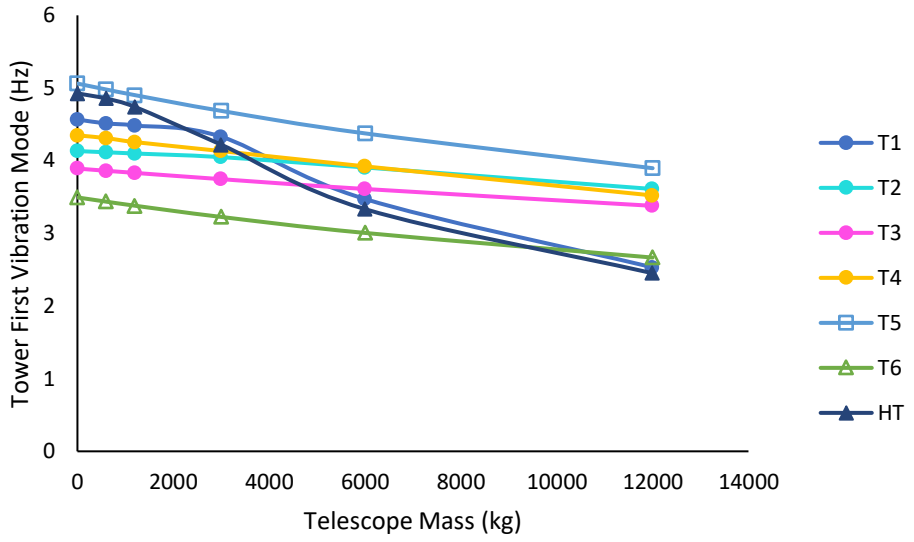

Figure 51. *Plot of each tower's first vibration mode against telescope mass.*

Additional simulations were conducted on T4 to identify the scaling law on key parameters, such as mass, first vibration mode, torsional mode, tilt, and field rotation. T4 was chosen since its modules are the same repetition of tetrahedra. Two cases are compared to T4, one where beam lengths and diameter are scaled to 80% the original size and the other to 60%. The results are presented in the tables and plots below.

Table 8. First Vibration Mode for T4 and 80% and 60% scaled towers for different telescope masses.

Telescope Mass (kg)	T4 (Hz)	Scaled 80% (Hz)	Ratio	Scaled 60% (Hz)	Ratio
0	4.35	5.47	1.26	7.30	1.68
600	4.31	5.36	1.24	6.94	1.61
1200	4.26	5.25	1.23	6.61	1.55
3000	4.13	4.93	1.19	5.76	1.39
6000	3.92	4.46	1.14	4.79	1.22
12000	3.52	3.78	1.07	3.66	1.04

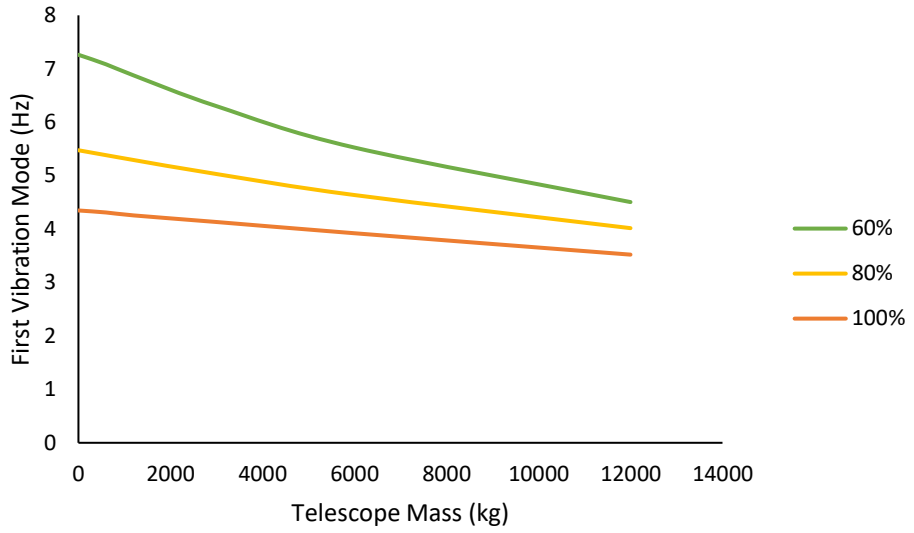

Figure 52. *Effect of tower scaling on first vibration mode for different telescope masses.*

Table 9. First Torsional Mode for T4 and 80% and 60% scaled towers.

T4 (Hz)	Scaled 80% (Hz)	Ratio	Scaled 60% (Hz)	Ratio
9.43	11.79	1.25	15.71	1.67

Table 10. Mass for T4 and 80% and 60% scaled towers.

T4 (tonnes)	Scaled 80% (tonnes)	Ratio	Scaled 60% (tonnes)	Ratio
77.15	42.42	0.55	18.29	0.24

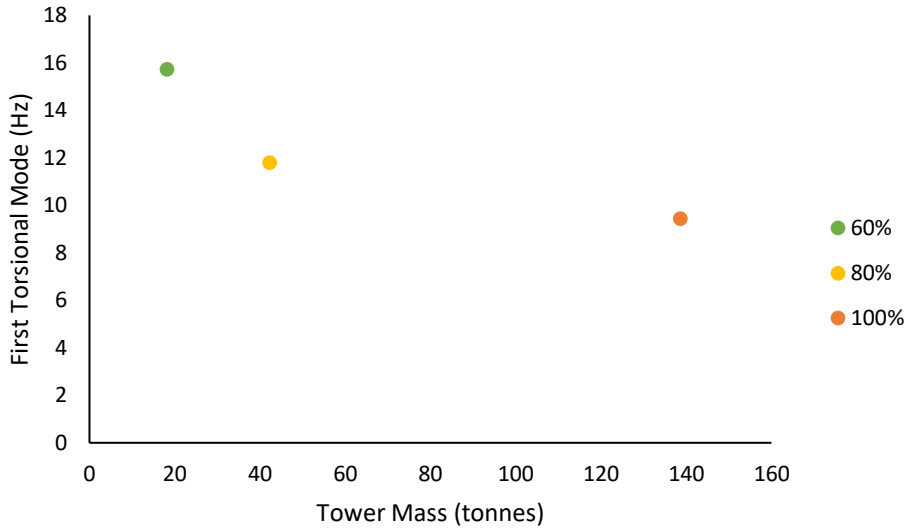

Figure 53. *Effect of tower scaling on tower mass and torsional mode.*

Table 11. Maximum Tilt and Field Rotation for T4 and 80% and 60% scaled towers.

Tower	Max Tilt (arcsec)	Max Base Rotation (arcsec)
T4	0.413	0.020
Scaled 80%	0.413	0.020
Scaled 60%	0.413	0.020

The results presented in Table 10 show length and mass are closely related to the cube of the scaling factor, 0.54 and 0.23 for 80% and 60%, respectively. Table 11 shows that maximum tilt and base rotation are constant. This can be attributed to simple scaling since the wind load and "spring" (beam lengths) are both decreasing by the same amount (40% and 20%). Torsional natural frequency increases for both cases and appear to be related to the inverse of the scaling factor, 1/0.6 and 1/0.8. This is also true for the first vibration mode but only for lighter telescope masses (0 kg to 1,200 kg). For masses greater than 1,200 kg, the frequency ratio begins to converge toward the 100% case (a 12,000 kg telescope has a frequency ratio of 1.07 and 1.04 for the 80% and 60% case).

An additional comparison was conducted on the performance of T6 if the smaller tube size of T5 was used, round HSS 7.625 in. x 0.328 in. This was done to compare T6 more fairly to T5 and infer how performance changes if only the beam cross section is scaled. A 31% mass saving is achieved compared to the original T6 but comes at a cost of increased tilt, up 50% from 0.66 arcsec to 0.99 arcsec, and decreased natural frequency of the first mode, down 9% from 5.3 Hz to 4.81 Hz, and torsional mode, down 13% from 2.67 Hz to 2.32 Hz. Although a significant mass savings is achieved, it comes at the cost of tower stiffness, but the reduced stiffness does not dramatically affect the frequency modes, which could be because of the significant mass reduction. Below are some plots of how this scaled T6 compares to the other tower designs:

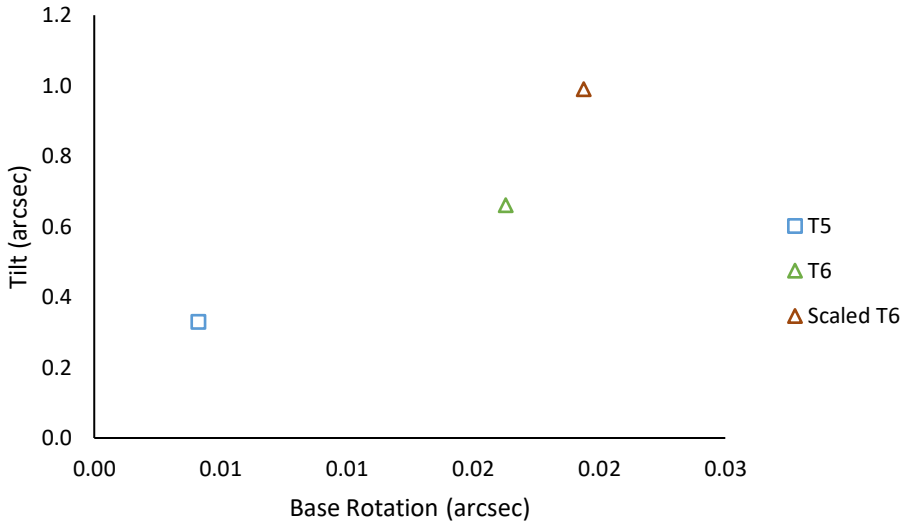

Figure 54. *Comparing maximum tilt and field rotation for scaled T6 against T5 and T6 during maximum operating condition.*

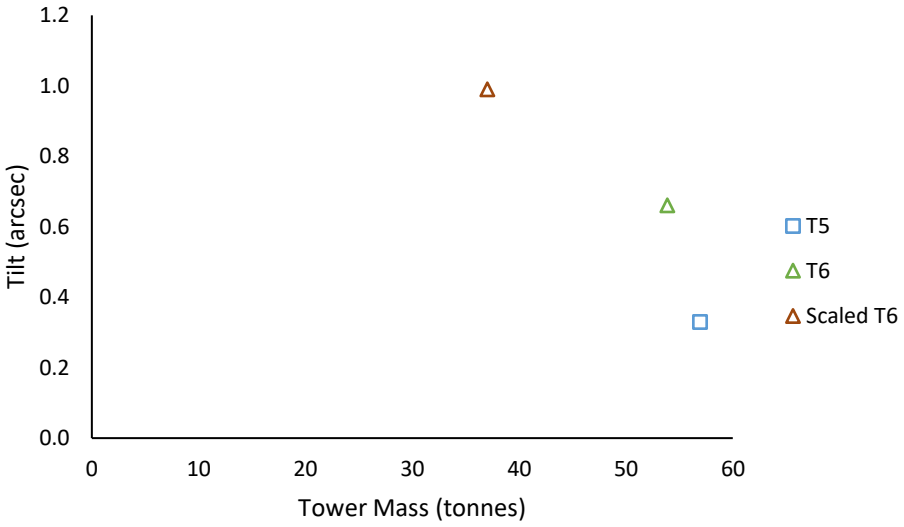

Figure 55. *Comparing maximum tilt and mass of scaled T6 against T5 and T6.*

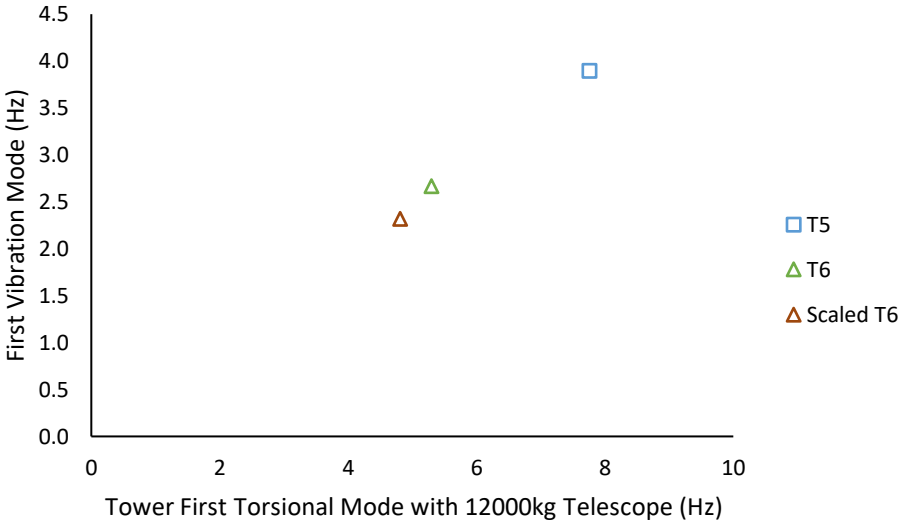

Figure 56. *Comparing first vibration mode and torsional mode of scaled T6 against T5 and T6.*

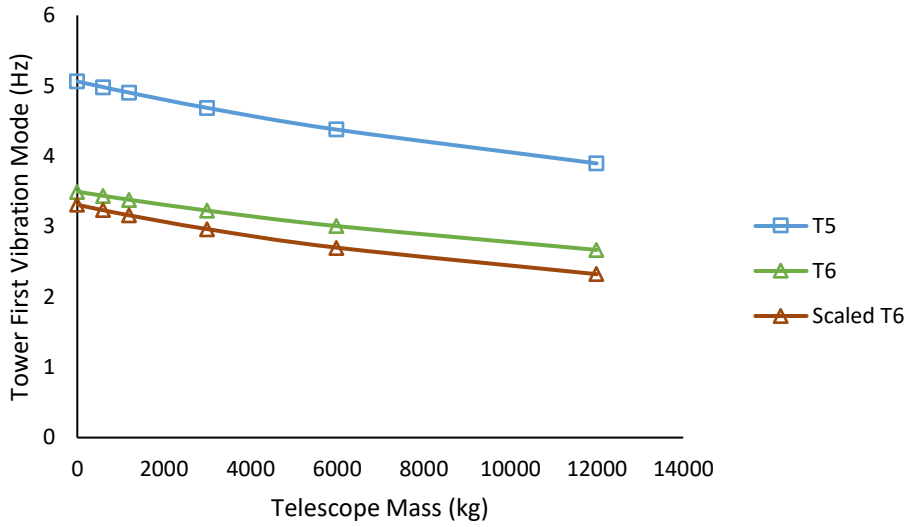

Figure 57. *Comparing effect of increasing telescope mass on tower first vibration mode for scaled T6 against T5 and T6.*

4.3.5 Tower Analysis Discussion & Summary

Only one tower design, T1 achieves a stability of less than 0.1 arcsec when subjected to the maximum operating condition of 10 m/s sustained winds. Its large module size, however, could make transporting and assembling them a logistical nightmare. Provided that some mitigation of rotation can be achieved in the telescope mount and control system, as appears to be the case (see Section 5.3), then it appears possible to optimize for lower logistical and assembly costs by adoption of T5 or T6. Although more unstable, T5 and T6 offer simpler logistics on the account that their modules are within the dimensions of a standard shipping container. That being said, tower design selection is incredibly dependent on the vibration suppression and mitigation methods to decouple telescope from the rotations of the tower. Should the telescope be completely isolated for either tower (as suggested below) then T6 should be selected since it is 30 m tall, compared to T5 being 24 m tall, and has slightly less mass than compared to T5. Even the scaled version of T6 could be considered since it offers a mass savings of 31%. If complete isolation is not possible, and only partial mitigation can be achieved, then T5 may become a more attractive solution since it is twice as stable as T6, 0.33” compared to

0.66”, with a first torsional mode 1.4 times greater than T6. Partial mitigation may open the possibility of scaled versions of T3 being explored since its stability is better than T5 by a factor of two. Should no mitigation be achieved, and this appears unlikely, then further investigation is needed in the power law analysis and module design to determine whether nonlinear scaling of T1 or T3 can achieve a stability of less than 0.1” while offering comparable logistical costs as T5 or T6.

Regardless of what tower design is ultimately chosen, additional methods are needed to decouple the telescope from the tower and provide sufficient margin for the stability budget. This need is amplified by the stability of each tower for its survival condition. It is important to note that there is not any published data on the 3-s wind gusts at Dome C and it is imperative that the frequency per day or per week that these gusts occur is known. Otherwise, if these gusts occur too frequently, the survival condition becomes a pseudo-operating condition.

Lastly, if more telescopes are to be deployed to Dome C and have a lower height requirement, say 15 m, but similar stability requirements, power law analysis suggests T3 and T1 could become viable candidates. When these designs are linearly scaled by 50%, their stability stays the same but their vibration modes increase and transportation becomes much easier since their module dimensions more closely resemble that of a cargo container.

5. Vibration Transfer & Suppression

Regardless of which tower design is ultimately selected, it is critical that all vibration transfer modes are investigated to maximize the telescope's pointing performance. One mode of vibration transfer is through frictional coupling of the telescope mount bearings. Of course, if bearings were completely frictionless on three orthogonal axes, then there would be no coupling; however, there is never zero friction, and we prefer an equatorial mount (only two axes) since this eliminates the need for image de-rotation. The deflection of the telescope must be assessed as a function of amplitude, or angular motion, of the top of the tower and the bearing friction characteristics. Are very low friction bearings, such as air bearings, required (as used in the SOFIA airborne observatory) or can cheaper rolling bearings be used?

Another option might be to mount the telescope to a vibration isolating pad or vibration absorber to reduce the displacement and force transmitted to the telescope, but it will be shown that these methods are impractical. Instead, the telescope can be isolated via friction mounts by selecting low friction bearings for the telescope mount. This is demonstrated by modeling displacement transmissibility as a function of bearing friction coefficient. The performance margin is small so some active suppression methods may still be desirable.

5.1 Characterizing Telescope Vibration

Can a compliant coupling between the tower and the telescope provide adequate vibration isolation? In this section, the telescope's lumped response due to oscillations of the tower will be examined in response to 10 m/s sustained winds and 72 m/s 3-s gusts and the next section will show how vibration isolators and absorbers are impractical.

A simple, linearized model can be constructed by treating the tower and telescope as two separate masses with their own natural frequency and damping as represented below:

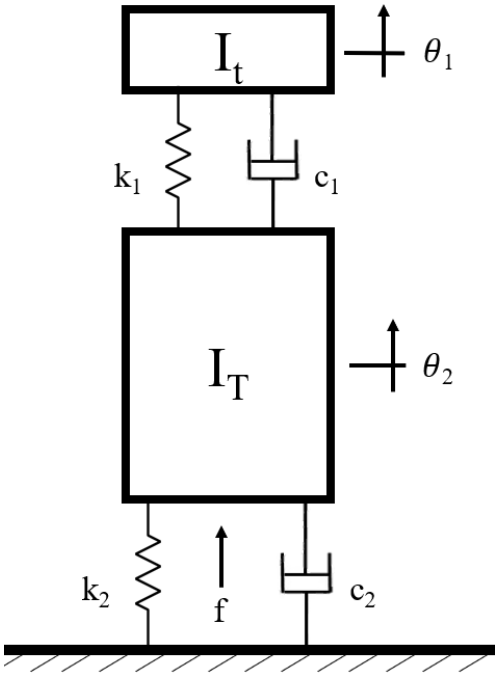

Figure 58. *Linearization of two mass model of tower and telescope.*

where *M* is the mass of the tower, *m* is the mass of the telescope, and the springs and dashpots represent the stiffness and damping of either structure. The forcing function, *f*, is the force applied due to wind loading. For sustained winds, *f* can be approximated as sinusoidal with a frequency, ω, between 0.01 Hz and 1 Hz, see Figure 7.

$$T = \tau \sin(\omega t) \tag{4}$$

The magnitude, τ, can be determined by using the spring force equation and the displacements from

Table *7*.

$$\tau = k\theta \tag{5}$$

The stiffness and damping coefficients can be determined from the following equations:

$$k = \omega_n^2 I \tag{6}$$

$$c = 2\zeta\sqrt{Ik} \tag{7}$$

The tower simulations conducted in MASTAN2 provided the natural frequency and area moment of inertia of each tower, but assumes an undamped structure, so the equivalent spring constant can be calculated from equation 6 and a damping ratio of 2% is assumed according to ref. 21 so the damping coefficient can be calculated using equation 7.

Using T3 as an example, τ is equal to 1,746 Nm since the tower deflection, θ, is 0.16" and k_1 is 2.25×10^9 Nm/rad since f_{n2} is 3.38 Hz, the mass is about 59.9 tonnes, and *I* from the 10 m by 30 m tower. From here the model for sustained winds begins to resemble a forced vibration problem with the equations of motion for the system being:

$$I_t\ddot{\theta}_1 = k_1(\theta_2 - \theta_1) + c_1\left(\dot{\theta}_2 - \dot{\theta}_1\right) \tag{8}$$

$$I_T\ddot{\theta}_2 = -k_1(\theta_2 - \theta_1) - c_1\left(\dot{\theta}_2 - \dot{\theta}_1\right) - k_2\theta_2 - c_2\theta_2 + f \tag{9}$$

Before solving for x_1, the response can be predicted by plotting the transmissibility transfer function. The forcing function is of the form:

$$y(t) = y_0 e^{i\omega t} \tag{10}$$

so the telescope response can be reasonably assumed to look something like:

$$x(t) = x_0 e^{i\omega t} \tag{11}$$

Plugging equations 10 and 11 into the equation of motion for the telescope, the result is:

$$[-m\omega^2 + i\omega c + k]xe^{i\omega t} = (k + i\omega c)y_0 e^{i\omega t} \tag{12}$$

Using the Laplace Transform, the transfer function of the system, $H_{x/y}(\omega)$, is:

$$H_{\frac{x}{y}}(\omega) = \frac{\left[1 + \left(2\zeta\frac{\omega}{\omega_n}\right)^2\right]^{1/2}}{\left[\left(1 - \frac{\omega^2}{\omega_n^2}\right)^2 + \left(2\zeta\frac{\omega}{\omega_n}\right)^2\right]^{1/2}} \tag{13}$$

where ω is the frequency that the tower is oscillating in rad/s and ω_n is the natural frequency of the telescope. When equation 13 is plotted against frequency ratio, r, where $r = \frac{\omega}{\omega_n}$, for different

damping ratios, Figure 59 shows that attenuation only occurs when the frequency ratio between the input excitation and the natural frequency of the isolator is greater than 1.4.

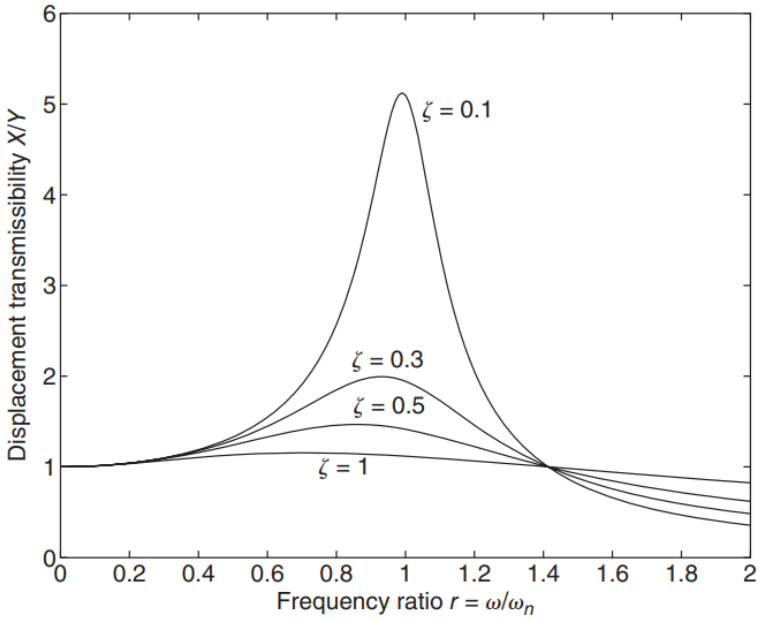

Figure 59. *Displacement transmissibility plot for mass-spring-dashpot system [22].*

However, recall from Figure 7 that 1σ of wind power density lies between 0.01 Hz and 0.1 Hz while 2σ is between 0.001 Hz and 1 Hz and

Table **6** shows that the natural frequency for each tower is greater than two. The tower will then oscillate at the same frequency as the wind so the telescope can only be isolated from the tower if the telescope or its isolation mount has a natural frequency well below 1 Hz, otherwise 100% of the displacement of the tower will be transferred to the telescope.

Using MATLAB's ode45 function, equations 8 and 9 are solved to find the telescope's response to 10 m/s sustained winds, which is plotted for different telescope natural frequencies and for different wind frequencies. The 3.38 Hz case illustrates the response when the wind excites T3 at its natural frequency.

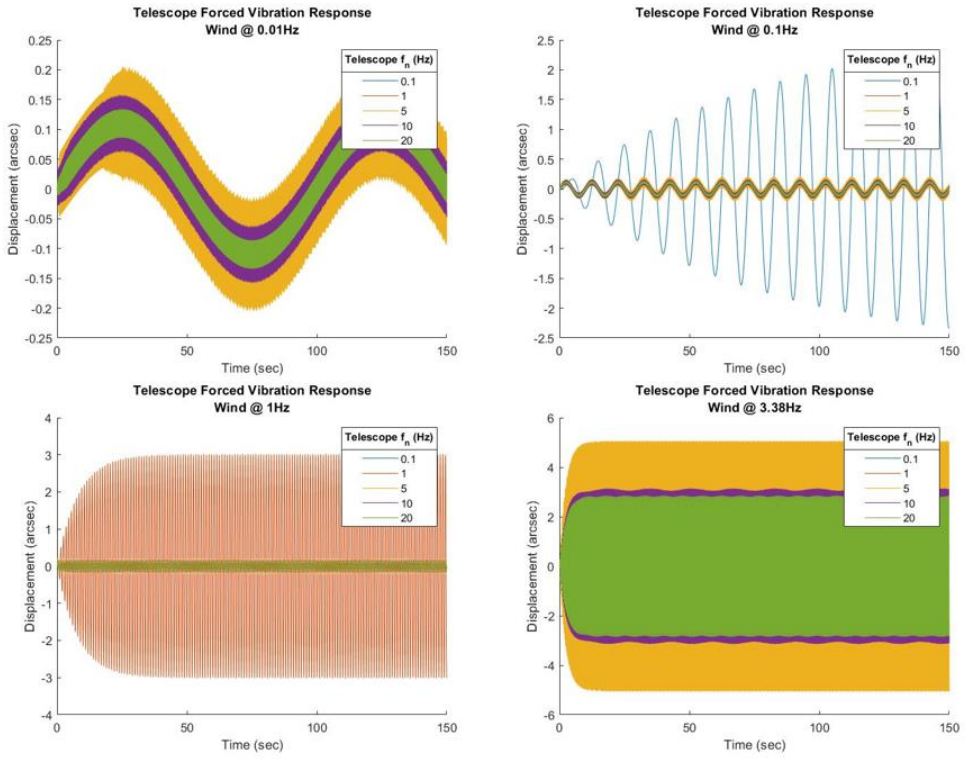

Figure 60. *Telescope response from forced vibration of tower.*

The calculated response confirms the reasoning from looking at the transmissibility plot, that the displacements of the tower are directly transferred to the telescope and are amplified if the wind frequency is close to the natural frequency of the telescope. Therefore, the telescope should have a natural frequency of 10 Hz or greater to avoid resonance from wind excitation.

From the same program, the free response is determined by removing the forcing function and plotting the position of the telescope mass until steady state is achieved. The response, shown in Figure 61, reinforces that the telescope should aim to have a high natural frequency, thus greater damping, and lower time constant, so perturbations caused by 3-sec wind gusts are quickly resolved.

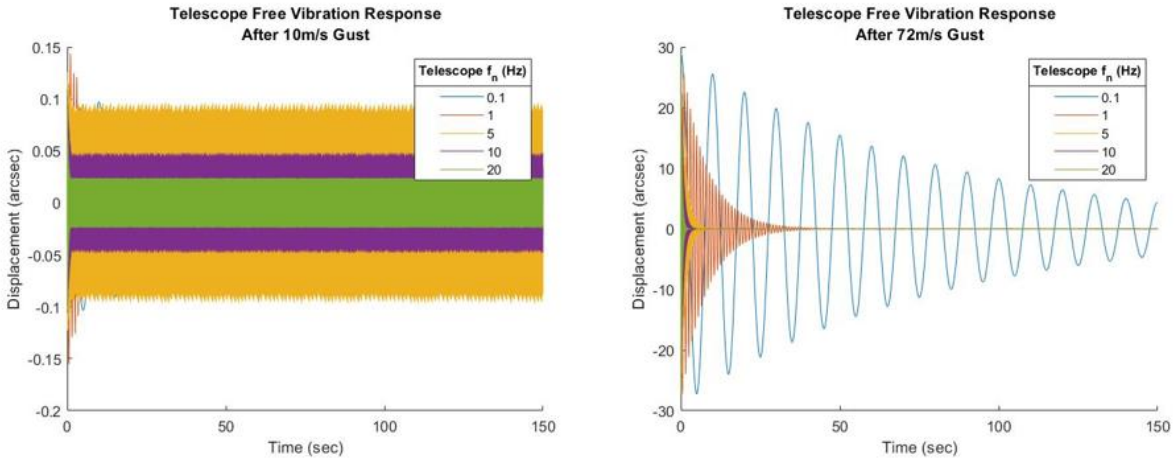

Figure 61. *Free response of telescope after 10 m/s and 72 m/s gust.*

5.2 Vibration Isolators & Absorbers

A vibration isolation mount can reduce vibration amplitude by providing a medium that is tuned such that the frequency ratio between the excitation and the mount is greater than 1.4. Based on this, an isolation pad or a vibration absorber seem like viable methods of decoupling the tower and telescope; however, for reasons outlined in this section, it is not.

The selection of an isolator is dependent on the frequency that the tower oscillates, ω. Recall the transfer function for the telescope:

$$H_{\frac{x}{y}}(\omega) = \frac{\left[1 + \left(2\zeta \frac{\omega}{\omega_n}\right)^2\right]^{1/2}}{\left[\left(1 - \frac{\omega^2}{\omega_n^2}\right)^2 + \left(2\zeta \frac{\omega}{\omega_n}\right)^2\right]^{1/2}} \tag{13}$$

If the design goal is to attenuate 90% of the input disturbance, assuming an undamped system, $\zeta = 0$, equation 13 can be solved as follows to find the natural frequency of the isolator:

$$H_{\frac{x}{y}}(\omega) = \frac{1}{\left|1 - \frac{\omega^2}{\omega_n^2}\right|} = 0.1 \tag{14}$$

$$\frac{\omega}{\omega_n} = \sqrt{11} = 3.31 \tag{15}$$

$$\omega_n = \frac{\omega}{3.31} \tag{16}$$

Although damping was excluded, it does not matter since equation 16 shows that to attenuate the displacement transfer by 90%, the natural frequency of the isolator must be 3.31 times less than the frequency of the excitation, which is impractical since the frequency of excitation ranges from 0 to 1 Hz. Therefore, other mitigation methods must be developed.

The same limitation applies to vibration absorbers (i.e., a tuned-mass damper), trying to null a range of input frequencies using a method better suited for nulling a single input frequency. Figure 62 below shows a simplified diagram of a TMD setup. The full derivation of the design equations will not be covered here since they are well known but can be viewed in ref. 22 from page 832 to 835. Essentially, the absorber is able to null the input excitation by having the same natural frequency, ω_{n_2}, as the input excitation, ω, but sine we are trying to null across a range of frequencies the absorber suffers from the same flaw as the isolator. One could try nulling at least 1σ of excitation by designing an absorber for 0.1 Hz of input excitation, but this would require an impractical amount of mass. The design equations are:

$$k_2 = \frac{F}{X_2} \tag{17}$$

$$m_2 = \frac{k_2}{\omega^2} \tag{18}$$

Using the 1,746 Nm calculated for T3 and assuming 10° of tolerable movement by the TMD, the mass required to null an input excitation of 0.1 Hz would be about 25,340 kg or 25.3 tonnes. Below is a brief derivation of the design equations, a more detailed derivation can be found in ref. 22 in pages 833 to 835.

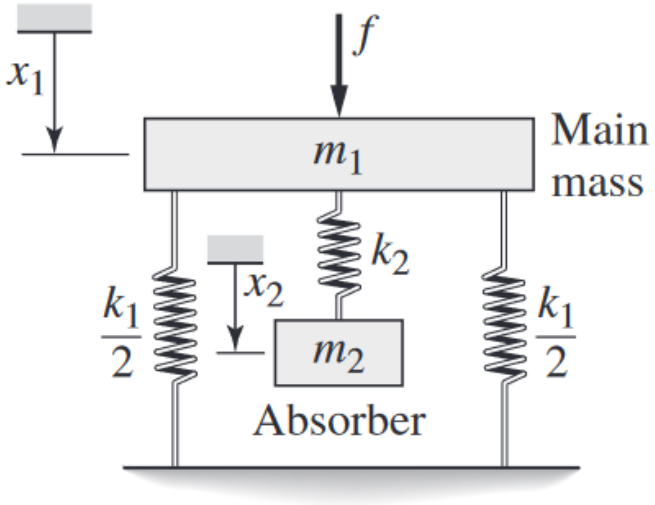

Figure 62. *Simplified linearized model of telescope, m_1, with vibration absorber, m_2 [22].*

Equations of motion:

$$m_1\ddot{x}_1 = -k_1x_1 - k_2(x_1 - x_2) + f \tag{19}$$

$$m_2\ddot{x}_2 = k_2(x_1 - x_2) \tag{20}$$

Transfer functions after taking the Laplace transform:

$$T_1(s) = \frac{X_1(s)}{F(s)} = \frac{m_2s^2 + k_2}{(m_1s^2 + k_1 + k_2)(m_2s^2 + k_2) - k_2^2} \tag{21}$$

$$T_2 = \frac{X_2(s)}{F(s)} = \frac{k_2}{(m_1s^2 + k_1 + k_2)(k_2s^2 + k_2) - k_2^2} \tag{22}$$

For a sinusoidal input with frequency ratios defined as:

$$r_1 = \frac{\omega}{\omega_{n_1}} = \frac{\omega}{\sqrt{k_1/m_1}} \tag{23}$$

$$r_2 = \frac{\omega}{\omega_{n_2}} = \frac{\omega}{\sqrt{k_2/m_2}} \tag{24}$$

the transfer functions can be written as:

$$T_1(j\omega) = \frac{1}{k_1}\frac{1 - r_2^2}{(1 + k_2/k_1 - r_1^2)(1 - r_2^2) - k_2/k_1} \tag{25}$$

$$T_2(j\omega) = \frac{1}{k_1}\frac{1}{(1 + k_2/k_1 - r_1^2)(1 - r_2^2) - k_2/k_1} \tag{26}$$

For m_1 to be motionless, X_1 must be equal to zero, which can be achieved if $T_1(j\omega)$ is equal to zero from $1 - r_2^2 = 0$, so $r_2 = \pm 1$. Since r_2 cannot be negative, $r_2 = 1$ such that:

$$r_2 = \frac{\omega}{\omega_{n_2}} = 1 \tag{27}$$

or:

$$\omega_{n_2} = \sqrt{\frac{k_2}{m_2}} = \omega \tag{28}$$

Thus, the mass m_1 will be motionless if the absorber has the same natural frequency, ω_{n_2}, as the frequency ω of the applied excitation. However, the range of excitations is from 0 to 1 Hz, so the same problem exists as with the vibration isolator.

5.3 Impact of Bearing Friction

Since bearing friction is never zero, there will be some coupling between the tower and the telescope. How this coupling is transferred to the telescope, and can be managed, is dependent on the kind of telescope mount in use. The coupling through an equatorial mount will be assessed since it is the preferred mount type for a cryogenically cooled telescope, as is the case for Cryoscope. Assuming purely Coulomb friction, modified friction models from earthquake engineering show that the amount of coupling is dependent on the friction coefficient of the bearing and the relative size of the bearing to the telescope. Vibration suppression below

the 0.1 arcsec stability requirement appears to be possible using air bearings in an equatorial mount, with field rotation being tolerable for as much as 1 arcsec of angular excitation, but active compensation may still be desirable for additional design margin. Given the high relative humidity, it is unclear whether air bearings can operate reliably, due to concerns of ice formation, and within power budget at Dome C unless the pumped air temperature is well above the very low ambient temperature or dehumidifiers are installed. This then poses a possible problem for image quality which relies on keeping all the air around the telescope very close to ambient temperature.

5.3.1 Bearings & Telescope Mounts

To sufficiently decouple the telescope from the tower's rotation in any arbitrary direction, bearings are required on any three orthogonal axes. Equatorial telescope mounts only have two rotation axes, thus require an additional bearing or friction isolation stage for complete coverage. Altitude-azimuth (alt-az) mounts must have a third axis for field de-rotation but if the instrument is a cryogenically cooled telescope (as is the case under consideration), then rotation of the field sensor is more difficult as the entire telescope must be rotated about its axis, to avoid cryogenic mechanisms.

An equatorial mount is preferred since it eliminates the need for field de-rotation by pointing one axis (Right Ascension) at the south celestial pole. The vibration isolation problem is complicated for telescopes on an equatorial mount, where rotating about the mount's right ascension axis changes the orientation of the declination bearing. As a consequence, the third axis (if provided) must align with the telescope tube and cannot be applied at the base of the telescope. Whether an additional bearing system or friction stage is required, though, depends on amount of rotation that is tolerable on the detector's imaging plane. The possibility that isolation on only the RA and DEC (declination) axes is sufficient will be examined.

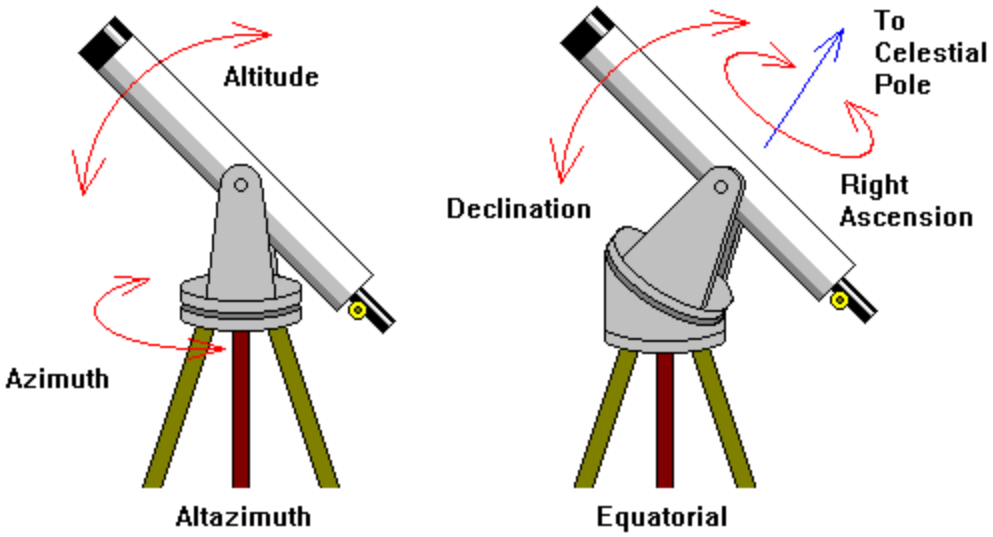

Figure 63. *Graphic depicting rotation axes for alt-az and equatorial mounts [23].*

When the tower rotates in a manner that is not covered by either bearing in the mount, the rotation will not be attenuated, and the telescope will want to rotate. The results from

Table ***7*** and the range wind frequencies presented in Figure 7 show that these rotations will be small angle, low frequency excitations (less than 1 arcsec and 1 Hz) so they could be compensated using the telescope's torque motor and star tracker. However, due to only having two-axis control, there will be some residual rotation that cannot be compensated, in the form of pure rotation of the image plane about its center. This field rotation 'stretches' objects in the image with increasing effect as the distance from the center of the image increases. A common example of field rotation is in long-exposure astrophotography where it appears like the sky is spinning (see Figure 64 blow).

Figure 64. *How field rotation affects an image in astrophotography [39].*

Notice that the objects at the focal point of the image appear stationary but objects farther away from the focal point become increasingly blurred and stretched as the distance from the focal point increases. Some field rotation may be tolerable depending on the telescope's image quality budget, the following is an estimation of field rotation given some premises:

1. Assertion: rotation about any axis direction can be decomposed into components along any three orthogonal axes.
2. Sufficient isolation is provided along RA and DEC axes so these components can be reduced to negligible levels.
3. RA and Dec Axes can be driven fast enough to keep the field center stationary.
4. The residual rotation is then about the field center, i.e., direction in which the telescope points.
5. Assume the component of mount rotation along the telescope tube axis maps 1:1 to image rotation. This is the worst case. The best case is when

the base rotation resolves into components aligned only to RA and/or DEC axes.

Given these premises, if a 1 arcsec rotation is applied along all three orthogonal axes then the only rotation transferred to the telescope is 1 arcsec of field rotation. To determine whether 1 arcsec of field rotation is tolerable, the distance rotated in units of pixels of the detector must be calculated. As per Figure 64 the impact of field rotation worsens as the distance from the center of the plane increases, so for a square image, the pixels most rotated will be at the corners. Given a square focal plane with width W in pixels and rotation angle in radians, α, tangential motion of the corner pixel is:

$$P = \frac{\alpha W}{\sqrt{2}} \tag{29}$$

For a Teledyne H2RG detector that is 2048 x 2048 pixels with 18 µm pixel pitch, W is 36864 µm and α is 4.848×10^{-6} radians, so P is 0.12 µm. This amount of field rotation is small compared to the PSF size for the Cryoscope telescope, which is 4.8 µm. Since the proposed tower tilt is below 1" at the maximum operating condition, an additional bearing or friction isolation mount is unneeded [47]. Should wind gusts in excess of 10 m/s occur frequently at Dome C, then an additional bearing or friction isolation mount may be needed but it is not apparent at the time of writing that this is the case.

Before discussing friction mount designs, it is important to consider which rotations are the most critical and beyond the 0.1" stability requirement. The results presented in

Table 7 show the largest rotations occur about the horizontal axes of the telescope base, causing the tower to tilt well beyond the tolerable pointing error. Rotations about the vertical axis (base rotation) for each tower design is tolerable but the amount of design margin varies by tower design. Therefore, friction stage designs should prioritize reducing the tilt of the tower

transferred to the telescope, seeking to reduce amplitudes below the 0.1” tolerance by at least an order of magnitude.

One bearing configuration that can provide tilt isolation is a double cradle design as in Figure 65 below. This method provides isolation from both horizontal axes and accommodates deploying a number of bearing types. Roller element bearings are the most common kind of bearing with low coefficients of friction depending on the type, with friction coefficients as low as 0.0008.

Table 12. Friction coefficients of various roller-type bearings [24].

Bearing Type	Friction Coefficient
Deep groove ball bearing	0.0010～0.0015
Angular contact ball bearing	0.0012～0.0020
Self-aligning ball bearing	0.0008～0.0012
Cylindrical roller bearing	0.0008～0.0012
Full complement type needle roller bearing	0.0025～0.0035
Needle roller and cage assembly	0.0020～0.0030
Tapered roller bearing	0.0017～0.0025
Spherical roller bearing	0.0020～0.0025
Thrust ball bearing	0.0010～0.0015
Spherical thrust roller bearing	0.0020～0.0025

One downside to using this method is the amount of mass required for the stage. Two panels are required to support the telescope, each as big as the base of the telescope and strong enough to not deform. This solution may be attractive for smaller telescopes where the mass is less than 3,000 kg but larger telescopes should seek alternative solutions.

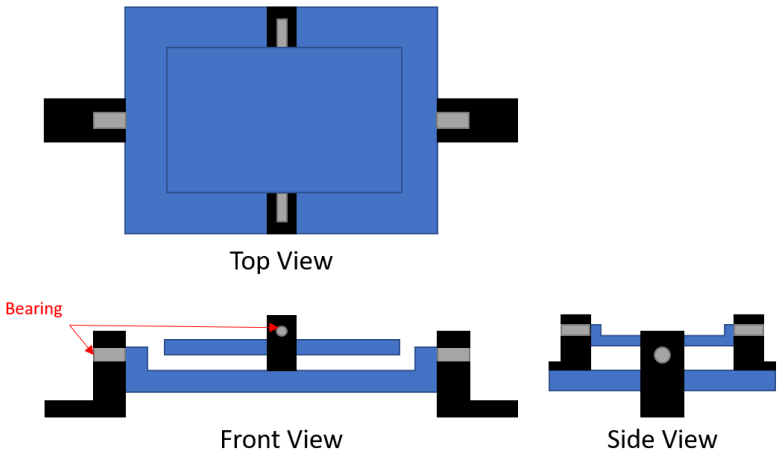

Figure 65. *Proposed double cradle design for bearing stage.*

Another attractive bearing configuration is to deploy the telescope mount on spherical sliding bearings (SSBs) or friction pendulum bearings (FPBs) which provides isolation from tilt and field rotation. SSBs and FPBs are like pendulums that slide on a concave surface, limiting the excitation transferred to the structure they are supporting to the friction force in the sliding motion. SSBs and FPBs are commonly found in earthquake engineering to isolate large structures, such as bridges and buildings, from seismic activity, which makes them good candidates to isolate larger telescopes (i.e., masses greater than 6,000 kg). They are designed for large amplitude excitation, so their friction coefficients are much greater than other bearing types, from 0.03 to 0.05, although recent developments in this area have caused their friction coefficients to drop to around 0.013 [25]. SSBs and FPBs are also attractive because of their deployment in cold regions like Japan and Alaska. The materials sliding against one another in these bearings are polished steel and PTFE impregnated with silicone oil. Although cold resistant models appear to only be rated to -40°C, it is conceivable that this operating temperature could be reduced further since there are silicone oils rated for temperatures as low as -110°C and PTFE retains its lubricity down to -200°C [26][27][28]. SSBs and FPBs are good candidates for this

application but further investigation is required to confirm that SSBs and FPBs can maintain a low friction coefficient of 0.013 or less in the Antarctic climate.

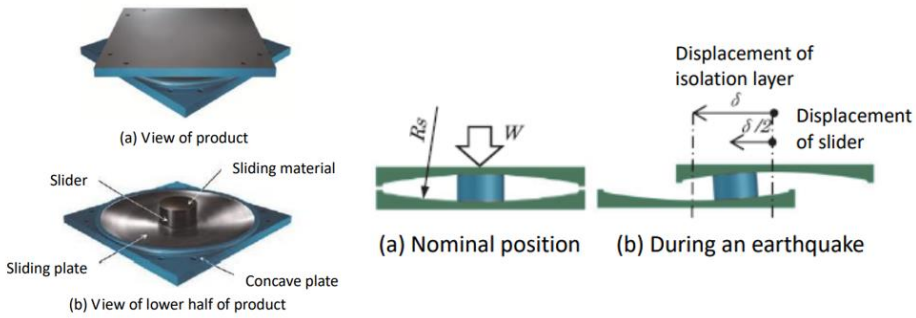

Figure 66. *Example of spherical sliding bearing [25].*

Should lower friction coefficients be required, spherical air bearings have been used in the past on telescopes such as SOFIA which was a telescope inside of a Boeing 747 and used air bearings to attenuate vibrations caused by the aircraft [48]. Air bearings are perhaps the most competitive bearing type if purely assessing them on their friction coefficient. With friction coefficients described as being as low as 0.00001, they are significantly better than roller element bearings in this regard [29]. Air bearings work by blowing a thin film of pressurized air through a porous media that creates a non-contact, 'zero friction' zone between it and another surface, see Figure 67.

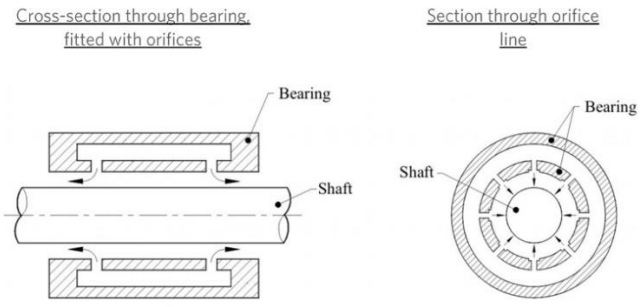

Figure 67. *Illustration of radial air bearing [38].*

Despite their dramatically lower friction coefficient, there are some trade-offs of implementing air bearings over a roller type bearing. One benefit of an air bearing is they do not require lubrication, unlike roller bearings, but they require clean air and piping, which raises concerns of ice crystal formation and how to mitigate it. If these pores become clogged, the bearing's effectiveness could be diminished, cause damage, or be destroyed. Although heater could be installed to prevent ice formation, it is important to understand the extent of which they are necessary. Additionally, these bearings require pumps and piping to transport the pressured air, increasing the mass and power budget and requiring additional infrastructure that roller bearings do not.

Ice formation occurs when the ambient temperature at a given humidity reaches its frost temperature. As the relative humidity decreases so does the dew point and frost point but the frost point is always higher than the dew point, due to the stronger molecular bonding on the surface of ice as compared to the surface of liquid water [49]. Given this, if the relative humidity is low enough, then the frost and dew points will be lower than ambient, and ice formation will not be an issue. Figure 68 highlights the relationship between the frost point and the relative humidity and temperature of the ambient air. To prevent ice formation within the air bearing, the relative humidity of the pumped air should be no greater than 40% but the humidity at Dome C often exceeds 50%, which causes frost to form at ambient [40][41].This can be mitigated by installing dehumidifier filters to the pumps, reducing the humidity of the pumped air in the bearing and preventing ice formation without having to install heaters.

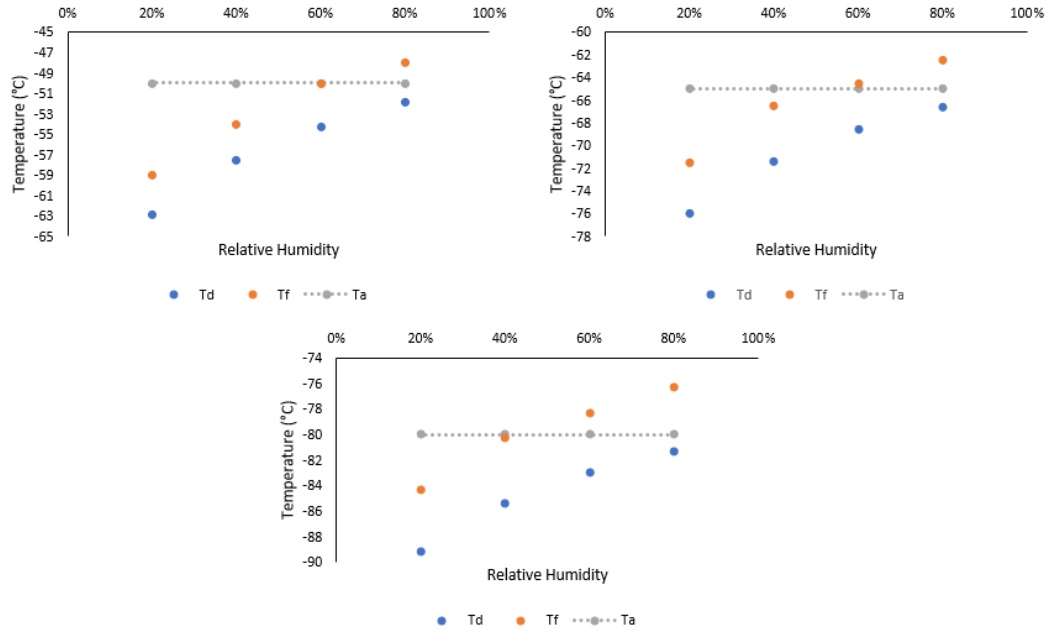

Figure 68. *Plots of freezing point, Tf, and dew point, Td, against relative humidity for three different ambient temperatures, Ta, at Dome C: -50℃ (top left), -65℃ (top right), -80℃ (bottom center).*

5.3.2 Coulomb Friction Model

Classical models of friction describe it as a force that opposes motion which is proportional to the normal force but independent of velocity. These models are known as Coulomb friction models and are represented as:

$$F = -\mu F_N \text{sign}(v) \tag{30}$$

Although simple, this model does not capture the behavior of the friction force when velocity is zero and fails to capture known phenomena like the Stribeck effect [30][31]. Despite these deficiencies, the Coulomb friction model overestimates the frictional force, which in the context of this work, implies greater frictional coupling, so it serves as a conservative approximation to estimate for the frictional coupling through the bearings.

5.3.3 Response of Sliding Bearing

The Coulomb friction model can be applied to represent the friction torque that opposes the torque applied to a bearing's outer ring and which is the only force acting on the bearing's inner ring, see Figure 69.

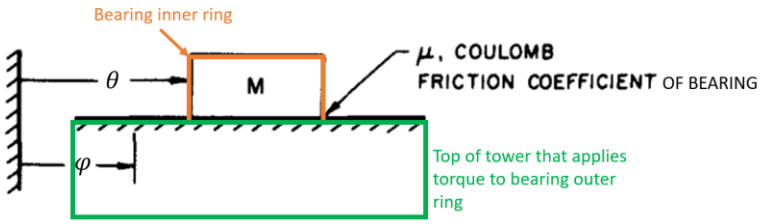

Figure 69. *Representation of bearing-tower system [32].*

This representation of the bearing-tower system is like that of base isolation friction mounts in earthquake engineering. The difference is that the excitation is an angular displacement, and the parameter of interest is the angular displacement transferred to the bearing's inner ring. Westermo and Udwadia (1983) present the formulation to solve for a linear sliding rigid block, and that same formulation can be used to assess the friction coupling in a bearing except linear representations are now angular.

The base excitation can be described as a sinusoidal input whose magnitude is equal to the maximum rotation of the tower under wind loads:

$$\varphi(t) = \varphi_{max} \sin(\omega t) \tag{31}$$

The acceleration of the tower can be described by taking the double derivative of the position equation, with the amplitude being:

$$\ddot{\varphi}_{max} = \varphi_{max}\omega^2 \tag{32}$$

For slip to occur in the bearing the following condition must be met:

$$\left|I_{t+m}\ddot{\theta}\right| \geq \mu r(gm + P) \tag{33}$$

$$I_{t+m} = \frac{1}{2} mR^2 \tag{34}$$

where I_{t+m} is the mass moment inertia of the telescope and mount, R is the radius of the telescope (approximated to radius of primary mirror), μ is the friction coefficient of the bearing, g is the gravity constant, m is the mass of the telescope or telescope and mount, r is the radius from the center of the bearing to the friction contact, and P is the preload on the bearing, if any. Assuming no preload, the angular acceleration of the inner ring during the sliding mode is then:

$$\ddot{\theta}(t_i) = \pm \frac{2\mu g r}{R^2} \tag{35}$$

And during the sticking mode the angular acceleration on the inner ring is:

$$\ddot{\theta}(t_i) = \ddot{\varphi}(t_i) \tag{36}$$

The velocity and position of the inner ring can be determined via integration:

$$\dot{\theta}(t_i) = \ddot{\theta}(t_i)(t_i - t_{i-1}) + \dot{\theta}(t_{i-1}) \tag{37}$$

$$\theta(t_i) = \ddot{\theta}(t_i)\left(\frac{1}{2}(t_i^2 - t_{i-1}^2) - t_{i-1}(t_i - t_{i-1})\right) + \dot{\theta}(t_{i-1})(t_i - t_{i-1}) + \theta(t_{i-1}) \tag{38}$$

Slip will occur when the following condition is met:

$$\eta < 1, \eta = \frac{2\mu g r}{\ddot{\varphi}_{max} R^2} \tag{39}$$

The mass will then stick when it reaches the end of its current slide mode, being in a slip-stick-slip state, if $\eta > 0.53$ or be constantly slipping, in a slip-reverse-slip state, if $\eta \leq 0.53$. If $\eta > 0.53$ and the block is sticking, then angular acceleration will be equal to that of the tower. Therefore, η should be less than 0.53 in order to minimize the angular acceleration, thus the resultant torque and angular displacement, of bearing's inner ring.

5.3.4 Bearing Angle & Torque Transfer Results

The impact of a bearing's coefficient of friction on the torque transferred to the bearing inner ring and the resulting angular displacement can determined by solving equations 31 through 39 using the results from Section 4.3.4.

Table 13. Parameters for Angle Transfer Model

Parameter	Case 1	Case 2
	Value	Value
φ_{max} (degrees)	1	1
a = b (m)	10	10
r (m)	0.006	0.0625
R (m)	0.125	1
ω (rad/s)	2π	2π

The performance of three bearing friction coefficients of 0.01, 0.001, and 0.00001 were assessed and the limitations of their attenuation are presented in Figure 70 through Figure 72 below. By using a very large angular deflection, in this case one degree is qualifies as such, the attenuation limit of a bearing can be found for each friction coefficient. The values for Case 1 are meant to simulate possible values for a 0.25 m-class telescope and Case 2 for a 2 m-class telescope.

As expected, when the friction coefficient is decreased so does the torque transferred to the bearing inner ring and its resulting angular displacement. However, the results from Case 1 and Case 2 show that the friction coefficient corresponding to roller bearings does not provide sufficient isolation below the 0.1" stability requirement. Roller bearings are only able to isolate down to 46.5" and 7.8" for Case 1 and Case 2, respectively. The difference of these values is driven by the ratio of radii (r/R^2) of the bearing (r) and the telescope (R), and Figure 72 shows how much an impact differences in the ratio of radii have on the attenuation limit. Air bearings,

on the other hand, can provide adequate isolation but only when the ratio of radii is less than 0.08, as with Case 2 which attenuates down to 0.07". Case 1 has a radii ratio of 0.384 and only attenuates down to 0.48". Therefore, air bearings with a ratio of radii of 0.08 or less should be deployed to achieve isolation below 0.1"; otherwise, **active compensation methods are required null the torque transmitted through the bearings and keep the telescope stable**.

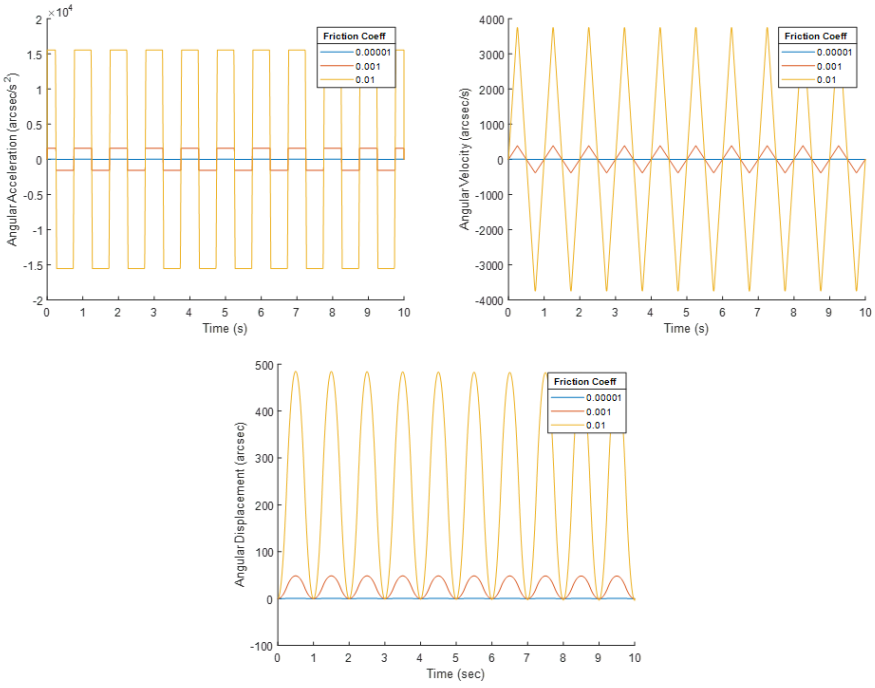

Figure 70. *Angular acceleration, velocity, and displacement of bearing inner ring for different friction coefficients for Case 1, 0.25m telescope.*

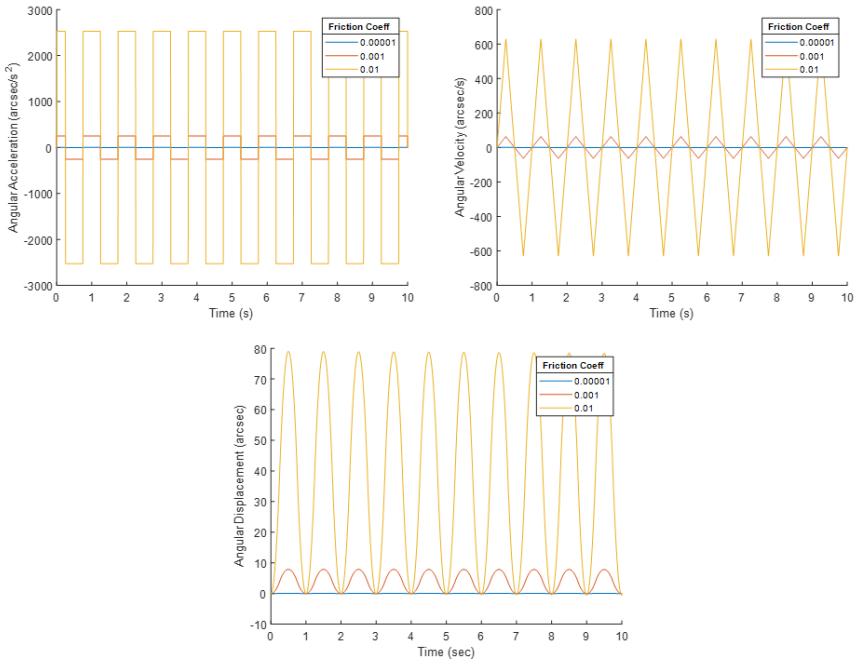

Figure 71. *Angular acceleration, velocity, and displacement of bearing inner ring for different friction coefficients for Case 2, 2m telescope.*

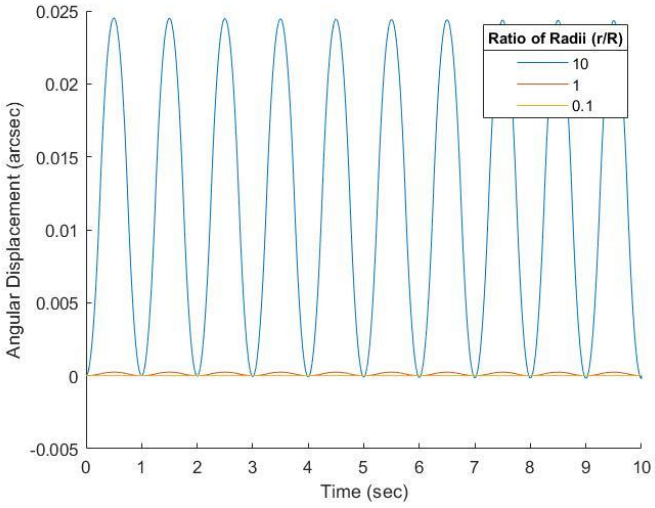

Figure 72. *Angular displacement of bearing inner ring for different ratio of radii (r/R).*

5.4 Canceling Remaining Angle Displacement: Rotary Flexure

As discussed in Section 5.3.2, the Coulomb friction model does not capture the true friction response, missing known phenomena like the Stribeck effect and not accounting for viscous effects. Although more accurate models exist, such as the Dahl and LuGre models,

friction is inherently nonlinear, making it difficult to predict the response accurately and precisely on a sub-arcsecond scale [31]. If active cancellation of sub-arcsecond residual angular displacements from friction coupling is to be effective, then one should not rely on friction models to feed the cancellation protocol. To circumvent this challenge, rotary flexures could be installed on the telescope and mount, converting the friction coupling problem to a beam bending problem. When the rotary flexure deflects, the torque required to rotate the flexure can be computed via beam theory or torsional spring equations and fed to the torque motor to provide the necessary torque to null the excitation. The flexure behaves as a torsional spring that is stiff in axial and radial directions but flexible in the theta direction. The angular stiffness should be minimized so deflections can be easily measured but this could introduce a component with a sub-hertz natural frequency. This is not a problem, however, if the natural frequency of the flexure is at least fifty times less than the bandwidth of the direct drive motors driving the telescope. If the flexure meets this requirement, then the torque transmitted by the flexure oscillating at its natural frequency can be adequately nulled by the motor.

5.4.1 Selecting a Flexure

The Riverhawk Free-Flex® flexural pivot is one example of a rotary flexure that could be viable for telescope masses below 1,400 kg; however, larger telescopes would require custom flexures to support the larger load or a tip-tilt mirror. The one inch, type-400 pivot from Riverhawk has a maximum load capacity of 735 kg so two pivots have a maximum load capacity of 1,470 kg with an equivalent zero-load torsional spring rate of 97.4 Nm/rad [33]. However, when a load is applied to the pivots the torsional spring rate changes, as indicated in Figure 74. If the two one-inch pivots are loaded with 1,400 kg, the multiplier is 0.00286, then the original 97.4 Nm/rad torsional spring rate becomes 194.72 Nm/rad when the pivots are in compression and

24.34 Nm/rad when they are in tension. The cases of “compression” and “tension” are dependent on the orientation of the flexure and are explained on their website, see Figure 75 for details.

Figure 73. *Riverhawk Cantilevered, single-ended Free-Flex® Pivot [33].*

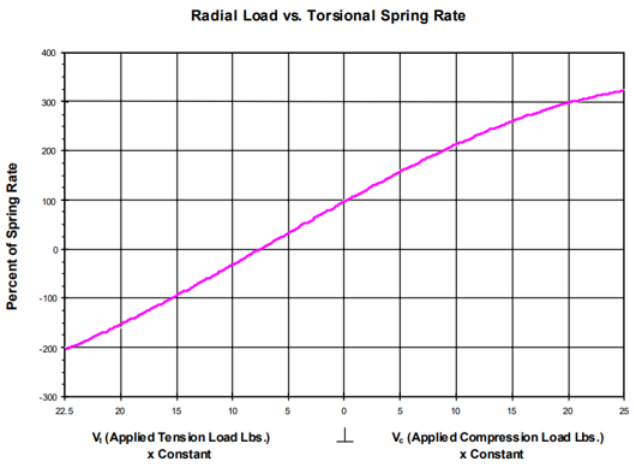

Table of Constants

**Pivot dia. (inches)	For Type 800*	For Type 600*	For Type 400*
0.1250	14.6	1.63	.204
0.1562	8.09	1.01	.126
0.1875	5.95	.743	.0895
0.2500	3.10	.387	.0485
0.3125	1.93	.241	.0309
0.3750	1.44	.173	.0217
0.5000	.784	.0980	.0123
0.6250	.450	.0576	.00720
.07500	.326	.0404	.00505
0.8750	.247	.0298	.00372
1.0000	.180	.0228	.00286

* This table applies only to standard pivots as defined herein.
** Diameter in inches.

Figure 74. *Information provided by Riverhawk on impact of applied load on spring rate [34].*

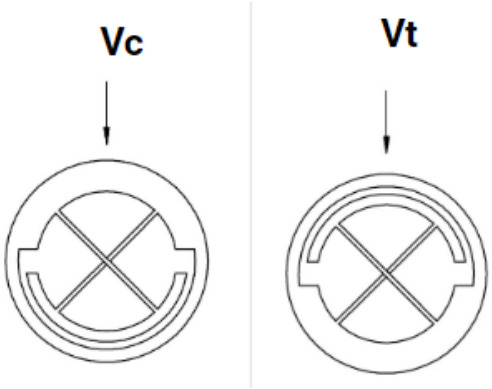

Figure 75. *Flexure orientation when loaded in compression (left) and tension (right) [33].*

The natural frequency of the flexure can then be calculated using the equation below:

$$f_n = \frac{1}{2\pi}\sqrt{\frac{K}{I}} \tag{40}$$

where K is the torsional spring rate and I is the mass moment of inertia of the telescope. Assuming a 0.5 m radius for a 1,400 kg telescope, I can be calculated using equation 34, then when the pivots are in compression the natural frequency is 0.11 Hz and 0.041 Hz when in tension. Therefore, the direct drive motors should have a bandwidth of at least 5.5 Hz if these flexures are used. Private conversations with Planewave Instruments, a telescope mount manufacturer and supplier, on the direct drive motors they use in their telescope mounts revealed that their motors have a bandwidth of 32 kHz but are limited to 50 Hz due to the driving software. Although this is just one example, it suggests that the bandwidth requirement for these flexures is well within the bandwidth of direct drive motors that could be used to drive the telescope.

5.4.2 Selecting an Encoder

Alongside the rotary flexure must be an adequate measurement device that can deliver sufficient precision that residual torque transmitted through the bearings and deflects the flexure can be detected. An encoder can be selected by either choosing one that has an accuracy below 0.1” as this is the stability requirement or calculating what the minimum flexure deflection is when the transmitted bearing torque is applied to it. If designers opt for the former, NASA Goddard Spaceflight Center advertises an optical encoder with an accuracy of 0.02” and Planewave Instruments has an optical encoder with an accuracy of 0.069” [35][36]. If the latter, the following calculations shows angular deflection of the one-inch, type-400 pivot discussed earlier from the residual torque transmitted by the bearings.

The torque can be calculated from equation 41, so for a friction coefficient of 0.001, bearing radius of 0.05 m, mass of 700 kg, and no preload, the torque is 0.34335 Nm. From here the torsional spring equation can be rearranged to calculate the angular deflection of the flexure:

$$T = K\theta \tag{41}$$

$$\theta = \frac{T}{k} \tag{42}$$

where *K* is the torsional spring rate of the flexure, *T* is the torque applied across the flexure, and θ is the angular displacement of the flexure. The torsional spring rate is 24.34 Nm/rad if the flexure is in tension and 194.72 Nm/rad if in compression. Therefore, for a flexure loaded in tension, the flexure deflects by 0.807°, and by 0.101° when the flexure is loaded in compression. Of course, these results are dependent on a few factors, such as which bearings are chosen and the size of the bearing, but if the torque was a thousand times less, the angular deflection of the rotary flexures would be greater than two arcseconds. This suggests that less precise encoders can be used to monitor the flexures. Renishaw is an example of one company whose optical encoders become viable, despite their encoder having precisions above 0.5" [37]. Regardless of which encoder is chosen, the deflection of the flexure can be accurately tracked and with a direct drive motor with a bandwidth greater than 5.5 Hz completes the vibration isolation scheme for a telescope atop the tower.

5.5 Vibration Suppression Analysis Discussion & Summary

The results presented above show that complete vibration isolation from the tower is possible through entirely passive means with active compensation providing additional design margin. Given that the tower will oscillate with the frequency of the input wind excitation since their frequency ratio is less than 0.5, damping mounts and tuned-mass dampers (TMD) were investigated as a possible isolation method. Although passive, TMDs are not effective for this

application since the range of excitation frequencies are less than 1 Hz, which risks the TMD resonating and displacing the telescope.

Friction isolation mounts were then investigated with the idea to assess whether the bearings already present in the telescope mount could provide adequate isolation, see Section 5.3. Assuming pure Coulombic friction, an angular friction model was created in Section 5.3.3 by modifying a linear friction model typically used in civil engineering friction mount design. From this model, it was determined that the amount of attenuation that friction isolation can provide is dependent on the friction coefficient and the relative size of the bearing to the telescope. Simulations in MATLAB for different bearing friction coefficients showed that air bearings could provide adequate isolation if the ratio of radii between the bearing and telescope is less than 0.08, see Section 5.3.4. Rolling-element bearings were unable to attenuate input excitations to below 0.1" and so were determined to be unsuited for isolation.

With air bearings able to attenuate excitations below the 0.1" stability requirement, an assessment on residual field rotation was done to determine whether the field rotation was tolerable if air bearings were used on an equatorial mount's RA and DEC bearings. Section 5.3.1 shows that as much as 1" of field rotation resulted in only 0.12 μm tangential motion, which is within the image motion budget for the Cryoscope telescope and, therefore tolerable. Note that tower angular deflections are less than 1", so the amount of tangential motion should be less than the expected 0.12 μm.

Since effectiveness of an air bearing is also dependent on the ratio of radii, active cancellation systems were investigated in order to provide additional design margin. As discussed in Section 5.4, friction is difficult to model and such models would likely be unable to achieve the level of precision necessary for the stability requirement, so flexures were considered as a workaround for the limitations of friction modeling. Riverhawk Free-Flex® pivots were

assessed as a candidate flexure for a telescope mass of less than 1,400 kg and were shown to be adequate flexures for this application, with custom flexures being needed for larger telescope masses, which Riverhawk has expressed willingness to collaborate on in private conversations. A concern of using flexures was that they would resonate due to their extremely low angular stiffness but calculations in Section 5.4.1 showed that the bandwidth requirement was sufficiently low to fall within the bandwidth of a candidate direct drive motor. Another concern was finding encoders with 0.1" accuracy or better to measure the small angular deflections of the flexure so the direct drive motor can provide the necessary torque to null the excitation. Two encoder candidates were found, one supplied by Planewave Instruments and another by NASA's Goddard Space Flight Center, with accuracies below 0.1" but Section 5.4.2 showed that less accurate encoders could be used, such that those from Renishaw which have accuracies as low as 0.5".

It is possible to passively isolate the telescope from the tower by employing air bearings in an equatorial mount. The residual motion in the form of field rotation was demonstrated to be tolerable for a Teledyne H2RG, showing that the telescope could be isolated well within the 0.1" stability requirement. Additional margin for the isolation could be provided by active suppression methods by measuring the deflection of rotary flexures with an optical encoder to calculate the torque transferred so the direct drive motor can null the excitation. This means that more unstable tower designs, like T5 and T6, become serious candidates since their deflections can be suppressed. T6 is likely to be the best candidate since it is the simplest to transport and construct while maintaining a natural frequency above 2 Hz and is has the second lowest mass of the tower designs considered.

6. Summary

Mechanical stability on the order of a fraction of an arcsecond for a telescope atop a 30-meter tower in Antarctica is feasible. The stability, natural frequency, and mass for several open-framework, 30-meter-tall, modular towers with tetrahedra geometries were assessed for a maximum operating condition of 10 m/s sustained winds and a survival condition of a 72 m/s 3-s wind gust at Dome C. The results of this analysis, presented in Section 4.3.4, on the towers proposed in Section 4.3.3 showed all the towers maintain sub-arcsecond stability with natural frequencies greater than 2 Hz, well beyond the peak spectral density of horizontal wind frequencies. One tower design, T1, maintains a stability of less than 0.1” but at the cost of significant mass and new transportation infrastructure. Other tower designs traded greater tilt for higher natural frequency, lower mass, and easier assembly and transportation, as discussed in Section 4.3.3.2. T6 is a notable design since all its modules readily fit within a standard 20 ft cargo container, while also maintaining a similar natural frequency as T1 with 30% less mass but 0.66” tilt in maximum operating conditions. With two modules fitting inside a single 40 ft shipping container, T6 is the easiest to transport and requires the least amount of resources and volume for a traverse.

Analysis of some passive vibration isolation methods were performed in Section 5 to assess whether tower tilt could be suppressed below the 0.1” stability requirement. Damping mounts, and by extension, tuned mass dampers were considered but were deemed unsuited since their natural frequencies would be within the range of excitation frequencies. Friction isolators were then considered, and it was investigated whether the bearings of an equatorial mount could provide adequate isolation. Using the formulation set up in Section 5.3.3, it was determined that the coefficient of friction of the bearing and relative size of the bearing to the telescope were the key variables. Typical bearing friction coefficients were assessed for some estimated radii values

for the bearing and telescope's mass moment of inertia. MATLAB simulations showed that an air bearing with radii ratio of less than 0.08 could provide sufficient isolation below 0.1", see Section 5.3.4, however if the radii ratio is greater than 0.08 then not even air bearings could isolate the telescope below 0.1". Therefore, air bearings could be installed in the telescope mount to maximize the friction isolation, but active cancellation methods may still be needed to provide adequate design margin in case the ratio of radii is greater than 0.08.

An active cancellation scheme was explored in Section 5.4 that would circumvent the challenges of friction modeling by instead measuring the torque transferred by the bearing through a rotary flexure. Rotary flexures behave like torsional springs and are governed by the same torque-displacement equations, so if the rotations of the flexure could be measured then the transmitted torque could be calculated and nulled by the direct drive motor. By mounting an optical encoder about the flexure these deflections can be measured, with several commercial encoders available that can adequately capture the flexure's rotations. Riverhawk Free-Flex® pivots were assessed as a candidate flexure for a telescope mass of less than 1,400 kg and were shown to be adequate, with custom flexures being required for greater telescope masses. These flexures, mounted with Planewave Instruments, NASA Goddard Space Flight Center, or Renishaw, provide the means for sufficient measurement and cancellation of residual torque transmitted by the bearing.

Since complete vibration isolation through passive and active means was shown to be possible, the criteria of evaluating tower designs can be changed. More weight can be given to criteria such as natural frequency, mass, and ease of construction and transportation and less to the stability of the tower during the maximum operating condition. This then makes T6 the best candidate due to its simple assembly, easy integration into existing transportation and traverse

infrastructure, low mass relative to the other tower designs, and natural frequency greater than 2 Hz. See Table 14 and **Figure 76** below for a description of T6.

Table 14. Characteristics of T6.

Characteristic	Performance
Maximum Tilt	0.660”
Maximum Base Rotation	0.016”
Mass	53.9 tonnes
First Vibration Mode with 12,000kg Telescope	2.67 Hz
First Torsional Mode	5.30 Hz
Overall dimensions (L x W x H)	5 m x 5 m x 30 m
Module Dimensions	2.5 m x 2.5 m x 4 m
Number of Modules	28
Number of Levels	7
Number of Modules per Level	4
Number of Cargo Containers Required (assuming 40ft container length)	7 (2 per container)

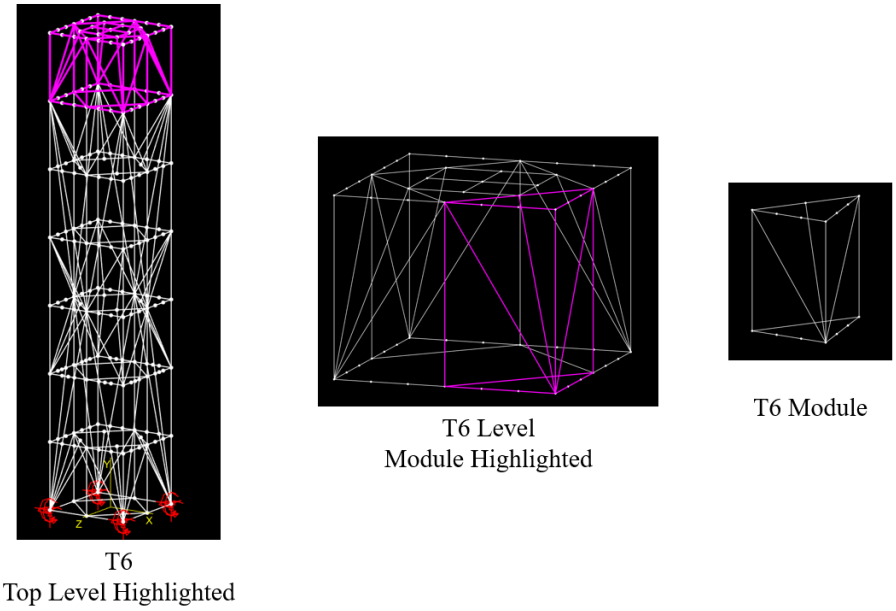

Figure 76. *T6.*

7. Conclusion

It is feasible to meet a 0.1 arcsec RMS tilt requirement atop a 30 m tower at Dome C by constructing T6 and equipping the telescope mount with rolling bearings and nested rotary

flexures. This path provides the lowest logistics cost and modular assembly, with the fewest modules. While tilts are about two times larger than other designs, such as runner-up T5, this can be addressed by using the direct drive motor to null the torque transmitted by the flexure by sensing the angular displacement of the flexure. This approach will require custom flexures as the load exceeds the largest available Riverhawk flexure by a factor of about 8.6. Should more design margin, or less reliance on an active cancellation system, be desired the rolling bearings can be replaced by air bearings but at the cost of an increased power budget, possibility of jitter from unequal airflow temperature around the telescope, and additional infrastructure to support the air bearings. If a more stable tower with a larger top platform is desired, then T5 could be selected since it is about twice as stable as T6 and 1.5 times wider but at the cost of requiring 1.7 times more modules, being only 24 m tall, and requiring a larger enclosure for the telescope, which would increase wind loading on the tower and lead to more tower tilt.

Revisiting the aims discussed in Section 1, it was found that it is possible to create a 30 m tower with less than 0.1 arcsec RMS tilt at Dome C but at significant transportation and construction costs. Instead, a tower with more tilt can be selected (T6), at significantly lower logistic cost and easier assembly, since the passive and active suppression methods in the form of air bearings and rotary flexures can sufficiently decouple the telescope from the tower.

8. Future Work

This work was intended to assess the feasibility and degree of difficulty of creating a 30 m tower for a telescope in Antarctica that could provide sufficient stability through passive and active means, so more detailed analysis is needed to flush out the design of the tower and vibration isolation methods. Additional work is required in designing and assessing the towers. Mass will drive the price of the tower so future work should include assessments into the effect of lighter spars and scaling widths on tower mass and natural frequency. The linear power law

analysis conducted in Section 4.3.4 shows that a tower design scaled down by 20% could provide the same mechanical stability for a mass reduction of 45% and a 25% increase of the first torsional mode. It would be interesting to know how these characteristics change if only a single dimension is scaled, such as height, width, and strut size, or if two different beam sizes are used in the design rather than one. Some of this analysis was already performed in Section 4.3.4 whereby the beam size of T6 was reduced by 20%. This showed a mass savings of 31% for a reduction of first torsional mode by 13%. Furthermore, additional analysis is needed for the effect of mounting a dome atop the tower and including a staircase on the tower's stability and natural frequency. Since the size and mass of the dome and stairs are unknown at the time of writing it was excluded from the analysis but should be included in future studies since the additional mass and surface area would affect the tower's performance. Additionally, the tower design is entirely dependent on the stiffness of its joints, therefore structural simulations and numerical analysis are needed to find the optimal design.

Future analysis must also be conducted on the addition of an enclosure or dome atop the tower that would house the telescope during observations. The enclosure would increase the amount of tower tilt since it introduces more surface for the wind to buffet so this effect must be quantified to more accurately determine the tower's stability during operating conditions. In addition, the added mass of the enclosure at the top of the tower would reduce the tower's natural frequency so the tower model must be updated as the design and mass of the enclosure become defined.

Another area that requires more analysis is the bearing friction model. The simplified model presented in Section 4.3.2 and 4.3.3 assumed pure Coulombic friction and did not account for viscous effects that would be present in an air or lubricated rolling bearing, which would increase the threshold by which isolation can be achieved. Although the rotary flexures complete

the isolation scheme and provide the means of nulling any residual torque the bearings cannot filter, this is still left to be proven by testing. So a rotary flexure and optical encoder assembly should be designed, built, and mounted to a bearing to test and confirm that residual torque transmitted by the bearing can be nulled using this system. Additionally, other angular deflection sensing methods should be assessed alongside the optical encoders as they may provide a more cost-effective solution.

References

1. Smith, Roger. “Cryoscope.” *The Palomar Observer*, https://sites.astro.caltech.edu/palomar/observer/newsletter/palomarobserver7.html.
2. Fossat, E. 2005, J. Astrophys. Astron., 26, 349
3. Storey, J. W. V., Ashley, M., C., B., Lawrence, J. S., & Burton, M. G. 2003, Mem. Soc. Astron. Italiana, 2, 13
4. Geissler, Kerstin, and Elena Masciadri. “Meteorological Parameter Analysis above Dome C Using Data from the European Centre for Medium-Range Weather Forecasts.” *Publications of the Astronomical Society of the Pacific*, vol. 118, no. 845, 7 June 2006, pp. 1048–1065., https://doi.org/10.1086/505891.
5. Genthon, Christophe, et al. “Ten Years of Temperature and Wind Observation on a 45-M Tower at Dome C, East Antarctic Plateau.” 2021, https://doi.org/10.5194/essd-2021-204.
6. Aristidi, E., et al. “An Analysis of Temperatures and Wind Speeds above Dome C, Antarctica.” *Astronomy & Astrophysics*, vol. 430, no. 2, 2005, pp. 739–746., https://doi.org/10.1051/0004-6361:20041876.
7. Wendler, G., Andre, J.-C., Pettre, P., Gosink, J., & Parish, T. 1992, Katabatic winds in Adelie coast, in Antarctic Meteorology and Climatology: Studies based on Automated Weather Stations, Antarctic Research Series, 61, 23
8. P. Sachs, Wind Forces in Engineering, Fig. 2.38 and 2.26, Pergamon Press, Oxford, 1972
9. Robert H. Hammerschlag, Aswin P. L. Jaegers, and Felix C. M. Bettonvil "Large open telescope: size-upscaling from DOT to LOT", Proc. SPIE 4853, Innovative Telescopes

and Instrumentation for Solar Astrophysics, (11 February 2003); https://doi.org/10.1117/12.460286

10. Hale, George E. “The 150-Foot Tower Telescope of the Mount Wilson Solar Observatory.” *Publications of the Astronomical Society of the Pacific*, vol. 24, 1912, p. 223., https://doi.org/10.1086/122165.
11. Hammerschlag, Robert H., et al. “Towers for Telescopes with Extreme Stability: Active or Passive?” *SPIE Proceedings*, 2006, https://doi.org/10.1117/12.670850.
12. “Mount Wilson Observatory Photographs and Audiovisual Materials, Approximately 1890s-2004 (Bulk 1925-1975).” *The Huntington Library*, https://catalog.huntington.org/record=b1881687.
13. Mark R. Swain and Hubert Gallée 2006 *PASP* **118** 1190
14. *21 Types of Beams in Construction*. The Constructor, 9 June 2020, https://theconstructor.org/structural-engg/types-beams-construction/24684/.
15. Kepler, Johannes. Harmonices mundi libri V. N.p., n.p, 1619.
16. “Demihypercube.” *Wikipedia*, Wikimedia Foundation, 30 May 2021, https://en.wikipedia.org/wiki/Demihypercube.
17. “Fracture Thermal - Massachusetts Institute of Technology.” *Modules in Mechanics of Materials*, Massachusetts Institute of Technology, https://web.mit.edu/course/3/3.11/www/modules/props.pdf.
18. *Packing and Shipping Instructions*. United States Antarctic Program, Aug. 2022, https://www.usap.gov/logistics/documents/tl-man-0002.pdf.
19. “SAM Low-Temperature Blue Hydraulic Fluid 1307010.” *Rural King - America's Farm and Home Store*, https://www.ruralking.com/sam-low-temperature-blue-hydraulic-fluid-1307010.

20. “Cryogenic Hydraulic Oil.” *Cryogenic Hydraulic Oil | Extreme Low Temperature | Superior Industries, Inc.*, Superior Industries Inc., https://www.superior-industries.com/products/synthetic-lubricants/synthetic-oils/cryogenic-low-temperature-oils/hydraulic/sch-60.html.
21. Kudu, Fatma Nur, et al. “Estimation of Damping Ratios of Steel Structures by Operational Modal Analysis Method.” *Journal of Constructional Steel Research*, vol. 112, Sept. 2015, pp. 61–68., https://doi.org/10.1016/j.jcsr.2015.04.019.
22. Palm, William. *System Dynamics*. Third ed., McGraw-Hill Science, 2014.
23. *Altazimuth and Equatorial Manual Mount*. Orwell Astronomical Society, http://www.oasi.org.uk/Telescopes/CFTOB/Mounts.gif.
24. “Frictional Coefficient (Reference).” *Basic Bearing Knowledge*, Koyo Bearings/JTEKT CORPORATION, https://koyo.jtekt.co.jp/en/support/bearing-knowledge/8-4000.html.
25. Nippon Steel & Sumikin Engineering Co., Ltd., 2018, *Spherical Sliding Bearing, NS-SSB®, Low Friction Type*, https://www.eng.nipponsteel.com/english/whoweare/r_and_d/reports/pdf/vol09_12.pdf.
26. “Spherical Bridge Bearing – Low Friction and Excellent Accommodation Feature.” *Spherical Bridge Bearings for Bridges and Building Structures*, Hengshui Jingtong Rubber Co., Ltd., https://www.bearing-pad.com/bearingpad/spherical-bridge-bearings.html.
27. *Low Temperature Range Down to -110 °C - FRAGOL*. Fragol, https://www.fragol.de/en/heat-transfer-fluids/silicone-oils/products/temperature-range/low-temperature-range-down-to-110-c.html#:~:text=Silicone%20oils%20are%20used%20especially,accordance%20with%20hazardous%20substances%20legislation.

28. *Low Temperature Rating*. Zeus Inc., 15 Nov. 2018, https://www.zeusinc.com/resources/summary-material-properties/low-temperature-rating/#:~:text=Fluoropolymers%20at%20Low%20Temperatures&text=PTFE%20has%20a%20working%20temperature,F%20(%2D73%20%C2%B0C).
29. *Air Bearing Application and Design Guide*. New Way Air Bearings, Jan. 2006, https://www.newwayairbearings.com/sites/default/files/new_way_application_and_design_guide_%20Rev_E_2006-01-18.pdf.
30. Geffen, V. van. 2009, *A Study of Friction Models and Friction Compensation*, http://coccweb.cocc.edu/bemerson/PhysicsGlobal/Courses/PH211/PH211Materials/PH211Breadcrumb/BreadcrumbDocuments/FrictionGeneral.pdf.
31. Olsson, H., et al. "Friction Models and Friction Compensation." *European Journal of Control*, vol. 4, no. 3, 1998, pp. 176–195., https://doi.org/10.1016/s0947-3580(98)70113-x.
32. Westermo, B., and F. Udwadia. "Periodic Response of a Sliding Oscillator System to Harmonic Excitation." *Earthquake Engineering & Structural Dynamics*, vol. 11, no. 1, Jan. 1983, pp. 135–146., https://doi.org/10.1002/eqe.4290110111.
33. "Cantilevered Pivot Bearings - Single-Ended Pivot Bearing." *Free-Flex® Pivots*, 17 May 2022, https://www.flexpivots.com/cantilevered-single-ende13d-pivot-bearings/.
34. *Free-Flex® Flexural Pivot Engineering Data*. Free-Flex® Pivots, https://www.flexpivots.com/wp-content/uploads/2022/03/Riverhawk-FlexuralPivotEngineeringData.pdf.
35. "Linear and Rotary Absolute Optical Encoders with Ultra-High Resolution." *Technology Opportunity*, NASA Goddard Space Flight Center, 9 Dec. 2005, https://itpo.gsfc.nasa.gov/wp-content/uploads/gsc_13703_optical_encoders.pdf.

36. *L-600 Direct Drive Mount*. PlaneWave Instruments, Inc., https://planewave.com/product/l-600-direct-drive-mount/.
37. Renishawplc. “Resolute™ with Resa30 Rotary (Angle) Ring.” *Renishaw*, https://www.renishaw.com/en/resolute-absolute-encoder-system-with-resa30-rotary-angle-ring--10939.
38. “What Is an Air Bearing?” *Westwind Air Bearing Spindles*, Celera Motion - A Novanta Company, 28 Apr. 2021, https://www.celeramotion.com/westwind/support/technical-papers/what-is-an-air-bearing/.
39. Haagh, Niels. “Astrophotography with Alt-Az Telescope Mounts.” *Telescope Mounts Explained*, Track The Stars, 11 May 2020, https://telescopemount.org/short-exposure-alt-az-astrophotography-learn-how-to-get-great-results/.
40. “Past Weather in Concordia Station, Antarctica.” *Weather in Concordia Station, Antarctica*, Time and Date, https://www.timeanddate.com/weather/antarctica/concordia-station/historic?month=9&year=2021.
41. Ricaud, Philippe, et al. “Trends in Atmospheric Humidity and Temperature above Dome C, Antarctica Evaluated from Observations and Reanalyses.” *Atmosphere*, vol. 11, no. 8, 2020, p. 836., https://doi.org/10.3390/atmos11080836. Accessed 9 Sept. 2022.
42. Ephraim Lanford, Mark Swain, Catherine Meyers, Tamao Muramatsu, Greg Nielson, Valerie Olson, Sebastien Ronsse, Emily Vinding Nyden, Robert Hammerschlag, and Patrick Little "Concept study and validation of Antarctic telescope tower", Proc. SPIE 6268, Advances in Stellar Interferometry, 626814 (27 June 2006); https://doi.org/10.1117/12.672346
43. Dargaud, Guillaume. “Antarctic Traverse.” *Antarctic Traverse*, 7 Aug. 2006, https://www.gdargaud.net/Antarctica/Traverse.html.

44. “Wide Load Regulations, Rules, Flags and Permit Costs by State.” *Wide Load Regulations, Rules, Flags and Permit Costs by State*, Oversize.io, https://oversize.io/regulations/maximum-width-by-state.
45. “Upbrella - Construction - without Cranes: 3L Innogenie.” *Upbrella - Construction - Without Cranes | 3L Innogenie*, 3L Innogenie, http://3l-innogenie.com/en/products/upbrella.
46. “MV American Tern.” *Wikipedia*, Wikimedia Foundation, 2 May 2022, https://en.wikipedia.org/wiki/MV_American_Tern.
47. Fucik, Jason, and Roger Smith. “The Optical Design for Cryoscope: A Wide-Field NIR Telescope with Low Thermal Emission.” *Ground-Based and Airborne Telescopes IX*, 2022, https://doi.org/10.1117/12.2630557.
48. Kaercher, Hans J., and H. Lautner. “Sofia Telescope Mounting on a Large Segmented Air Bearing.” *Cryogenic Optical Systems and Instruments IV*, 1990, https://doi.org/10.1117/12.23042.
49. Haby, Jeff. “The Forecasting of Dew.” *Dew and Frost Development*, https://www.weather.gov/source/zhu/ZHU_Training_Page/fog_stuff/Dew_Frost/Dew_Frost.htm.